KATHOLIEKE UNIVERSITEIT
LEUVEN

Arenberg Doctoraatsschool Wetenschap & Technologie
Faculteit Ingenieurswetenschappen
Departement Elektrotechniek

STEADY-STATE AND DYNAMIC MODELLING OF VSC HVDC SYSTEMS FOR POWER SYSTEM SIMULATION

Stijn COLE

Proefschrift voorgedragen
tot het behalen van de
graad van doctor in de
ingenieurswetenschappen

September 2010

STEADY-STATE AND DYNAMIC MODELLING OF VSC HVDC SYSTEMS FOR POWER SYSTEM SIMULATION

Stijn COLE

Examencommissie:
Prof. dr. ir.-arch. H. Neuckermans, voorzitter
Prof. dr. ir. R. Belmans, promotor
Prof. dr. ir. W. D'haeseleer
Prof. dr. ir. J. Driesen
Prof. dr. ir. G. Deconinck
Prof. dr. ir. M. Ghandhari
(Royal Institute of Technology, Zweden)
Prof. dr. ir. F. Milano
(University of Castilla-La Mancha, Spanje)

Proefschrift voorgedragen
tot het behalen van de
graad van doctor in de
ingenieurswetenschappen

U.D.C. 621.315

September 2010

D/2010/7515/78
ISBN 978-94-6018-239-6

Abstract

This work deals with the modelling of Voltage Source Converter High Voltage Direct Current (VSC HVDC) systems for power system analysis. The main contribution of the models is that they are valid for every topology of the DC grid. Therefore, they can be used to simulate multi-terminal VSC HVDC systems. Additionally, tools are developed for the steady-state and dynamic simulation of power systems with VSC HVDC connections. Together, the models and tools allow simulation of integrated AC/DC systems.

A simplified VSC HVDC steady-state model is first proposed, that can be used for power flow analysis. Next, the model is extended to a detailed model, by adding converter losses, limits, a full DC system representation, and filters. A sequential AC/DC power flow computation algorithm that can handle multi-terminal systems, is developed. Lastly, continuation methods are extended to allow AC/DC power system simulation.

A detailed dynamic VSC HVDC model is proposed in this work. It contains control systems, and detailed representations of the AC and DC side. Aspects such as control loop design, influence of the phase-locked loop and filter are discussed in detail. Reduced order models are then formally derived by eliminating certain time constants. A MATLAB based power system simulation software, *MatDyn*, is developed. This software is used to research the implementation aspects of dynamic multi-terminal VSC HVDC models in power system simulation software, and to test the proposed models. All models and tools are thoroughly validated.

Samenvatting

Dit werk handelt over de modellering van Voltage Source Converter High Voltage Direct Current (VSC HVDC) systemen voor de analyse van elektrische hoogspanningsnetwerken. De belangrijkste bijdrage van de modellen is het feit dat ze geldig zijn voor om het even welke topologie van het DC netwerk. Ze kunnen dus gebruikt worden om multi-convertor VSC HVDC systemen te simuleren. Ook worden programma's ontwikkeld voor simulatie van elektrische hoogspanningsnetwerken in evenwichts- en dynamisch bedrijf. Samen laten de modellen en programma's toe geïntegreerde AC/DC netwerken te simuleren.

Eerst wordt een eenvoudig VSC HVDC model voorgesteld dat kan gebruikt worden voor vermogenstroomanalyse. Het model wordt vervolgens uitgebreid tot een gedetailleerd model, door convertorverliezen, limieten, een volledig voorstelling van het DC netwerk en filter toe te voegen. Een sequentiële methode voor vermogenstroomberekeningen van AC/DC netwerken is ontwikkeld. Tenslotte zijn continueringsmethodes uitgebreid zodat ze voor AC/DC simulatie gebruikt kunnen worden.

Een gedetailleerd dynamisch VSC HVDC model wordt voorgesteld in dit werk. Het bevat regelkringen en een gedetailleerde voorstelling van AC en DC zijde. Aspecten zoals ontwerp van de regelkringen en de invloed van de filter worden in detail besproken. Modellen van gereduceerde orde worden vervolgens formeel afgeleid, door bepaalde tijdsconstanten te elimineren. Een MATLAB-gebaseerde software voor simulatie van hoogspanningsnetwerken, $MatDyn$, is ontwikkeld. Het wordt gebruikt om de implementatieaspecten van dynamische multi-convertor VSC HVDC modellen in programma's voor simulatie van hoogspanningsnetwerken te onderzoeken, en om de modellen te testen. Alle modellen en programma's worden grondig gevalideerd.

Voorwoord

Na eerst een maand vakantiewerk te hebben gedaan bij Electa, ging ik er in oktober 2005 aan de slag als doctoraatsstudent. Rond die tijd bereikte mij vage informatie over een project in samenwerking met ABB over een nieuwe technologie in hoogspanningsnetten, VSC HVDC. Het was Prof. Ronnie Belmans die me suggereerde om verder onderzoek te verrichten naar VSC HVDC en dan vooral naar het gebruik in vermaasde netten. Ik wens hem hartelijk te bedanken om het promotorschap op zich te nemen, en om interessante projecten aan te brengen. Hij heeft me ook de kans gegeven om gedurende bijna drie maanden onderzoek te doen bij ABB in Zweden. De juryleden Prof. Johan Driesen, Prof. Geert Deconinck, en Prof. William d'Haeseleer bedank ik voor hun vragen en opmerkingen bij de tekst, Prof. Herman Neuckermans daarenboven voor het voorzitterschap. Many thanks to Prof. Federico Milano and Prof. Mehrdad Ghandhari for their interest in the work and pertinent questions and suggestions. Bedankt ook David, Jef, Simon en Jan voor het nalezen. Thanks to Kailash, Reza, and Georgios for inviting me to ABB Corporate Research, and giving me a warm welcome in a cold Sweden. Their help is much appreciated.

Het einde van dit doctoraat betekent ook het afscheid van ELECTA. Bedankt aan alle collega's voor een s(t)imulerende werkomgeving en voor alle toffe momenten. Speciale vermelding voor Leonardo en Dirk, die me hebben begeleid gedurende het eerste jaar. Ook bedank ik iedereen van het secretariaat; ze stonden altijd klaar voor mij.

Speciale dank aan mijn familie en vrienden voor hun steun, en aan Karolien natuurlijk, voor alles wat ze voor mij gedaan heeft.

Stijn Cole
September, 2010

List of Symbols and Abbreviations

List of Symbols

Symbol	Description
F	Set of dynamic equations
G	Set of algebraic equations
G_2	Set of power flow equations
G_1	Set of non power flow, algebraic equations
P	Set of parameters
L	Constraint manifold
S	Infeasible manifold
ω	Pulsation
ω_s	System's pulsation
$\mathsf{C_S}$	Symmetrical components' transformation matrix
$\mathsf{C_P}$	Park's transformation matrix
$\mathsf{C_K}$	Kron's transformation matrix
u_s	System voltage
u_c	Converter voltage
u_f	Filter voltage
u_s^{dq}	d- or q-axis system voltage
u_c^{dq}	d- or q-axis converter voltage
u_f^{dq}	d- or q-axis filter voltage

(Continued on next page)

Symbol	Description
$\underline{U}_s$	System voltage phasor
$\underline{U}_c$	Converter voltage phasor
$\underline{U}_f$	Filter bus voltage phasor
i_{pr}	Phase reactor current
i_{tr}	Transformer reactor current
i_{pr}^{dq}	d- or q-axis phase reactor current
i_{tr}^{dq}	d- or q-axis transformer reactor current
$\underline{I}_{pr}$	Phase reactor current phasor
$\underline{I}_{tr}$	Transformer current phasor
$\underline{S}_s$	VSC's power injection in the system
$\underline{S}_c$	Power injection at converter
$\underline{S}_f$	Power flowing to the grid at filter bus
Y_{dc}	DC bus admittance matrix
$\mathsf{Y}_{\mathsf{bus}}$	AC bus admittance matrix
P_{loss}	VSC HVDC system's losses
L_{pr}	Phase reactor inductance
R_{pr}	Phase reactor resistance
L_{tr}	Transformer inductance
R_{tr}	Transformer resistance
L_{eq}	Transformer + phase reactor inductance
R_{eq}	Transformer + phase reactor resistance
C_f	Filter capacitance
u_{dc_i}	DC voltage at converter i
i_{dc_i}	i^{th} converter's injected DC current
i_{cc}	DC conductor current
U_{dc}	Steady-state DC voltage
I_{dc}	Steady-state converter's injected DC current
I_{cc}	Steady-state DC conductor current
L_{dc}	DC circuit inductance
R_{dc}	DC circuit resistance
C_{dc}	DC circuit capacitance

(Continued on next page)

Symbol	Description
α	Continuation parameter(s)
H_F	Test function for fold
H_H	Test function for Hopf bifurcation
H_S	Test function for singularity induced bifurcation
H_L	Test function for limit induced bifurcation
λ	Eigenvalue
h	Step size
$K_{p,i}^{dq}$	d- or q-axis PI current controller's proportional gain
$K_{i,i}^{dq}$	d- or q-axis PI current controller's integral gain
$K_{p,q}^{dq}$	d- or q-axis PI reactive power controller's proportional gain
$K_{i,q}^{dq}$	d- or q-axis PI reactive power controller's integral gain
$K_{p,u}^{dq}$	d- or q-axis PI system voltage controller's proportional gain
$K_{i,u}^{dq}$	d- or q-axis PI system voltage controller's integral gain
$K_{p,p}^{dq}$	d- or q-axis PI active power controller's proportional gain
$K_{i,p}^{dq}$	d- or q-axis PI active power controller's integral gain
$K_{p,dc}$	PI DC voltage controller's proportional gain
$K_{i,dc}$	PI DC voltage controller's integral gain
Δu_c^{dq}	d- or q-axis current controller cross-coupling term
$i_{pr^{ref}}^{dq}$	d- or q-axis phase reactor reference current
Q_{ref}	Reactive power reference
U_{ref}	System voltage reference
P_{ref}	Active power reference
u_{dcref}	DC voltage reference
$i_{dc_n^{ref}}$	Slack converter's injected DC current reference
T_σ	Converter's time constant
T_{dc}	Converter's time constant seen from DC side
t	Time
P_m	Turbine power
E_{fd}	Excitation or field voltage

List of Abbreviations

Abbreviation	Description
AC	Alternating Current
COI	Centre of Inertia
CSC	Current Source Controller
DC	Direct Current
DAE	Differential Algebraic Equation
DSP	Digital Signal Processor
EC	European Commission
EMF	Electromotive Force
EMTP	Electromagnetic Transients Program
ENTSO-E	European Network of Transmission Operators for Electricity
EWEA	European Wind Energy Association
EWIS	European Wind Integration Study
FACTS	Flexible Alternating Current Transmission Systems
GTO	Gate Turn-Off Thyristor
HVDC	High Voltage Direct Current
IGBT	Insulated Gate Bipolar Transistor
IEM	Internal Electricity Market
LF	Loop Filter
LIB	Limit Induced Bifurcation
LQG	Linear-Quadratic-Gaussian
MI	Mass-Impregnated
MTDC	Multi-terminal Direct Current
NDF	Numerical Differentiation Formulas
ODE	Ordinary Differential Equation
PD	Phase Detector
PDE	Partial Differential Equation
PF	Power Flow
PI	Proportional-Integral
PIP	Priority Interconnection Plan
PLL	Phase-Locked Loop

(Continued on next page)

Abbreviation	Description
PSAT	Power Systems Analysis Toolbox
PSS/E	Power System Simulator for Engineers
PWM	Pulse Width Modulation
RES	Renewable Energy Sources
RMS	Root Mean Square
SCR	Short Circuit Ratio
SIB	Singularity Induced Bifurcation
TEN-E	Trans-European Energy Networks
TSO	Transmission System Operator
VCO	Voltage Controlled Oscillator
VSC	Voltage Source Controller
XLPE	Cross-linked Polyethylene

Contents

Chapter 1

Introduction

1.1 Historical Background of HVDC Transmission

Electric power is commonly transported by three-phase Alternating Current (AC) power systems. Today, AC power systems are so widespread and universally accepted that it is hard to believe that at the dawn of the electricity era this was far from evident. While the first transmission line in Europe was an AC connection between Laufen and Frankfurt, in America electric power transmission and distribution was first attempted using Direct Current (DC). DC transmission has been around from as early as the 19th century, when the inventions of Thomas Edison became the drivers for the development of a DC network. The DC standard for power transmission was challenged by Westinghouse and the mathematical genius, Tesla, both proponents of AC transmission. A debate ensued on the best technology for power transmission, AC or DC, whereby the advocates of both sides had recourse to ideological arguments as much as to technical ones. This 'War of the Currents' as the AC versus DC debate was coined, was eventually won by AC. One of the main contributing factors to the victory of AC was the invention of the transformer that allowed using more and higher voltage levels and led to economic transport of electric power over longer distances. Furthermore, it is convenient producing rotating fields for electrical machines using AC [1].

The victory of AC did not lead to the immediate demise of DC networks. One of the last remnants of DC was a small network near Pearl Street in New York City operated by Con Edison. It was only shut down in 2007 [2]. In Europe, René Thury introduced arguably the first High Voltage Direct Current (HVDC) system. The so-called "Thury System" consisted of DC generators connected to the loads through conductors. High voltages were achieved by connecting DC

generators in series. The first installation consisted of a circuit of 120 km, at a voltage of 14 kV. This system, that only deserved the epithet 'high voltage' by comparison with the Edison system, was built in 1889 in Italy. In 1910, an even by today's standards respectable 125 kV DC system was introduced in France. The DC connection between Moutiers and Lyon had a total length of over 180 km, with a short underground section [3, pp. 94-95]. The main drawback of the Thury system was the low reliability due to the series connected loads. The last Thury systems went out of operation by the 1930s, but they had by then shown the potential of HVDC systems.

Research on DC technology was never completely abandoned: AC technology being well-established, one of the fields of interest was the mercury arc valve, that could rectify AC current. Even though mercury arc valves had been around for quite a long time, much research and experiments were needed to develop valves with a rating high enough to make them suitable for power transmission. After this breakthrough development, many years of continued work were still needed to build a commercial system: the world's first HVDC system between the island of Gotland and Sweden. It is thanks to the unrelenting efforts of Uno Lamm, the 'father of HVDC', that DC transmission made its definitive comeback in the 1950s [1].

In the '70s, high power thyristors were developed as an alternative to mercury arc valves. Solid-state switches entail numerous advantages over mercury arc valves. The voltage of thyristor valves can be increased by simply series connecting thyristors in a 'stack', while current rating could be increased by parallel connecting such stacks. It was thus easy to achieve very high power ratings which meant a big step forward for HVDC and the bulk transmission of electric power. Thyristor valves do not suffer from the drawbacks of mercury arc valves, such as the need for frequent overhauls, and mercury emission. Consequently, mercury arc valves were not further developed and were gradually replaced from the '70s onwards. Today only a few converter stations with mercury arc valves remain.

Since the first project in 1954, the principles of HVDC transmission have essentially remained the same. Developments and experience have increased steadily, allowing ever higher power and voltage rates, and continue to do so today. Currently, the cumulative installed capacity amounts to almost 100 GW [4].

With the advent of the high power Insulated Gate Bipolar Transistor (IGBT), a new era in HVDC technology has commenced. This new component was introduced as main building block of the valves of a new generation of HVDC converters. The main difference between thyristors and IGBTs in operation of the power converter is the turn-off capability of the latter. This seemingly small difference has completely revolutionised the world of HVDC: the use of IGBTs instead of thyristors is not a development comparable to the transition from

mercury-arc valves to thyristor valves, but a rupture that required a complete change of the layout and design philosophy of the converter stations, greatly expanding the range of applications of HVDC [1]. Converters with IGBTs did not replace converters with thyristors: both systems exist because their field of application is not the same. To distinguish between both systems, the term Current Source Converter (CSC) HVDC is used for the thyristor converter HVDC, and Voltage Source Converter (VSC) for the IGBT converter HVDC. Alternatively, they are referred to as respectively line-commutated and self-commutated converters. The first commercial installation of VSC HVDC was commissioned in 1999 on the island of Gotland, Sweden. This system has a rated power of 50 MW at a DC voltage of ± 80 kV. From that moment on, ratings have been steadily increasing: the more recent 'Estlink' (2006) has a rated power of 350 MW at ±150 kV DC, and in the same year, a manufacturer claimed he can deliver installations breaking the 1 GW barrier [5]. In Table 1.1, the state-of-the-art of HVDC systems is shown. Clearly, VSC HVDC cannot compete with CSC HVDC in the area of bulk transmission of power, which remains the apanage of conventional HVDC. On the other hand, VSC HVDC is more flexible than CSC HVDC: it is technically superior and has less space requirements. VSCs open up a wide range of new applications, hitherto not viable for HVDC.

Table 1.1: HVDC systems: state-of-the-art

	State-of-the-art: installed		State-of-the-art: possible	
	CSC HVDC	VSC HVDC	CSC HVDC	VSC HVDC
P [MW]	6300	350	6400	1100
U_{dc} [kV]	±600	±150	±800	±300

1.2 Rationale for VSC HVDC

HVDC systems are more flexible than their AC counterparts. This offers distinct advantages for the operation of the modern power grid, confronted with all-pervading changes. One of the most salient changes in the power system world was the development of the Internal Electricity Market (IEM), that targets easy international trade of electricity. However, national grids were originally interconnected only to aid in case of emergency conditions. The interconnections were never dimensioned with international trade in mind. Hence, the European network consists of strong national grids that are weakly interconnected. The scarcity of cross-border transmission capacity seriously impedes international trade. The lack of sufficient cross-border capacity has been identified as a barrier

for the development of a single IEM [6]. This was recognised by the European Commission (EC), that published guidelines facilitating financing Trans-European Energy Networks (TEN-E) [7]. The most recent list of projects is identified in the 2007 Priority Interconnection Plan (PIP) [8]. The efforts of the EC notwithstanding, we cannot but find that only five projects of this list have been completed thus far [9]. Some key obstacles that many PIP projects face, would disappear if VSC HVDC were to be used. It is recognised by the European Network of Transmission Operators for Electricity (ENTSO-E) that new technologies, such as VSC HVDC, are valuable investment options [10].

International trade causes variable flows that make the grid more challenging to operate. If the flows are contracted exchanges, the TSO can take measures to deal with them. Often, the variable flows are unidentified or unscheduled and cannot be easily dealt with by the operator. Tie-lines can then become dangerously highly loaded. VSC HVDC can offer power control, which is instrumental to deal with loop flows [11].

Another trend in power systems is the increasing number of renewable energy sources (RES) connected to the grid. This trend exemplifies the increasing political commitment to battle climate change, that started with the ratification of the Kyoto-protocol by many countries. In Europe, the European Council set a binding target for renewable energy as part of the '20 20 by 2020' policy: by 2020, 20% of consumed energy must have a renewable origin [12]. Wind energy will be the main contributor to this target. The vertiginous rise of wind power has exceeded the expectations of the European Wind Energy Association (EWEA), that adopted a target of 10 GW by 2010 in 1997, and revised it three years later to 60 GW. The European Commission estimated 22.6 GW of installed capacity in 2010 [13]. Both predictions proved too conservative: in 2009, 10 GW of wind energy was installed in the EU-27, bringing the total installed capacity at 76 GW by the end of 2009 [14]. The EWEA sets the target for installed capacity at 180 GW for 2020 and at 300 GW for 2030 [15]. This would correspond with respectively a 18.1% and 25.5% share of wind energy in the total installed capacity in the EU [15]. Wind power is an intermittent energy source. As such, it creates problems for the power grid, where at any time generation and load have to be balanced. The European Wind Integration Study (EWIS)[16], a study conducted by the European TSOs, identified a number of problems associated with integrating large scale wind power into the European network:

- large unidentified flows, that could reduce system stability and impede trading;
- need for grid reinforcements;
- problems due to disconnection of wind farms after faults;
- heavily loaded lines and the need for more reactive power.

Furthermore, RES are often located far away from the load centres, necessitating long distance transmission, that again requires more reactive power if AC is used. RES can even be located offshore, where it is notoriously difficult to connect them, especially far from shore. VSC HVDC converters can be installed offshore: the first offshore HVDC converter was installed in the North Sea in 2005 to feed an offshore platform [17], and a second one is expected to go in operation in 2010 [18]. An offshore converter to be used for connecting wind farms was deblocked on 05/03/2010. The application of VSC HVDC to offshore wind farms receives much attention in research [19], [20], [21], [22]. VSC HVDC systems have the capability to deal with other problems related to connection of RES: they provide reactive power, and can control the power flow.

The benefits of VSC HVDC are widely recognised: its promising prospects lead to a growing body of literature devoted to possible applications of VSC HVDC. References [23] and [24] propose to use VSC HVDC to supply power to large cities. CSC HVDC systems have been proposed for city infeed as early as 1940. Some schemes were even built, but the concept was found to be not economically efficient. It was argued in [24] that the new possibilities that VSCs offer, warrant reconsidering HVDC for city infeed. In [25] control algorithms are derived for VSC HVDC systems supplying industrial networks, requiring high quality power that could be provided by VSC HVDC. The system can provide frequency control, and ride-through capability in case of voltage disturbances. Lastly, with VSC HVDC, it is straightforward to connect more than two converters to the same DC network. This possibility has led to the vision of a DC 'supergrid', that could connect many RES to a common DC network [26]. At the time of writing (2010), more than ten VSC HVDC projects are completed, many more are under construction or in the planning stage.

1.3 Goals of the Work

When considering VSC HVDC for a transmission project, the power system engineer needs models of the various power system components at every stage of the project. For the basic power system equipment such as transmission lines, transformers, and generators with their controls, such models already exist. The same can be said for CSC HVDC: in section 1.1 it was indicated that experience with CSC HVDC goes back to the 1950s, and that the technology remained essentially unchanged since the '70s. CSC HVDC is now well-known, with a large number of installations. Several models exist, and are available in the literature and in all relevant software packages. The same level of experience does not exist for VSC HVDC, a fairly new technology. In most power system analysis and design software, no VSC HVDC models are available. While it may be true that manufacturer delivered models exist, one should not loose sight of the fact that

those models are closed, and limited to the specific implementation of VSC HVDC by that particular manufacturer. Accordingly, the power system engineer sees himself obliged to take recourse to user defined modelling, as opposed to standard models. Thanks to the work of the IEEE, that has always been very active in the field of standardisation, standard models now exist for numerous power system equipment, such as excitation systems [27], and steam and hydro turbines [28]. However, to the author's best knowledge, no standard models for VSC HVDC have been proposed in the literature. We believe there is a need for standard models for VSC HVDC systems, that can be readily implemented in power system simulation software. Using standard models for power system equipment has clear advantages. Data exchange between utilities, and the transition to new software packages proves much more convenient if standard models are used.

The absence of standard models for VSC HVDC does not mean that no efforts are spent on HVDC modelling: there is a growing body of literature dedicated to the subject. Steady-state models, with different level of detail, and different assumptions have been developed [29], [30], [31], [32], [33], [34], all discussed in Chapter 4.

The group of dynamic VSC HVDC models proposed in literature is very heterogeneous. The models are often developed *ad hoc*, and are not suitable for standard models. Also, very few dynamic models are explicitly developed with multi-terminal operation in mind. Nevertheless, quite a lot of publications are devoted to the subject of VSC Multi-Terminal Direct Current (MTDC). They deal with various aspects of MTDC operation such as localisation of DC faults and protection [35], [36], control strategy [37], harmonics [38], and applications in wind farms [39], [40]. The multi-terminal models used in the aforementioned papers on MTDC have a fixed topology, i.e. are not generally valid: it is not explained how to extend the models to other topologies. Some papers exist on modelling of multi-terminal CSC HVDC systems and the implementation of those models in stability programs, e.g. [41] and [42]. As for basic modelling of VSC MTDC systems in power system stability programs, the literature is limited to non-existent.

This work aims to redress these lacunae by developing a set of steady-state and dynamic models, that could serve as standard models of VSC HVDC systems for the analysis of large scale integrated AC/DC systems. Additionally, it is explained how the models can be efficiently implemented in power system software. To this end, power system tools are developed. A major feature of the models is that they are all 'general', i.e. valid for every possible topology of the DC network and every possible connection with the AC network. The simplest AC/DC system is an AC network with asynchronous infeed, which could represent for instance the connection of an offshore wind farm to the power system, or a standard two-terminal HVDC system whereby the second converter is located in a different system (Fig. 1.1). Fig. 1.2 shows a system wherein the two converters are located

in the same AC system. The most general AC/DC system is a meshed DC system connected to the AC system through many converters (Fig. 1.3). Furthermore, the models are 'generic', i.e. valid regardless of the technology used for the actual implementation. This means that VSC HVDC systems of different manufacturers can be represented by the same model.

1.4 Scope of the Work

The power system is complex with dynamic behaviour, characterised by time constants ranging from microseconds to hours. It would require a huge modelling effort to develop models that can be used for the whole frequency spectrum of the power system's dynamic behaviour. Solving the system would necessitate substantial computational power. It is the *de facto* standard to decouple the power system on basis of time frames. Models of power system components can broadly be divided into three categories: steady-state, electromechanical, and electromagnetic. These three categories correspond to different phenomena in the power system, studied with different simulation tools. Mathematically, this classification makes sense in that it is based on the smallest time constant of interest: when it is very small, electromagnetic models are used, when it is larger, electromechanical models, and when it is large, steady-state models.

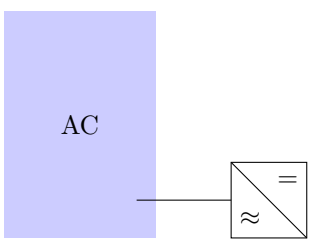

Figure 1.1: Asynchronous infeed.

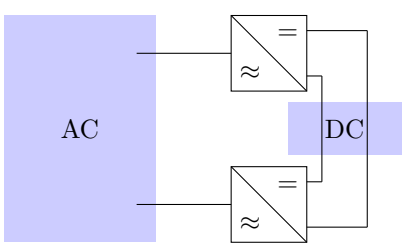

Figure 1.2: Two-terminal system.

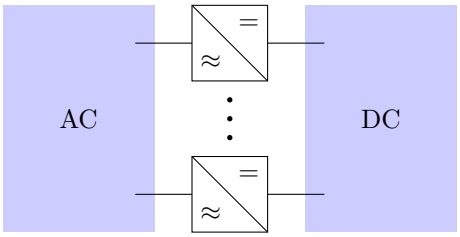

Figure 1.3: General MTDC system.

Electromagnetic phenomena are local in nature, caused by events such as switching actions, lightning, and faults. Such phenomena have very small time constants, and are studied using EMTP (Electromagnetic Transients Program) type tools, that use a very small integration step size. The integration interval is usually also small, as electromagnetic transients die out fast.

Electromechanical phenomena are essentially associated with the interaction between electrical and mechanical energy in the generators. Electromechanical transients are much slower than electromagnetic ones. Electromagnetic transients have negligible influence on slower phenomena. Conversely, they are not influenced by slower dynamics, that can be assumed constant during the short simulation interval of interest. This provides the basis for the decoupling of the different dynamic phenomena. Electromechanical transients are traditionally studied with transient stability type programs. The phenomena of interest are slow compared to the fundamental frequency. Larger step sizes can be used, but at the cost of neglecting harmonics and fast phenomena.

When electromagnetic and electromechanical transients have died out, the system is in steady-state. Steady-state models can then be used. Such models are implemented in power flow or optimal power flow tools. Table 1.2 gives an overview of the properties of the different models.

The focal point of this work is steady-state and electromechanical models. Electromagnetic models are characterised by a large set of state variables and associated set of equations; the parameter set is generally large as well. In case of VSC HVDC, an electromagnetic model requires for instance knowledge of the precise converter topology and valve characteristics. For each topology, a different model should be developed. It is thus hard to come up with a generic model. The level of detail can also vary within each category: for each category different models with different level of detail can be developed. It is important to understand that detailed models are not always the best choice: often, it is hard to collect all data, especially in the planning stage. A few unknown data entries can nullify the effort spent in acquiring a detailed model. Such models are, and can only be, provided by the manufacturers of the equipment, but contain proprietary information and

are technology dependent and, hence, not generic. Furthermore, as the number of state variables of detailed models is large, the number of equations to be solved is also large, which places a heavy burden on computing power, especially for large systems. If the model is described by differential equations, as is the case for electromechanical and electromagnetic models, the integration step size needs to be increased to arrive at acceptable simulation speed. On the other hand, it is not correct to state that models should be 'as simple as possible', as the adage has it, but they should be 'as detailed as necessary'. This is why in this work, both detailed and simplified models are proposed.

Table 1.2: Categories of power system modelling

	Steady-state	Electromechanical	Electromagnetic
Time frame	large	small	very small
State variables	few	more	many
Time step	indefinitely large	small	very small
Phenomena	loading	stability	harmonics
Data requirements	small	moderate	high

1.5 Overview

In Chapter 2, an explanation of the technological aspects of a VSC HVDC system is given. Its main components, operating principles, converter topologies and operating range are discussed. The purpose of the chapter is to provide a clear understanding of the operation of a VSC HVDC system, and to determine which elements need to be modelled. The chapter is followed by the more theoretical Chapter 3, that provides the mathematical background of the general power system model. The models fit within the framework of the general power system model and are subjected to its limitations and assumptions. The aim is to clearly define the range of validity of the model. In Chapter 4, steady-state VSC HVDC models are developed. First a simple model is proposed to which subsequently more detail is added. A sequential AC/DC power flow computation algorithm that can handle MTDC systems, is developed. Chapter 5 deals with time-domain simulation of power systems. A computer program is developed, that can be used to simulated AC/DC systems. In Chapter 6, dynamic VSC HVDC models are developed. A detailed model is proposed. Reduced order models are then formally derived by eliminating certain time constants. The models are tested using the program developed in Chapter 5. The work is concluded with Chapter 7, which provides conclusions and suggestions for future work.

Chapter 2

VSC HVDC

2.1 Introduction

Before starting to model a VSC HVDC system, it is essential to have a clear understanding of its components, operating principles, and operating range. In section 2.2, the key components constituting a VSC HVDC system are enlisted. The purpose of the component in the whole system is discussed, as well as some technological and constructional aspects. The emphasis lies on component modelling. Different converter topologies and their influence on modelling are discussed as well. In the next section, the operating principles of VSC HVDC are explained. Lastly, the capability chart, defining the operating range of a VSC HVDC system, is discussed.

2.2 VSC HVDC Components

In Fig. 2.1, a representation of a VSC HVDC system is shown. The AC grid is connected to the converter through a transformer, a shunt connected filter and a phase reactor. All are three-phase elements, but are shown by their single-line representation. On the DC side, the DC capacitors and the conductors are shown. Filters, phase reactor, valves and DC capacitors are located in a building, depicted by the shaded area. Only the transformers are located outside.

Not all elements are shown. Some elements, not important for steady-state and dynamic modelling, are omitted, as e.g. the indispensable cooling system. It is located outside and provides cooling for the semiconductors. Obviously, it is not part of the electrical system and can safely be discarded in the analysis. On

the AC side, a number of breakers are present, assumed closed at all times and hence need not be modelled. On the DC side, harmonic filters, radio frequency interference filters and the common mode blocking reactor are omitted. The DC reactor reduces harmonics. It is usually very small, but influences the rate of current change and thus the DC dynamics. Its effect must therefore be taken into account. This can easily be achieved by aggregating its reactance with the conductor's reactance: an explicit representation is not necessary. DC harmonic filters have a negligible influence. Common mode reactors are installed to reduce common mode currents, that can cause electromagnetic interference. They do not, however, influence differential mode components. Consequently, there is no influence on dynamics or power flows and they may be discarded [43]. On the other hand, some important elements that need or may need to be modelled, such as the control scheme and measuring equipment, are not shown.

2.2.1 Transformer

The transformer is an important element in an HVDC system. In CSC HVDC systems, there is some concern on increasing transformer failures [44]. Converter transformers exhibit higher losses due to the harmonic content of the current and are subjected to high vibration levels caused by saturation of the core due to small DC current components [44, p.18]. Therefore, special care is needed in the design of these transformers. For VSC HVDC systems, standard transformers can be used, as the filter is located between converter and transformer. Often the transformer is equipped with a tap changer to increase the reactive power range (section 2.5). In future, it may be possible to discard the transformer from the scheme by an appropriate choice of the DC voltage. This would be beneficial for reliability and cost. The transformer can be represented by a combination of a π

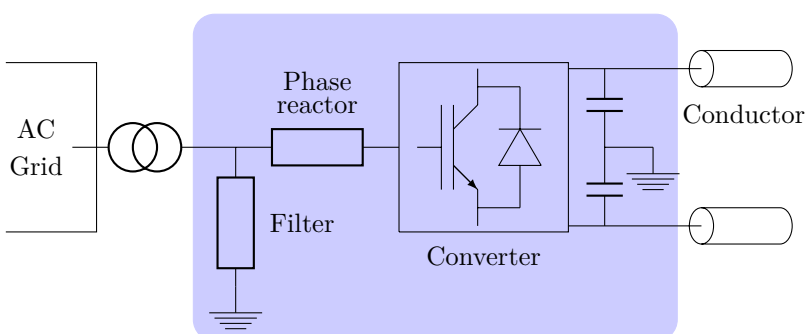

Figure 2.1: VSC scheme.

equivalent and an ideal transformer. Alternatively, it can be represented simply by its leakage reactance.

2.2.2 Phase Reactors

The phase reactor is the dominant element on the converter's AC side. It is a large, inductive element with small resistance. Its purpose is to control the complex current. By doing so, it can control active and reactive power. Also, it is part of the low pass filter that disallows high frequency signals to enter the transformer. The phase reactor's size determines the dynamic behaviour of the converter's AC side; hence, the phase reactor is an important element in modelling VSC HVDC systems.

2.2.3 Filter

The filter essentially forms a low-pass filter together with the phase reactor, tuned so that the fundamental frequency is magnified, low frequency signals are not altered, but high frequency signals are strongly attenuated. Low order filters can be added if needed [43]. The shunt filter is installed between converter and network. It prevents harmonics from entering the AC system, and filters high frequency components so that the transformer is not exposed to high frequency stress. This allows using standard transformers.

Contrary to CSC HVDC systems, there is no need for switching more or less filters depending on the active power set point: a single, small filter bank suffices. The filter changes the power flow in that it provides reactive power to the network.

The filter consists of shunt inductances and capacitors. The precise layout is not important here: being interested in the fundamental frequency signal only, the filter needs not be modelled in great detail. Around the fundamental frequency, the filter can be represented by a capacitor.

Whether the filter needs to be included at all in steady-state and dynamic modelling cannot be determined at this point. If and how it should be done, is discussed in subsequent chapters.

2.2.4 Valves

The valves are arguably the most important elements of the HVDC system. Their main purpose is to switch voltages, much higher than the voltage of their constituent switching elements. To achieve high voltage switching capability, switching elements are connected in series. Some redundant elements are included,

to ensure that the valve can continue operating when an element fails. The most widely used switching element for VSC HVDC systems is the Insulated Gate Bipolar Transistor (IGBT). Although some VSC HVDC systems with Gate Turn-off Thyristors (GTO) and thyristors with forced commutation have been developed, at the end of 2004 all VSC valves used IGBTs [43, p.5-3]. A diode is connected in anti-parallel with each IGBT. Apart from the IGBT and diode, a single IGBT module also has a snubber circuit, gate drive, and heat sink.

For Root Mean Square (RMS) modelling, the valves need not be modelled: the switching is so fast compared to the phenomena of interest, that it can be assumed infinitely fast. However, to account for the dynamic behaviour of the converter bridge, consisting of many switches, as a whole, the bridge can be modelled as a simple time delay.

2.2.5 DC Capacitors

The DC capacitors provide the voltage of the converter's DC side. They are the most important elements in the DC circuit: they act as energy storage, vital for the operation of VSC HVDC. The DC voltage is kept within a narrow band by charging or discharging the capacitors. Their size determines the dynamic behaviour of the DC circuit. Hence they are important for the dynamic modelling.

2.2.6 Conductors

Extruded cables are predominantly used for VSC HVDC transmission. Currently, there are 500 kV AC cross-linked polyethylene (XLPE) cables in operation [45]. AC XLPE cables cannot be directly used for DC transmission because of a phenomenon called space charges. The direct voltage gives rise to an electric field, which would cause space charges to move and accumulate in certain spots of the insulation, resulting in its degradation. Special XLPE cables have been developed that do not exhibit space charge problems. A precondition for such cables is that the voltage polarity does not change rapidly, as this causes high stresses in the insulation. CSC HVDC systems require voltage polarity reversal for a reversal in power direction. Hence, XLPE cables are not used in conjunction with CSC's. Other types such as mass-impregnated (MI) (e.g. NorNed), or gas-filled (e.g. the New Zealand inter island link) conductors are used. The polarity of the DC voltage in VSC HVDC systems does not change. Hence, XLPE cables can be used, which have some advantages over liquid insulated cables:

- XLPE is lighter than other cable types. MI cables weigh up to 80 kg/m for a voltage level of 500 kV. The weight and bulk of the cable limit the maximum length of one cable section. It is advantageous to have long cable

sections, as the number of cable joints can be reduced, the joint being the most failure-prone component in the cable system. They are assembled in environments with controlled humidity and temperature [46, p.107].

- XLPE cables have a smaller bending radius. Hence, smaller drums can be used, leading to easier transport, and more flexible routing.
- As XLPE is lighter and has a smaller bending radius, installation of the cable is easier.
- XLPE is a solid insulator. There is no risk of oil leakage.

Today (2010), manufacturers can deliver cables with a maximum voltage of ± 320 kV DC. In the literature, as early as 2004, a DC XLPE cable at a remarkable voltage of 500 kV, including joints, has been reported, subjected to long-term (one year) tests and found to be suitable for HVDC transmission [47].

A special type are submarine cables, which face harsh environmental conditions. They are armoured with galvanised steel wire for mechanical sturdiness. Furthermore, the insulation needs to be protected from water, and also from humidity: while solid insulation is water-tight, it can still diffuse humidity, which causes the dielectric strength and ageing resistance to decrease [46, p.22]. The joints of submarine cables need to be water-tight as well, achieved by soldering the joint's lead sheaths against the cable's lead sheaths [5]. While jointing submarine cables certainly proves much more difficult than jointing their conventional counterparts, this difficulty is offset by the fact that very few, or even no joints are needed: submarine cables are wound on large ship mounted drums that can carry more than 100 km of cable.

The DC voltage of a VSC HVDC system is limited by the maximum voltage of the conductors. It is thus possible to develop VSC HVDC systems with higher DC voltage using other conductors such as overhead lines or non-extruded cables. Obviously, the advantages of XLPE conductors would then be lost. As there is almost always opted for XLPE cables, underground transmission with extruded cables is clearly seen as an advantage. All VSC HVDC systems in operation now, are equipped with XLPE cables. Of all projects in construction or planning phase, only one will use overhead DC lines: the Caprivi link, connecting Namibia and Zambia, expected to go in operation in 2010.

The risk of a DC fault is reduced when using cables. This is an important aspect, as no DC breakers are present in VSC HVDC systems. When a DC fault does occurs, the IGBTs are blocked, but the free-wheeling diodes in the converter continue to feed the fault. The fault has to be cleared by the AC breakers; the VSC HVDC is thus disconnected from the system, even when the fault is transitory.

HVDC conductors, be it cables or overhead lines, are modelled by a π circuit, sufficiently accurate for short to middle-long distances. For long conductors,

chained π sections are a good approximation. In case the VSC HVDC has a back-to-back configuration, i.e. has no cable connection, no π section needs to be included.

2.2.7 Control Systems

The control schemes have a large impact on system dynamics. It is an important task to determine the modelling requirements of the control schemes.

The VSC HVDC control system is implemented on high performance Digital Signal Processors (DSPs). It is a cascaded system, where every level accepts the input of the previous one and feeds its output signal to the next level. This is schematically represented in Fig. 2.2. Firing control is the lowest level. It acts very fast, with a cycle time in the μs range. Inner control, outer control and supplementary control are used for increasingly higher level functions, and have increasingly higher cycle times.

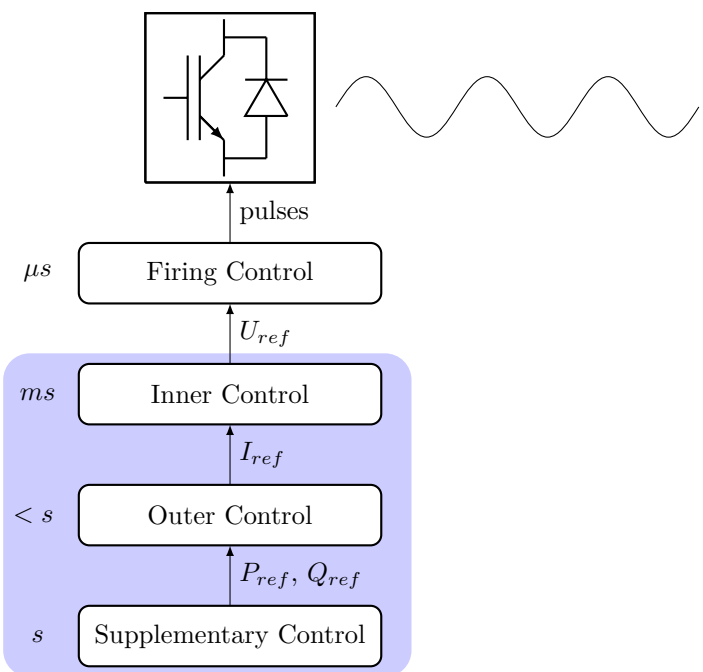

Figure 2.2: Schematic representation of control system hierarchy.

Firing Control

Firing control or valve control is the lowest level control. It takes the desired converter waveform as an input, and determines by means of the valve firing logic the pulses that need to be generated. The firing logic is communicated to the IGBTs, and pulses are generated that switch the IGBTs at the appropriate instants. The firing instances are synchronised using a Phase-Locked Loop (PLL). The pattern of the pulses depends on the topology of the bridge and the switching method.

As converters are considered to be a black box, the details of the converter topology are not known and modelling the firing control is impossible. However, firing control has cycle times in the μs range, very much faster than the phenomena set forth to study, and hence need not be modelled. It is simply assumed that the desired converter waveform is generated by the firing control.

Current Control

The current, or inner, control system controls the current through the phase reactor. Decoupled control is used, which means that voltages and currents are decomposed in d- and q-components, controlled independently. The output of the current control is the desired converter voltage. The current control loop is designed to be much faster than the outer controllers. It is not fast enough, however, to warrant neglecting its dynamics. This means current controllers and all relevant controllers higher in the hierarchy must be modelled.

Outer Controllers

The outer controllers determine the behaviour of the converter at the system bus. Several targets can be set:

- Active power control: determines the active power exchanged with the AC grid.
- DC voltage control: used to keep the DC voltage control constant.
- Reactive power control: determines the reactive power exchanged with the AC grid.
- AC voltage control: instead of controlling reactive power, AC voltage can be directly controlled, determining the voltage of the system bus.

The outer controllers have in common that they provide a current set point in the *dq*-frame for the inner current controller. Their behaviour directly influences the dynamics of the AC system and are therefore of paramount importance in modelling VSC HVDC systems.

Supplementary Controllers

Supplementary controls set high level system targets such as damping or system wide loss reduction. They are not necessary for the operation of the VSC HVDC system, but greatly enhance their functionality.

- Frequency control: Frequency control is indispensable when a converter is located in a passive system, but it can also be used in an active power system. Frequency is regulated by modulating active power.
- Damping control: A converter can damp oscillations occurring in the AC power system by an additional controller. Input signals can be local, or not local, such as generator speeds, which may require communication. The output signal modulates active power, so that the active power swing is counteracted.
- AC voltage control: Instead of directly controlling AC voltage in the outer controller, an additional loop can be created around the reactive power control. The reactive power set point is determined from the desired AC voltage.

In this work, no models for supplementary controllers are developed. Apart from the fact that VSC HVDC systems can operate perfectly well without supplementary controllers, the reason is that it is not desirable to come up with generic models of supplementary controllers.

2.3 Converter Topologies

Valves are connected in a three-phase bridge. Many layouts are possible. The most simple three-phase topology is a six-pulse bridge, switching between two voltage levels (Fig. 2.3). A diode is connected in anti-parallel with the IGBT. When the IGBTs are blocked, the valves form an uncontrolled diode bridge. As the diodes cannot be blocked, they are dimensioned to withstand short circuit currents.

Switching between two voltage levels only generates a signal with high harmonic content. The harmonics can be attenuated by using Pulse Width Modulation

(PWM). PWM is a technique that produces a voltage by modulating the width of pulses. The switching frequency should be high, usually around 2 kHz, to reduce harmonics. An additional advantage of PWM is that extra flexibility is obtained: every 'chop' of the waveform provides a degree of freedom, that can be used for harmonic cancellation [48]. PWM comes in different flavours, going from sinusoidal PWM with third harmonic injection to optimal PWM [49]. Two-level topologies are most used, but three-level topologies are also available.

If the number of voltage levels is increased further, the waveform that is produced by switching between multiple intermediate voltage levels contains less harmonics compared to the waveform obtained by the two-level scheme. Consequently, it is no longer necessary to use PWM in higher level schemes, although it would be possible. This is avoided, however, because the absence of PWM eliminates high frequency components introduced by fast switching. A wide variety of higher level topologies is proposed, such as diode-clamped, flying capacitor, cascaded H-bridge, and modular multilevel schemes [50], [51]. All are alternatives to PWM. The drawback of most higher level schemes is their prohibitive cost. Although higher level schemes reduce harmonics and losses, lower level schemes in combination with PWM can achieve the same by other means such as an adapted switching strategy.

Today (2010), three manufacturers offer VSC HVDC systems. The pioneer offers two and three-level PWM topologies. Its two competitors opted for a modular multilevel topology.

2.4 Operating Principles

The most basic three-phase VSC using IGBTs is the six-pulse bridge (Fig. 2.3). It can be shown that, for square wave operation, the converter's RMS line voltage $\underline{U_c}$ is: ([52, pp.107-108], [43, p.3-4])

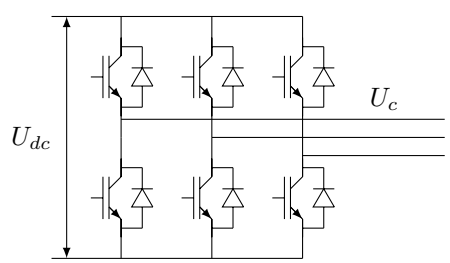

Figure 2.3: Three-phase six-pulse VSC bridge.

$$\underline{U}_c = \frac{\sqrt{6}}{\pi} k U_{dc} e^{j\delta_c}, \tag{2.1}$$

with k the voltage ratio factor, which equals one for square wave operation. Two variables remain in the equation: the phase angle δ_c, and the DC voltage U_{dc}. The magnitude of the converter voltage depends on the DC voltage. If a number of converters are connected through a common DC network, controlling one converter's voltage magnitude requires changing the DC voltage, which in turn affects the other converters' voltage magnitude. In other words: voltage magnitude of the converters are interdependent.

The two-level bridge of Fig. 2.3 is never operated in square wave mode because its output waveform would have a large harmonic content. PWM reduces the harmonics, but also introduces flexibility: the voltage ratio factor can be controlled, allowing to keep the DC voltage constant. Converters with common DC network can then independently control the voltage magnitude.

As stated in section 2.3, PWM is no longer necessary for high level schemes. However, if PWM is not used, the VSC cannot control the voltage ratio factor. Consequently, the DC voltage has to be changed in order to control converter's voltage magnitude. However, even if PWM is not used, it is possible to control reactive power independently. A first possibility is to introduce a chop in the output waveform. A second possibility is a double-group cascaded H-bridge scheme, wherein every group has a voltage phasor with controllable phase angle. By adjusting the phase angle difference between both phasors, the amplitude can be controlled, independently of the DC voltage [52].

In the remainder of this work, it is assumed at all times that voltage magnitude control is independent of DC voltage, i.e. that all proposed methods and simulations are *not valid* for only those VSC topologies that:

1. do not use PWM and
2. are not of the modular multilevel type, which can control voltage independently, and
3. do not use special techniques to accommodate DC voltage independent voltage control such as chopping or double-grouping.

It has to be noted that it is very unlikely that a scheme that satisfies the above three conditions will ever be built. All installations that have been built up till now, are two or three level schemes with PWM. In the near future, multilevel schemes will be built. However, for HVDC, multi modular topologies have advantages over diode-clamped, flying capacitor, and cascaded H-bridge topologies. All manufacturers who develop multilevel schemes have opted for the multi modular type.

2.4.1 Power Control

The principles of power control are the same for every converter topology. The important element on the AC side is the phase reactor, or more generally: the series reactance, which can include the effect of the transformer. The presence of filters does not change the operating principles. Therefore, it suffices to analyse the simplified diagram of Fig. 2.4.

Active and reactive power injected in the grid can be expressed using the well-known equations:

$$P = \frac{U_s U_c \sin(\delta_c)}{X}, \tag{2.2}$$

$$Q = -\frac{U_s^2}{X} + \frac{U_s U_c}{X} \cos(\delta_c). \tag{2.3}$$

$\underline{U}_s = U_s \angle 0$ is the system voltage, $\underline{U}_c = U_c \angle \delta_c$ the converter voltage. Changing the phase angle δ_c has a large influence on the active, but negligible influence on the reactive power, since δ_c is rather small. Conversely, the magnitude of the converter voltage compared to that of the system voltage has a large influence on reactive but negligible one on active power. Active and reactive power control are therefore practically independent. By varying the magnitude of the converter voltage, the reactive power can be controlled. If the converter voltages magnitude is higher than the system voltages, reactive power is injected in the AC system; if it is smaller, reactive power is absorbed by the converter (Fig. 2.5). By varying the phase angle of the converter voltage with respect to the angle of the system voltage, the active power can be controlled. If the converter voltage leads the system voltage, active power is injected in the AC system; if it lags the system voltage, active power is absorbed by the converter. In Fig. 2.6, the converter voltage is lagging, active power is absorbed by the converter; it is operating as rectifier.

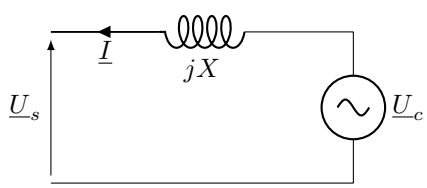

Figure 2.4: Simplified equivalent AC circuit.

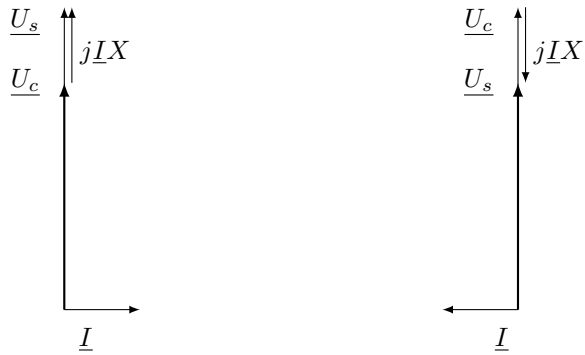

Figure 2.5: Left: reactive power consumption. Right: reactive power generation.

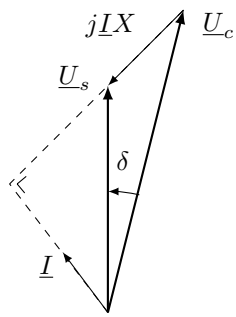

Figure 2.6: Converter in rectifier mode, absorbing active power.

Each converter has thus two degrees of freedom: the angle and magnitude of the converter voltage, which can be used to independently control active and reactive power.

2.4.2 Converter Coordination

Converters of a VSC HVDC systems are coupled by a DC system. There is no active power storage in the DC network, so incoming active power must equal outgoing power minus losses. Mathematically, a system of n converters must satisfy the equation:

$$\sum_{i=1}^{n} P_{inj_i} = P_{loss}. \tag{2.4}$$

This additional equation reduces the degrees of freedom with one, to $2n - 1$. One converter must set its active power to satisfy (2.4). This is achieved in practice by controlling the DC bus voltage, but as shown further on, some models set the slave converter's power order as a function of the master converter's power order. We call the voltage controlling converter the 'slack' converter, because it compensates for losses in the DC network and thus has a similar function as a slack node in an AC grid.

2.4.3 DC Voltage Control

The most important element of the DC circuit is the capacitor. Therefore, the DC circuit is reduced to just the capacitor, shown in Fig. 2.7 for a two-terminal system. The reasoning applies equally well to multi-terminal systems. When the active power reference of a converter is increased, the capacitors discharge. As a result, the DC voltages drop (Fig. 2.7). The DC voltage controller detects the voltage drop, and requests more active power. The capacitors are charged, and the voltage rises (Fig. 2.8). When the DC voltage reaches the set point in steady-state, the active powers are balanced again.

In principle, every converter can act as the DC voltage controller. When energising

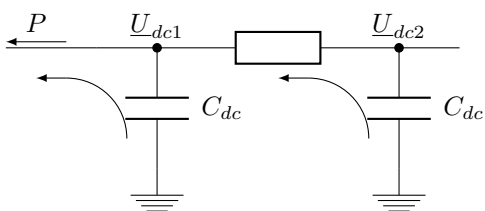

Figure 2.7: DC voltage control, step 1: an increased power set point of the inverter causes the capacitors to discharge and the DC voltage to drop.

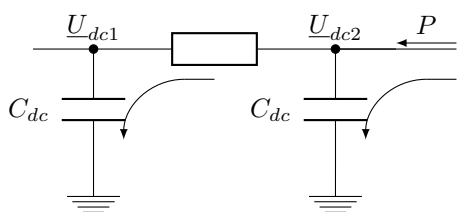

Figure 2.8: DC voltage control, step 2: the DC voltage controller responds to a decreased DC voltage by requesting more power from the rectifier, which charges the capacitors.

the HVDC system, the converters are blocked and feeding the capacitor via the diode bridge. The diode bridge's DC voltage is however not equal to that obtained with the IGBT bridge. When the first converter is deblocked, it regulates the DC voltage to the desired reference value before the other converters are deblocked. In practice, it is thus the first converter that is deblocked during energising that controls the DC voltage.

2.4.4 Advanced DC Voltage Control

It is vital that the DC voltage be restricted to a narrow band. Large deviations from rated DC voltage are unacceptable as they result in damage of the equipment. The DC voltage control as described in the previous section cannot guarantee that the DC voltage remains within bounds in all situations. Therefore, in practice, every converter is equipped with a DC voltage controller.

Example 2.1. *Consider the system shown in Fig. 2.9. Two converters inject 100 MW, two absorb 100 MW. The lower right converter is the slack converter. If the lower left converter fails, there is an unbalance of 100 MW and the DC voltage rises. The slack converter increases active power up to its rated power, which may be lower than 200 MW. This will lead to an unacceptably high DC voltage.*

2.5 Capability Chart

Active and reactive power can be independently chosen, but must remain within certain limits. Failure to model operating limits can lead to unrealistic behaviour of the model. The operation range of a VSC HVDC system is limited by three factors: current through the converter, DC voltage, and rating of the cable.

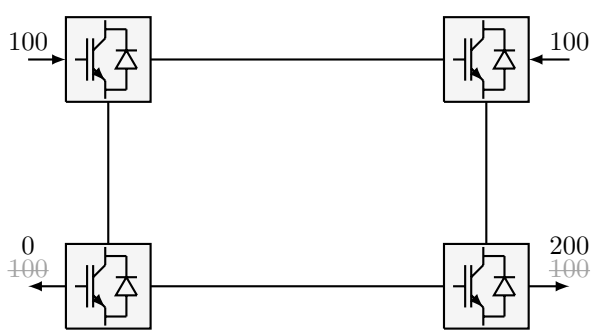

Figure 2.9: Loss of lower left converter.

The current through the converter needs to be limited in order to protect the switching elements. During faults, the converter is blocked: the diodes take over the current and the switching elements are protected. The locus of maximal current in the PQ diagram is a circle with centre at the origin, and radius $U_s \cdot I_{eq}^{max}$:

$$U_s \cdot I_{eq}^{max} = \sqrt{P^2 + Q^2}. \tag{2.5}$$

The voltage across the converter U_c is also limited. Indirectly, it depends on the DC voltage. For systems adopting PWM, the modulation factor is limited. However, as the aim is a model that is generally valid, converter voltage instead of modulation index is limited. The locus of this limit can be found by applying the power flow equations to the circuit in Fig. 2.4:

$$P = \frac{U_s U_c}{X_{eq}} \sin\delta \tag{2.6}$$

$$Q = -\frac{U_s^2}{X_{eq}} + \frac{U_s U_c \cos\delta}{X_{eq}}, \tag{2.7}$$

and eliminating $\cos\delta$ and $\sin\delta$:

$$\cos^2\delta + \sin^2\delta = 1 = \left(\frac{P X_{eq}}{U_s U_c}\right)^2 + \left[\left(Q + \left(\frac{U_s^2}{X_{eq}}\right)\right)\frac{X_{eq}}{U_s U_c}\right]^2, \tag{2.8}$$

which leads to the equation of a circle in the PQ diagram with centre in $(0, -U_s^2/X_{eq})$ and radius $U_s U_c / X_{eq}$:

$$\left(\frac{U_s U_c}{X_{eq}}\right)^2 = P^2 + \left(Q + \frac{U_s^2}{X_{eq}}\right)^2. \tag{2.9}$$

The third limit is the maximum current through the conductors. This limit is a vertical in the PQ diagram at rated DC voltage. The three limits are shown in Fig. 2.10. Often the transformer is equipped with a tap changer that can regulate the filter bus voltage. When the filter bus voltage is increased, the radii of the circles increase. The centre of the current limit circle remains at the origin, but the centre of the voltage limit circle lowers. The net effect is a more restrictive voltage, but a less restrictive current limit and vice versa for a decreased filter bus voltage (Fig. 2.11). The capability chart differs in steady state and dynamic operation. In steady-state, the converter voltage limit is less restrictive because a set point that lies outside the range, can be attained by tap change operation that shifts the limit. In dynamic operation, the tap changer is too slow to change the voltage limit.

Synchronous generators have similar limits as VSC HVDC systems. Maximum current through the converter corresponds to maximum stator current, converter voltage limits correspond to maximum field current or Electromotive Force (EMF),

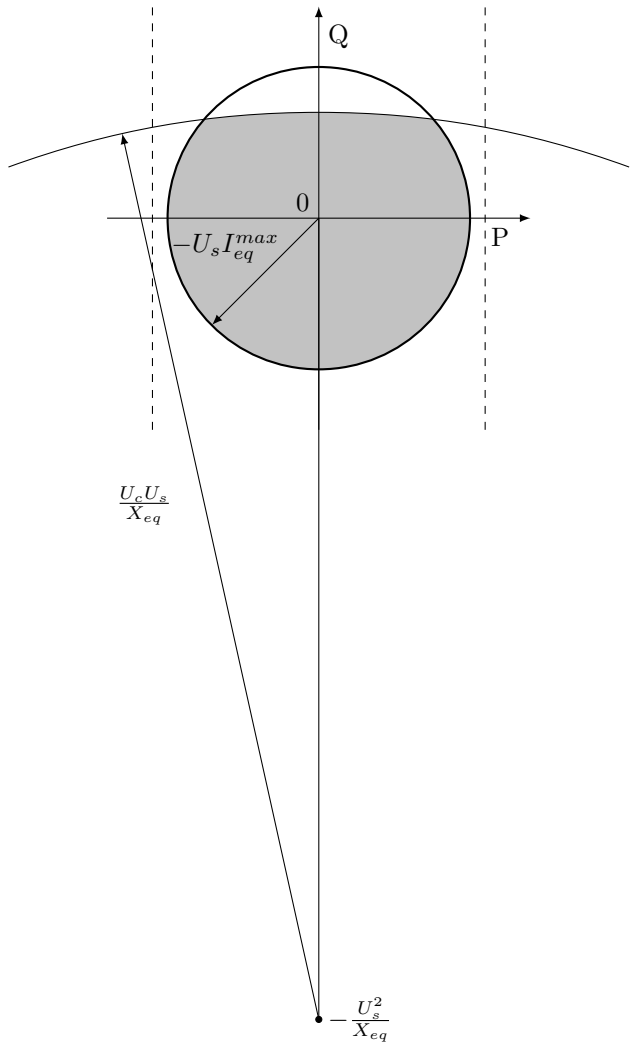

Figure 2.10: PQ diagram.

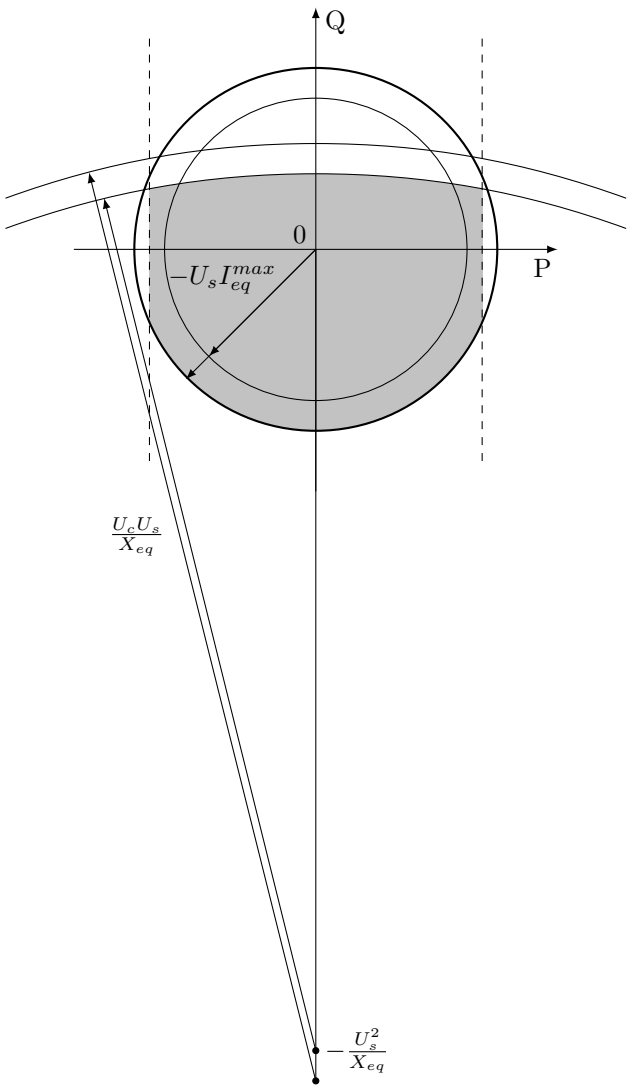

Figure 2.11: PQ diagram: effect of increased filter bus voltage.

and maximum power through the cable to maximum turbine output. The capability charts of generators and converters are therefore very similar. There are however some important differences. The generator's operating range is further restricted by some additional limits, that do not come into play for VSC HVDC systems. The first one is the end region heating limit: during underexcited operation, the axial flux in the end region of the stator increases and causes heat due to the eddy currents in the laminations [53, p.194]. The second one is the static stability limit, which limits the angle δ to 90°. This limit corresponds with a horizontal through $(0, -U_s^2/X_{eq})$ in the PQ diagram. The practical stability limit is more restrictive, as a security margin is applied that increases with increasing active power. These two restrictions limit underexcited operation of the generator, i.e. limit operation in the fourth quadrant. With the exception of some generators installed in pumped hydro facilities, operation in the second and third quadrant is not possible. Furthermore, for most generators, minimal active power output is larger than zero due to restrictions on the thermo-mechanical energy system driving the turbine.

Another difference between HVDC and generators does not influence the capability diagram *per se*, but has a large influence on operation. As the converter's thermal inertia is much lower than the generator's windings, overcurrents have to be limited immediately. Generators can withstand moderate overcurrents for a short period of time, so that limiters are not activated immediately after detection of a current limit violation.

2.6 Conclusions

In this chapter, components, converter topologies, operating principles, and the capability chart of VSC HVDC systems are explained. It can be concluded that the minimal requirements for VSC HVDC modelling include models for the AC side reactance, DC capacitor, conductors and control systems. A generic model should not include models of valves and converter topologies, as they can vary greatly from one implementation to another. Models of these components are not needed for relatively slow phenomena. It has been explained that all topologies can be represented by a generic model, except those that do not use PWM, are not of the modular multilevel type and do not use special techniques such as chopping or double-grouping. Inner and outer control systems must be modelled. For a correct representation of the capability chart, three limits need to be modelled, which have to be enforced immediately after being violated.

Chapter 3

Mathematical Model of the Power System

3.1 Introduction

An important part of modelling is to clearly establish the model's range of validity. The general power system model for steady-state and electromechanical analysis is first derived. This model is a Differential-Algebraic Equations (DAE) model, whose mathematical properties will be shown to inherently restrict the range of validity of every model developed in its framework. A series of transformations and additional simplifications, frequently used in conjunction with the DAE model in order to reduce calculations, and their ramifications for model validity are subsequently discussed in detail. The underlying assumptions of the power system model, and its precise conditions for validity, are in this manner established in a rigorous way. The VSC HVDC models fit in the general power system framework and are hence subject to the same underlying assumptions.

3.2 Derivation of the Power System Model

The electric power system has been hailed as the most complex system devised by man. It consists of a variety of equipment and control systems, that interact in a complex way. The network itself consists mainly of buses, transmission lines and transformers. Synchronous generators, driven by power plants, feed electric power into the network, that is consumed by various types of loads such as induction motors, lighting, and heating systems. Several control systems such as speed

governors, excitation systems and other equipment such as Flexible Alternating Current Transmission Systems (FACTS) complete the system.

3.2.1 Power System Components

Synchronous Generators and their Controls

Synchronous generators are arguably the most crucial elements in the power system. Much effort has been spent on their accurate modelling, including their controlling equipment. The generator itself is a dynamic system wherein both electromechanical and electromagnetic phenomena play important and interacting roles. Mechanical dynamics are governed by the balance between electric power P_e and mechanical power P_m, and depend on mechanical parameters such as rotor inertia H and damping D. They are modelled by the swing equation [53]:

$$\frac{2H}{\omega}\frac{d^2\delta}{dt^2} = P_m - P_e - D\frac{d\delta}{dt}, \tag{3.1}$$

with δ the rotor angle, and ω rotor speed. The more complex electromagnetic dynamics are caused by the interactions of the various windings in the machine, and depend on electric parameters. The number of windings and their electric parameters in their turn depend on the type and construction of the machine. Different generator models exist to represent the variation in electromagnetic dynamics. The analysis of the synchronous machine's electromagnetic dynamics is simplified by using Park's transformation: inductances vary with angle, but can be made time-invariant by an appropriate transformation to a rotating reference frame. The stator equations have to be consistent with the network representation: stator dynamics are taken into account in electromagnetic simulations, but neglected in electromechanical ones.

The behaviour of the generator cannot be separated from the turbine's and energy system's dynamics, and from their controlling equipment. The turbine and energy system are mechanical systems that can be described by Ordinary Differential Equations (ODEs). Their controllers are mechanical-hydraulic, electrohydraulic or digital. They influence the mechanical power P_m, and hence the dynamics governed by the swing equation. The excitation system regulates the generator's EMF. Its influence enters the electromagnetic equations through the generator's field voltage.

Branches

Branch voltages and currents vary with time and position. Their relation is given by the wave equation:

$$-\frac{\partial u(x,t)}{\partial x} = Ri(x,t) + L\frac{\partial i(x,t)}{\partial t} \tag{3.2a}$$

$$-\frac{\partial i(x,t)}{\partial x} = Gu(x,t) + C\frac{\partial u(x,t)}{\partial t}. \tag{3.2b}$$

These Partial Differential Equations (PDEs) can be solved if the boundary conditions are known. The solution of the boundary-value problem can be written as a lumped-parameter π circuit, which can be transformed to a nominal π circuit if the line length is small compared to the wavelength. The PDEs can be written as time-delay equations [54, p.576]. The time it takes the wave to reach the receiver and reflect back is negligible compared to the time range of the phenomena of interest. Setting the time-delay to zero reduces the equations to the well-known algebraic equations, using the bus admittance matrix formulation. This formulation can be used for both AC and DC lines. For very long lines, the time delays are not negligible. However, a good approximation can be obtained by representing the lines by cascading sections, each section modelled by a nominal π section. Transformers can be modelled by a combination of a π section and an ideal transformer with complex transformation ratio, which can also be represented in admittance matrix formulation.

Loads

Various types of loads are connected to the network. Distinction is made between static and dynamic loads. Static loads are represented by algebraic equations. This is acceptable when loads have a fast response and reach steady-state. However, in many cases this is not true, e.g. for motor loads. In recent years, it is recognised that dynamic behaviour of the load is important in voltage stability, long-term stability, and interarea oscillations [53, p.274]. Loads then need to be modelled by differential equations.

FACTS and HVDC

HVDC and most FACTS devices are fast acting devices with electronic switching elements, and few to no mechanical components that influence dynamics[1]. They can be represented with various levels of detail. They are modelled by differential

[1]The Phase Shifting Transformer is a well-known exception.

or by a combination of algebraic and differential equations. Currents and voltages are transformed to a rotating reference frame to aid control system design.

System Wide Controllers

A variety of supplementary controls, such as secondary frequency and voltage control, and protection schemes are present in power systems. The outputs of the system wide controllers are auxiliary signals to capacitor banks, FACTS, HVDC systems and generators control systems. They are mostly fairly slow and need not be modelled in most steady-state and electromechanical studies. In long term dynamic studies they are represented as differential equations.

3.2.2 The Power System's Mathematical Model

Fig. 3.1 shows the schematic representation of the mathematical model of a power system. The network is described by algebraic equations. The equipment connected to the network is modelled using differential equations. Some parts are algebraic equations such as the generators' stator equations, and static load models. The interface between the network and equipment consists of transformations described by algebraic equations, as treated in section 3.3.3. In short, all parts of the power system are modelled by algebraic equations and/or differential equations, leading to a DAE system description of the power system, used in electromechanical power system studies:

$$\dot{\boldsymbol{X}} = F(\boldsymbol{X}, \boldsymbol{Y}, \boldsymbol{P}), \qquad F : \mathbb{R}^{n+m+p} \to \mathbb{R}^n \tag{3.3a}$$

$$0 = G(\boldsymbol{X}, \boldsymbol{Y}, \boldsymbol{P}), \qquad G : \mathbb{R}^{n+m+p} \to \mathbb{R}^m \tag{3.3b}$$

$$\boldsymbol{X} \in \mathcal{X} \subset \mathbb{R}^n, \boldsymbol{Y} \in \mathcal{Y} \subset \mathbb{R}^m, \boldsymbol{P} \in \mathcal{P} \subset \mathbb{R}^p,$$

wherein $\boldsymbol{X}$ are the dynamic state variables, $\boldsymbol{Y}$ the instantaneous variables, and $\boldsymbol{P}$ the parameters.

Example 3.1. *Consider the system in Fig. 3.2, based on a system in [55]. The system includes a generator, which can represent a network, connected to a constant power load with a transmission line, and a VSC connected to the load bus. The generator is modelled by an equation, only including voltage dynamics (type IV.2 in [54, p.123]):*

$$\dot{E}'_q = \frac{1}{T_d}\left[-\frac{x_d}{x'_d}E'_q + \frac{x_d - x'_d}{x'_d}U_1\cos(\delta_1 - \delta) + E_{fd}\right], \tag{3.4}$$

with E_{fd} the excitation voltage, E'_q voltage behind transient reactance, and x_d, and x'_d, respectively steady-state and transient reactance. Constant excitation is

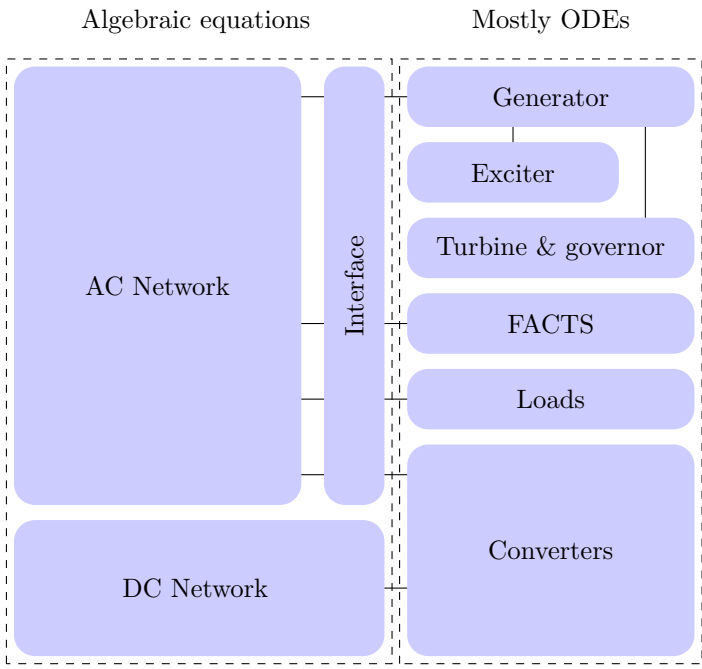

Figure 3.1: Structure of the power system model.

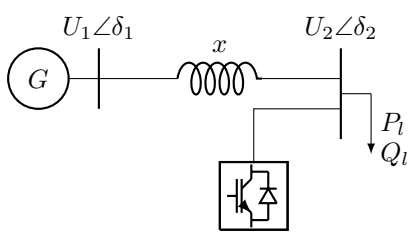

Figure 3.2: Single-line diagram of the example system.

assumed. For sake of simplicity, it is assumed that the converter's active power P_{VSC} is constant, and that its reactive power controller can be described by the following dynamic equation:

$$\dot{Q}_{VSC} = \frac{1}{T_{VSC}} \left[-K(U_2 - U_2^{(ref)}) \right]. \tag{3.5}$$

The algebraic equations consist of the active power flow at bus 1:

$$0 = \frac{U_1 E'_q}{x'_d} \sin(\delta_1 - \delta) + \frac{U_1 U_2}{x} \sin(\delta_1 - \delta_2), \tag{3.6}$$

the active power flow at bus 2:

$$0 = \frac{U_2 U_1}{x} \sin(\delta_2 - \delta_1) + P_l - P_{VSC}, \tag{3.7}$$

the reactive power equilibrium at bus 1:

$$0 = \frac{1}{x'_d}(U_1^2 - U_1 E'_q \cos(\delta_1 - \delta)) + \frac{1}{x}(U_1^2 - U_1 U_2 \cos(\delta_1 - \delta_2)), \tag{3.8}$$

and the reactive power equilibrium at bus 2:

$$0 = \frac{1}{x}(U_2^2 - U_1 U_2 \cos(\delta_2 - \delta_1)) + Q_l - Q_{VSC}. \tag{3.9}$$

A system as simple as this one already has a fairly large number of state variables and parameters. However, for this specific case, it is possible to simplify the equations by noting that the angles only occur in pairs: all angles and U_1 can be eliminated from the equations [56]. Define:

$$P = P_l - P_{VSC}, \tag{3.10}$$

$$Q = Q_l - Q_{VSC}, \tag{3.11}$$

and

$$x' = x'_d + x. \tag{3.12}$$

The system can now be written as:

$$F : \dot{E}'_q = \frac{1}{T_d} \left[-\frac{x + x_d}{x'} E'_q + \frac{x_d - x'_d}{x'} \frac{U_2^2 + x'Q}{E'_q} + E_{fd} \right] \tag{3.13a}$$

$$\dot{Q}_{VSC} = \frac{1}{T_{VSC}} \left[-K(U_2 - U_2^{(ref)}) \right] \tag{3.13b}$$

$$G : 0 = (E'_q U_2)^2 - (x'P)^2 - (x'Q + U_2^2)^2 \tag{3.13c}$$

which is a DAE system. This simple system is used in subsequent examples. Only three state variables remain, allowing a full graphical representation in state space: dynamic state variables $\boldsymbol{X} = [E'_q, Q_{VSC}]$, algebraic variables $Y = U_2$. The parameter vector is $\boldsymbol{P} = [T_d, T_{VSC}, E_{fd}, U_{ref}, x_d, x'_d, x', x, P_{VSC}, P_L, Q_L, K]$.

3.3 Transformations and Simplifications

A general three-phase signal can be represented by the following set of equations:

$$f_a(t) = \sqrt{2}F_a(t)\cos(\omega t + \phi_a(t)), \tag{3.14a}$$

$$f_b(t) = \sqrt{2}F_b(t)\cos(\omega t + \phi_b(t)), \tag{3.14b}$$

$$f_c(t) = \sqrt{2}F_c(t)\cos(\omega t + \phi_c(t)). \tag{3.14c}$$

The representation in the abc reference frame is the most general formulation: every type of equipment can be modelled in its domain. Simulations using this representation are accurate, and are used in e.g. EMTP type simulation software [57].

In steady-state, the magnitude F_a, F_b, F_c and the reference phases ϕ_a, ϕ_b, ϕ_c are constant. The equations reduce to:

$$f_a(t) = \sqrt{2}F_a\cos(\omega t + \phi_a), \tag{3.15a}$$

$$f_b(t) = \sqrt{2}F_b\cos(\omega t + \phi_b), \tag{3.15b}$$

$$f_c(t) = \sqrt{2}F_c\cos(\omega t + \phi_c). \tag{3.15c}$$

According to the Nyquist criterion, the time step in the simulation is limited by the maximum frequency of the signal [58]. As can be seen, these equations are still time-dependent, which means that even when the system is at steady-state, a small time step has to be chosen. The abc representation of power systems is therefore not suitable for long-term simulations. The maximum frequency can be reduced by simplifications or in some cases by a suitable transformation.

3.3.1 Transformations

In the modelling paradigm, already some simplifying assumptions were made, notably neglecting electromagnetic dynamics. Still, a wide range of time constants is present in the system, from generator flux decay to boiler dynamics. The solution of such a system is numerically difficult, especially because the number of equations is very large. The mathematical transformation of variables can make the solution of the system easier. While (3.3) represents an underlying physical system, it can be treated as any mathematical system: it can be solved in a transformed domain where variables have not necessarily physical meaning, and transformed back to the original domain. The best-known transformation is Park's equation, which simplifies synchronous machine modelling. For the solution of (3.3), many more transformations can be used, many of them listed in [58].

Symmetrical Components

The currents and voltages of a three-phase system can be decomposed in a system of symmetrical components. Symmetrical components and abc variables are related by the following transformation, and its inverse:

$$\boldsymbol{f_{abc}} = \mathsf{C_S} \cdot \boldsymbol{f_a^{(p,n,z)}}, \tag{3.16}$$

with

$$\mathsf{C_S} = \begin{bmatrix} 1 & 1 & 1 \\ a^2 & a & 1 \\ a & a^2 & 1 \end{bmatrix}, \tag{3.17}$$

and $a = e^{(j120^\circ)}$. Applying the symmetrical transformation (3.16) to (3.15), abc components can be written as a sum of symmetrical components:

$$f_{abc}(t) = f_{abc}^{(p)}(t) + f_{abc}^{(n)}(t) + f_{abc}^{(z)}(t), \tag{3.18}$$

with

$$f_{abc}^{(p)}(t) = F_p \begin{bmatrix} \cos(\omega t + \theta_p) \\ \cos(\omega t + \theta_p - \frac{2\pi}{3}) \\ \cos(\omega t + \theta_p + \frac{2\pi}{3}) \end{bmatrix}, \tag{3.19}$$

$$f_{abc}^{(n)}(t) = F_n \begin{bmatrix} \cos(\omega t + \theta_n) \\ \cos(\omega t + \theta_n + \frac{2\pi}{3}) \\ \cos(\omega t + \theta_n - \frac{2\pi}{3}) \end{bmatrix}, \tag{3.20}$$

and

$$f_{abc}^{(z)}(t) = F_z \begin{bmatrix} \cos(\omega t + \theta_z) \\ \cos(\omega t + \theta_z) \\ \cos(\omega t + \theta_z) \end{bmatrix}. \tag{3.21}$$

For balanced networks, the impedance matrix is diagonal, and the three-phase system reduces to three single-phase ones. For symmetric networks, one single-phase system remains, greatly reducing computational effort.

Baseband

A bandpass signal $f(t)$ can be written as an analytic signal $f_a(t)$, in terms of the Hilbert transform of the signal:

$$f_a(t) = f(t) + j\hat{f}(t), \tag{3.22}$$

with $\hat{f}(t)$ the Hilbert transform $\mathcal{H}(f(t))$ of $f(t)$. In the analytic signal, negative frequencies are removed. The idea behind applying this transformation is that negative frequencies do not contain additional information, due to the symmetry of the spectrum. The resulting signal can then be shifted towards 0 Hz, to reduce the highest frequency of the signal, which allows using larger step sizes. Power system transients have a frequency spectrum centred around system frequency, and can be seen as bandpass signals [58]. Bandpass signals can be represented by analytic signals, i.e. signals that contain no negative frequency components.

The benefit of this transformation is now shown by considering a signal $f(t) = f_m(t)\cos(\omega t + \phi)$. Its Hilbert transform is $\hat{f}(t) = f_m(t)\sin(\omega t + \phi)$. Applying (3.22) to the signal, its analytic signal can be written as

$$f_a(t) = f(t) + j\hat{f}(t) = f_m(t)(\cos(\omega t + \phi) + j\sin(\omega t + \phi)). \tag{3.23}$$

Applying Euler's formula gives:

$$f_a(t) = f(t) + j\hat{f}(t) = f_m(t)e^{j(\omega t+\phi)}. \tag{3.24}$$

The analytic signal can now be shifted by ω. Multiplying the right hand side of (3.24) by $e^{-j\omega t}$ gives $f_m(t)e^{j\phi}$. The frequency content of this transformed signal is centred around 0 Hz. If the signal $f(t)$ contains higher harmonics, the baseband representation is not interesting as the signal is only shifted by ω. A high frequency spectrum then remains, and the analytic signal representation has no advantages over the abc representation.

Park Transformation

ABC coordinates can be transformed to $dq0$-components by the generalised Park transformation, a transformation to an arbitrary reference frame with speed ω:

$$\boldsymbol{f_{dq0}} = \mathsf{C_P} \cdot \boldsymbol{f_{abc}}. \tag{3.25}$$

The transformation is defined by the transformation matrix $\mathsf{C_P}$:

$$\mathsf{C_P} = \frac{2}{3}\begin{bmatrix} k_1\cos\theta & k_1\cos(\theta - \frac{2\pi}{3}) & k_1\cos(\theta + \frac{2\pi}{3}) \\ -k_2\sin\theta & -k_2\sin(\theta - \frac{2\pi}{3}) & -k_2\sin(\theta + \frac{2\pi}{3}) \\ \frac{1}{2}k_3 & \frac{1}{2}k_3 & \frac{1}{2}k_3 \end{bmatrix}, \tag{3.26}$$

with

$$\theta = \omega t + \theta_0. \tag{3.27}$$

The angle δ is the angular displacement of the arbitrary reference frame at $t = 0$ from a synchronously rotating reference frame. The constants k_1, k_2, and k_3 can

be chosen freely. For example, in the original Park transformation, $k_1 = 1$, $k_2 = 1$, and $k_3 = 1$. The zero sequence component can be calculated as $f_0 = \frac{1}{3}(f_a + f_b + f_c)$. For a balanced system $f_a + f_b + f_c = 0$ and, therefore $f_0 = 0$.

Applying Park's transformation to symmetrical components gives:

$$f_{dq0}^{(p)}(t) = F_p \begin{bmatrix} \cos(\theta_p) \\ \sin(\theta_p) \\ 0 \end{bmatrix}, \tag{3.28}$$

$$f_{dq0}^{(n)}(t) = F_n \begin{bmatrix} \cos(2\omega t + \theta_n) \\ \sin(2\omega t + \theta_n) \\ 0 \end{bmatrix}, \tag{3.29}$$

$$f_{dq0}^{(z)}(t) = F_z \begin{bmatrix} 0 \\ 0 \\ \cos(\omega t + \theta_z) \end{bmatrix}. \tag{3.30}$$

Under balanced operation, only the positive sequence component remains. As can be seen from (3.28), the frequency content is concentrated around 0 Hz. However, under unbalanced operation, negative and zero sequence components are present that respectively introduce harmonics at frequencies 2ω and ω. The benefits of the $dq0$-transform are then lost [58].

3.3.2 Simplifications: The Phasor Modelling Paradigm

In the previous section, transformations were proposed that have computational advantages under certain circumstances. They are just mathematical transformations: the results are calculated in the transformed domain and transformed back. Hence, there is no negative influence on the accuracy of the results. This section deals with simplifications, not transformations of (3.14). The simplifications lead to a loss of accuracy, but are guaranteed to speed up calculation, unlike transformations, which only speed up calculation if certain conditions are met.

Dynamic Phasors

HVDC converters cause harmonics. The frequency spectrum is composed of spectra around system frequency, and around the harmonic frequencies. The harmonic frequencies can be thought of as frequency shifted spectra:

$$X(j\omega) = \sum_{k=-\infty}^{+\infty} X_k(j\omega - jk\omega_s), \tag{3.31}$$

or in the time domain:

$$x(t) = \sum_{k=-\infty}^{+\infty} X_k(t) e^{jk\omega_s t}. \tag{3.32}$$

A signal $x(\tau)$ can be represented in the interval $\tau \in (t-T, t]$ by a Fourier series

$$x(\tau) = \sum_{k=-\infty}^{+\infty} X_k(t) e^{jk\omega_s t}, \tag{3.33}$$

with $\omega_s = \frac{2\pi}{T}$, and

$$X_k(t) = \frac{1}{T} \int_{t-T}^{t} x(\tau) e^{-jk\omega_s \tau} d\tau. \tag{3.34}$$

$X_k(t)$ are the Fourier coefficients [59], [60], also called dynamic phasors or time-varying phasors. During transients, the signal is not periodic and the Fourier coefficients are time dependent, while in steady-state, the signals are periodic, and $X_k(t) = X_k$ are constants. The original signal can be approximated by a finite sum:

$$x(t) \approx \sum_{k \in K} X_k(t) e^{jk\omega_s t}. \tag{3.35}$$

The level of accuracy depends on the selection of Fourier coefficients. Some information is inevitably lost, but a more efficient computation is achieved.

Quasi-stationary Phasors

A more crude approximation are phasors, also called 'quasi-stationary' phasors to distinguish them from dynamic phasors. They were introduced by Steinmetz to simplify calculations with alternating current [61]. A signal

$$f(t) = \sqrt{2} F \cos(\omega t + \phi), \tag{3.36}$$

can be written by Euler's formula as:

$$f(t) = \frac{\sqrt{2}F}{2} e^{j(\omega t + \phi)} + \frac{\sqrt{2}F}{2} e^{-j(\omega t + \phi)}, \tag{3.37}$$

or

$$f(t) = \Re\mathfrak{e}\{\sqrt{2} F e^{j(\omega t + \phi)}\} = \Re\mathfrak{e}\{\sqrt{2} F e^{j\omega t} e^{j\phi}\}. \tag{3.38}$$

The phasor is $Fe^{j\omega t}e^{j\phi}$, $Fe^{j\phi}$, or $F\angle\phi$. In the latter two representations, the pulsation of the sinusoid is implicit. The signal is the projection of the phasor on the real axis of the complex plane.

3.3.3 Interfacing the F and G Set

The use of transformations for the F and G set entails benefits for the simulation of power systems. Often, the equations of each generator and its associated equipment are transformed to a rotating reference frame, attached to the generator's rotor. The G set is transformed to the phasor domain. While it would be possible to express the whole set in terms of phasors, this would lead to a quite complicated set of equations and this is consequently never done in practice. On the other hand, a unified representation of F and G in terms of dq-components is chosen in some power system analysis software.

In a lot of power system software, a (large) subset of F is expressed in a rotary reference frame. The entire G set consists of quasi-stationary phasors; the network equations are solved in the phasor domain. At the buses where generators or converters are connected, phasor variables need to be transformed to the dq-domain and vice versa, whereby it has to be borne in mind that, while the phasor domain is common to all buses, the dq-frame is different for every generator and converter. We are thus looking for a transformation that relates the phasor and dq-domain.

A balanced system of steady-state voltages or currents can be written as:

$$f_a(t) = F\sqrt{2}\cos(\omega_s t + \phi_0) = \Re\mathfrak{e}\left\{F\sqrt{2}e^{j\phi_0}e^{j\omega_s t}\right\} \tag{3.39a}$$

$$f_b(t) = F\sqrt{2}\cos(\omega_s t + \phi_0 - \frac{2\pi}{3}) = \Re\mathfrak{e}\left\{F\sqrt{2}e^{j(\phi_0-2\pi/3)}e^{j\omega_s t}\right\} \tag{3.39b}$$

$$f_c(t) = F\sqrt{2}\cos(\omega_s t + \phi_0 + \frac{2\pi}{3}) = \Re\mathfrak{e}\left\{F\sqrt{2}e^{j(\phi_0+2\pi/3)}e^{j\omega_s t}\right\} \tag{3.39c}$$

The signals vary sinusoidally with pulsation ω_s, the synchronous speed. The angle ϕ_0 is the angular displacement of phase a with respect to the reference axis. Applying Park's transformation (3.25) gives [62, p.127]:

$$f_d(t) = F\sqrt{2}\sin((\omega_s - \omega)t + \phi_0 - \theta_0) = \Im\mathfrak{m}\left\{F\sqrt{2}e^{j(\phi_0-\theta_0)}e^{j(\omega_s-\omega)t}\right\} \tag{3.40a}$$

$$f_q(t) = F\sqrt{2}\cos((\omega_s - \omega)t + \phi_0 - \theta_0) = \Re\mathfrak{e}\left\{F\sqrt{2}e^{j(\phi_0-\theta_0)}e^{j(\omega_s-\omega)t}\right\} \tag{3.40b}$$

The zero component is absent as the system is balanced. When assumed, as customary in transient stability type simulations, that the rotor speed does not deviate significantly from synchronous speed, i.e., $\omega = \omega_s$, then (3.40) simplifies

to:

$$f_d = F\sqrt{2}\cos(\phi_0 - \theta_0) \tag{3.41a}$$

$$f_q = F\sqrt{2}\sin(\phi_0 - \theta_0), \tag{3.41b}$$

whereby $\sqrt{2}$ can be dropped, if f_d and f_q are expressed in p.u. Writing in function of δ instead of θ_0 yields:

$$f_d = F\sin(\phi_0 - \delta) \tag{3.42a}$$

$$f_q = F\cos(\phi_0 - \delta). \tag{3.42b}$$

The d- and q-components are not phasors, but real quantities. However, when a complex plane is associated with the dq-plane, the voltage expressed in dq-components is mathematically equivalent to a phasor, and can be regarded as a phasor in the dq-plane. The rotation implicitly associated with phasors stems from the voltage or current variations in time. For f_d and f_q, the rotation comes from the rotation of the rotating frame. The phasor that can be related to dq-components is (Fig. 3.3):

$$\underline{F} = f_q + j f_d = F\left(\cos(\phi_0 - \delta) + j\sin(\phi_0 - \delta)\right) = F e^{j(\phi_0 - \delta)}. \tag{3.43}$$

A voltage or current signal $\mathsf{f}_{\mathsf{abc}}$, can be transformed to a common, synchronously rotating reference frame by the transformation

$$\boldsymbol{f_{DQ0}} = \mathsf{C_K} \cdot \boldsymbol{f_{abc}}, \tag{3.44}$$

termed Kron's transformation [63, p.65]. It is defined by the transformation matrix $\mathsf{C_K}$:

$$\mathsf{C_K} = \frac{2}{3}\begin{bmatrix} k_1\cos\theta & k_1\cos(\theta - \frac{2\pi}{3}) & k_1\cos(\theta + \frac{2\pi}{3}) \\ -k_2\sin\theta & -k_2\sin(\theta - \frac{2\pi}{3}) & -k_2\sin(\theta + \frac{2\pi}{3}) \\ k_3\frac{1}{2} & k_3\frac{1}{2} & k_3\frac{1}{2} \end{bmatrix}, \tag{3.45}$$

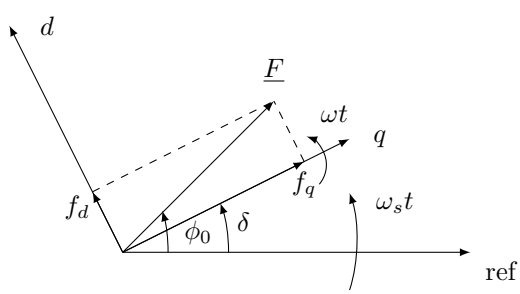

Figure 3.3: Transformation from phasor to dq-components.

with

$$\theta = \omega t + \beta. \tag{3.46}$$

As this transformation is common to the whole network, β is a constant. For convenience, β is set to zero, which has the effect of aligning the Q-axis with the reference axis with respect to which the a phase is displaced by ϕ_0. The DQ-components are then obtained:

$$f_D = F \sin(\phi_0) \tag{3.47a}$$

$$f_Q = F \cos(\phi_0). \tag{3.47b}$$

Finally, it can be easily verified that, if k_1, k_2, and k_3 are the same for $\mathsf{C_K}$ and $\mathsf{C_P}$, the following holds:

$$\mathsf{C_K} = \mathsf{T}\mathsf{C_P}, \tag{3.48}$$

with T the rotation matrix:

$$\mathsf{T} = \frac{2}{3}\begin{bmatrix} \cos\theta & \sin\theta & 0 \\ -\sin\theta & \cos\theta & 0 \\ 0 & 0 & 1 \end{bmatrix}. \tag{3.49}$$

This leads to the expression

$$f_Q + j f_D = e^{j\theta}(f_q + j f_d), \tag{3.50}$$

that can be used to express all variables in a common reference frame (Fig. 3.4), and that, together with (3.43) relates phasor and dq-domain.

3.4 Structure of the DAE System

The mathematical structure of the power system is a DAE system (3.3). This formulation, which appears quite general, neglects in fact some difficulties such as the presence of discrete variables, e.g. tap positions, constrained variables, and discontinuities in the power system. The notation of (3.3) is used in the rest of this work for the sake of notational simplicity, but it can be readily extended to reflect all the intricacies of the power system model. Such an attempt was made in [58]. Moreover, a power system model including discrete variables, and discontinuities is theoretically problematic; holding on to the notation (3.3) allows to use the extensive mathematical theory developed for DAE, and especially ODE systems. It is indeed tempting to reduce (3.3) to a system of ODEs. It is intuitively clear that this is indeed possible. At all times, $G = 0$ must be satisfied. This set of

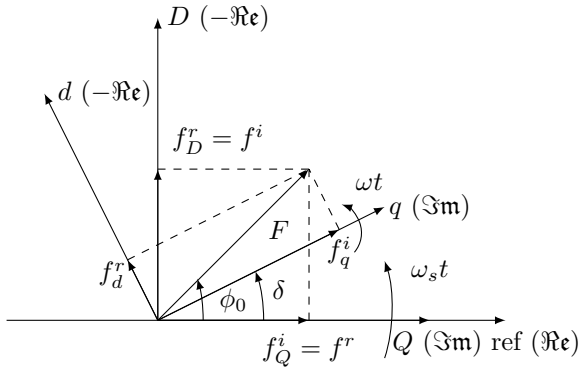

Figure 3.4: Transformation from phasor to DQ-components.

equations can thus be seen as a constraint. All trajectories in state space follow the vector field produced by the pure ODE set F. This vector field is restricted to a subset L of state space, defined as:

$$L = \{(\boldsymbol{X}, \boldsymbol{Y}) \in \mathbb{R}^{n+m} : G(\boldsymbol{X}, \boldsymbol{Y}, \boldsymbol{P}) = 0, \boldsymbol{P} = \boldsymbol{P_0}\}. \tag{3.51}$$

The theoretical justification uses the implicit function theorem.

Implicit Function Theorem. *Consider a map* $(x, y) \mapsto F(x, y)$. *Let* $F : \mathbb{R}^{n+m} \to \mathbb{R}^m$ *be a* C^1 *function, defined in a neighbourhood of* $(x, y) = (a, b)$, *such that* $F(a, b) = 0$. *If*

$$\left(\frac{\partial F_i(x,y)}{\partial y_j}\right)\Bigg|_{(x,y)=(a,b)}$$

is invertible, then there exists a unique, locally defined C^1 *function* $y = f(x)$, $f : \mathbb{R}^n \to \mathbb{R}^m$, *such that* $F(x, f(x)) = 0$, *for all* x *in some neighbourhood of* $(x,y)=(a,b)$.

Applying the implicit function theorem to (3.3), there exists a function $f(\boldsymbol{X}, \boldsymbol{Y}, \boldsymbol{P})$ defined locally, with $\boldsymbol{Y} = f(\boldsymbol{X}, \boldsymbol{P})$ that satisfies $G(\boldsymbol{X}, f(\boldsymbol{X}, \boldsymbol{P}), \boldsymbol{P}) = 0$. Hence, (3.3) can be reduced to a locally equivalent system of zero time derivative ODEs:

$$\dot{\boldsymbol{X}} = F(\boldsymbol{X}, f(\boldsymbol{X}, \boldsymbol{P}), \boldsymbol{P}). \tag{3.52}$$

The function F can be found by the Schur complement of the linearised system's Jacobian. Linearising (3.3) yields:

$$\begin{bmatrix} \boldsymbol{\Delta}\dot{\boldsymbol{X}} \\ 0 \end{bmatrix} = \mathsf{J} \begin{bmatrix} \boldsymbol{\Delta X} \\ \boldsymbol{\Delta Y} \end{bmatrix}, \tag{3.53}$$

with J the Jacobian of (3.3). Using the Schur complement of the Jacobian, (3.53) reduces to an ODE:

$$\boldsymbol{\Delta}\dot{\boldsymbol{X}} = \left(\frac{\partial F(\boldsymbol{X},\boldsymbol{Y},\boldsymbol{P})}{\partial \boldsymbol{X}} - \frac{\partial F(\boldsymbol{X},\boldsymbol{Y},\boldsymbol{P})}{\partial \boldsymbol{Y}} \cdot \left(\frac{\partial G(\boldsymbol{X},\boldsymbol{Y},\boldsymbol{P})}{\partial \boldsymbol{Y}} \right)^{-1} \cdot \frac{\partial G(\boldsymbol{X},\boldsymbol{Y},\boldsymbol{P})}{\partial \boldsymbol{X}} \right) \boldsymbol{\Delta}\boldsymbol{X}, \tag{3.54}$$

locally equivalent with (3.3).

In order for this reduction to be possible, $\partial G/\partial \boldsymbol{Y}$ must be invertible. There are points in L where $\partial G/\partial \boldsymbol{Y}$ is not invertible. These points form the singular set S, defined as:

$$S = \{(\boldsymbol{X},\boldsymbol{Y}) \in L : det(\partial G/\partial \boldsymbol{Y}(\boldsymbol{X},\boldsymbol{Y},\boldsymbol{P})) = 0\}, \tag{3.55}$$

a codimension one (or higher) submanifold of L, that divides the constraint manifold in disconnected components, where the implicit function theorem can be applied, sufficiently far away from the singular manifold S. At points of S, the system solution is not defined: $G = 0$ cannot be solved for the algebraic variables. Trajectories cannot pass through such points where a solution is not defined. Hence, the trajectory simply 'stops'. Practically, this means that numerical time integration of (3.3) fails in the neighbourhood of S. The DAE is no longer of index 1[2] at points where $det(\partial G/\partial \boldsymbol{Y})$ is equal to zero. This means that, arriving at a point of the set S, the solution ceases to exist: the system then has no time solutions, what clearly defies logic. The way out of this paradox is to remember that the system (3.3) is a mere representation of reality. In real systems, trajectories cannot stop: arriving at S, they are guided by fast dynamics that are not modelled, such as the travelling wave phenomena on transmission lines. The DAE system (3.3) can indeed be seen as a limit system of a singularly perturbed ODE system [65, p.244]:

$$\dot{\boldsymbol{X}} = F(\boldsymbol{X},\boldsymbol{Y},\boldsymbol{P}), \qquad F : \mathbb{R}^{n+m+p} \to \mathbb{R}^n \tag{3.56a}$$

$$\epsilon\dot{\boldsymbol{Y}} = G(\boldsymbol{X},\boldsymbol{Y},\boldsymbol{P}), \qquad G : \mathbb{R}^{n+m+p} \to \mathbb{R}^m, \tag{3.56b}$$

where the parameter ϵ tends to zero. For very small ϵ, $\epsilon\dot{\boldsymbol{Y}} = G(\boldsymbol{X},\boldsymbol{Y},\boldsymbol{P})$ describes indeed very fast dynamics. Trajectories of the singularly perturbed system (3.56) can be approximated by those of the DAE system if the fast dynamics are stable along the trajectory. All eigenvalues of $\partial G/\partial \boldsymbol{Y}$ must have negative real parts [66].

The reduction of (3.3) to a locally equivalent system (3.54) is of theoretical importance only. The system response is obtained directly by solving (3.3). This

[2] A DAE is of index 1 around a point $(\boldsymbol{X_0},\boldsymbol{Y_0},\boldsymbol{P_0})$ if $\partial G/\partial \boldsymbol{Y}$ is invertible at $(\boldsymbol{X_0},\boldsymbol{Y_0},\boldsymbol{P_0})$ and $G(\boldsymbol{X_0},\boldsymbol{Y_0},\boldsymbol{P_0}) = 0$ is satisfied [64].

is treated in Chapter 5. For practical power system models, the DAE system is of index 1. If not, the model can be reformulated by moving some algebraic variables to the dynamic state variables set. This operation is always possible since algebraic variables can be considered as dynamic variables with indefinitely fast dynamics. In practice, it often suffices to change some load models [67, p.443].

Example 3.2. *The system from example 3.1 is revisited. The constraint manifold L can be directly computed from G:*

$$L = \left\{ \pm\sqrt{(x'P)^2 + (x'Q + U_2^2)^2}/U_2^2, Q_{VSC}, U_2 : Q_{VSC} \in \mathbb{R}, U_2 \in \mathbb{R} \right\} \quad (3.57)$$

It can be seen that the constraint manifold consists of four disjoint sections: U_2 only appears squared, and there is a positive and negative solution for E'_q. The singular set consists of points that are the solution of the following system:

$$(E'_q U_2)^2 - (x'P)^2 - (x'Q + U_2^2)^2 = 0 \quad (3.58a)$$

$$\frac{\partial G}{\partial U_2} = {E'_q}^2 - 2(x'Q + U_2^2) = 0 \quad (3.58b)$$

Eq. (3.58b) *can be written as:*

$$E'_q = \pm\sqrt{2(x'Q + U_2^2)} \quad (3.59)$$

or

$$U_2 = \pm\sqrt{\frac{{E'_q}^2}{2} - x'Q}. \quad (3.60)$$

Substituting (3.59) in (3.58a) gives:

$$0 = (E'_q U_2)^2 - (x'P)^2 - \left(\frac{{E'_q}^2}{2}\right)^2, \quad (3.61)$$

or:

$$E'_q = \pm\sqrt{2U_2^2 \pm 2\sqrt{U_2^4 - (x'P)^2}} \quad (3.62)$$

Back substitution of E'_d in (3.60) gives:

$$U_2 = \sqrt{\frac{2U_2^2 \pm 2\sqrt{U_2^4 - (x'P)^2}}{2} - x'Q}, \quad (3.63)$$

which after some manipulation can be written as

$$U_2 = \pm\sqrt[4]{(x'P)^2 + (x'Q)^2}. \quad (3.64)$$

Back substitution of U_2 in (3.62) finally gives:

$$E'_q = \pm\sqrt{2\sqrt{(x'P)^2 + (x'Q)^2} + 2x'Q}. \tag{3.65}$$

The analytical locus of the singularity in state space,

$$S = \{(U_2, Q_{VSC}, E'_q) : Q_{VSC} \in \mathbb{R}\} \tag{3.66}$$

is thus from (3.64) and (3.65):

$$S = \left\{ \pm\sqrt[4]{(x'P)^2 + (x'Q)^2}, Q_{VSC}, \pm\sqrt{2\sqrt{(x'P)^2 + (x'Q)^2} + 2x'Q} : Q_{VSC} \in \mathbb{R} \right\}. \tag{3.67}$$

It can be seen from this equation that the singular set also consists of four disjoint sections, which is not surprising since it is a subset of L. Numerically evaluating the expressions for the constraint manifold and the singular set for a range of values for Q_{VSC} leads to the state space plot in Fig. 3.5. It can be verified that constraint manifold and singular set consist indeed of four disjoint sections.

3.5 Overall Modelling Assumptions

Now that the mathematical preliminaries are dealt with and the theoretical foundations have been laid, we are in a position to clearly define the modelling assumptions, to which the rest of the work is submitted. It is common practice in electromechanical simulation software to use quasi-stationary phasors. Here, we comply with the quasi-stationary phasor paradigm. However, this introduces some major, albeit acceptable, assumptions. Quasi-stationary phasors can be seen as analytic signals with constant amplitude, phase and frequency, or as a special case of dynamic phasors, where only the fundamental frequency component is retained, and the Fourier coefficients are not time independent. In other words, the two assumptions that lie at the base of the quasi-stationary assumption are:

- all harmonics are neglected,
- a perfectly sinusoidal signal is assumed.

Consequently, quasi-stationary phasors are only valid when harmonics are absent and the system is at steady-state. Strictly speaking, the quasi-stationary assumption is incompatible with power system transient analysis as during transients the pulsation changes. However, under quasi-stationary conditions,

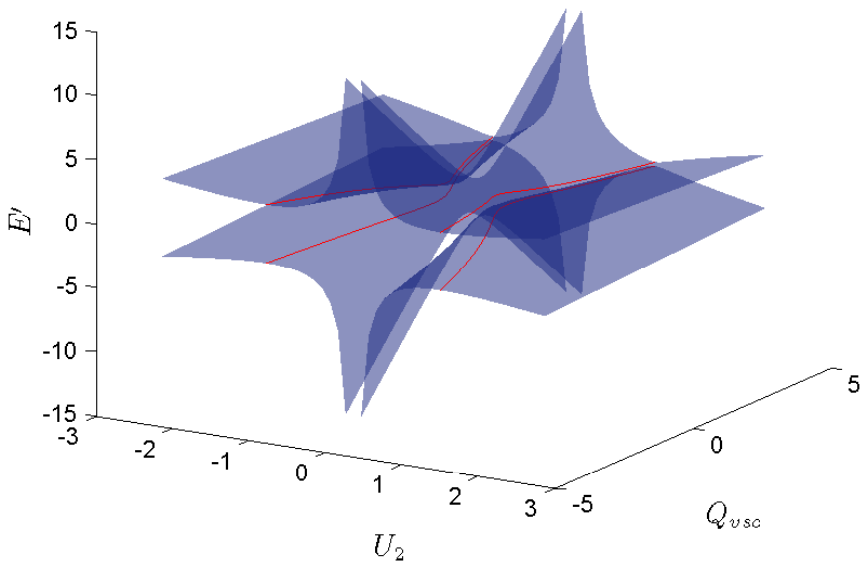

Figure 3.5: Representation of the expression for constraint and singular manifold in state space. The shaded surface represents the constraint manifold L, the lines represent the singular manifold S.

when the transients are sufficiently slow compared to the signal's pulsation ω, quasi-stationary phasors can be used. Electromechanical transients comply with the quasi-stationary condition. That is why in early transient stability programs quasi-stationary phasors were used. Quasi-stationary phasors have since become the *de facto* standard in transient stability type software, and are also used today in modern power system analysis software. In fact, they are so widely used in analysis of power systems, that their inherent limitations are often forgotten. The VSC HVDC models we develop in subsequent chapters fit in the framework of the phasor paradigm. This means that the models we set forth to develop are only guaranteed to be valid if the quasi-stationary assumption is valid.

As a corollary, the models are not valid for the simulation of very fast trajectories; they must be slow with respect to the carrier frequency. Any behaviour at or close to the infeasible set, should not be investigated using the proposed models, and off-manifold dynamics are neglected, irrespective of their stability. In the remainder of this text, unless otherwise specified, it is assumed that dynamics are constrained

to the set $L \backslash S$ and operation is sufficiently far away from the set S, i.e. a pure ODE formulation of (3.3) is possible, although in practice we still use the DAE formulation. Sufficiently far away means that the quasi-stationary assumption is valid.

Lastly, a balanced system is assumed at all times, also during faults, as is a symmetric voltage system. Together with neglecting harmonics, this guarantees that great speed is achieved in the simulation of machines and converters, allowing the simulation of large integrated AC/DC systems.

For the VSC system itself, very few additional assumptions are needed. In manufacturer delivered models, control loop parameters are often hard coded: only one set of parameters is then available, resulting in a restriction of the systems Short Circuit Ratio (SCR) because one set of parameters can not account for VSC operation in systems with widely differing SCRs. In the models we develop, this assumption is not necessary, as parameters can be changed. One assumption to be made is that there is no passive grid operation. In practice, a parallel control loop needs to be designed for passive grid operation. Also, protection schemes, such as converter blocking, are not taken into account. This restriction can be translated to a restriction in voltage drop at the converter's point of common coupling in the order of 30%.

3.6 Conclusions

The mathematical model of the power system, for phenomena with a narrow frequency spectrum around fundamental frequency, is a DAE system with quasi-stationary phasors. Such a formulation has consequences for the validity of a model developed in such a framework: trajectories are restricted to the $L \backslash S$ set, a sinusoidal carrier wave is assumed, and harmonics are neglected. Furthermore, a balanced system and symmetric network is assumed at all times. Every VSC HVDC model that is to be developed, needs to fit in the modelling and simulation framework of the rest of the power system. The above mentioned restrictions do not pertain to the model itself, but to the transient stability modelling paradigm, wherein the model is developed. Some restrictions, however, are specific to the VSC model, such as no passive grid operation and no protection schemes. The result of the simplifications and also of the transformations is that the solution methods can be made to be very efficient.

Chapter 4

Steady-State Models

4.1 Introduction

Power flow is arguably the single most important and most widely used calculation in power system analysis. It is used for planning, scheduling, to obtain a starting point for dynamic analysis, and used in economic algorithms, real time dispatching, and N-1 contingency analysis. The aim of this chapter is to derive simplified and detailed VSC HVDC models to be incorporated into power flow computations and to implement power flow computation methods that can handle MTDC systems. The simplified model is shown to be a good approximation of commercially available models. The detailed model should overcome the shortcomings of the available models, and those proposed in the literature. The models are thoroughly validated by comparing them with a manufacturer delivered model and a model that comes with the commercial power system software 'Power System Simulator for Engineers' (PSS/E) [68].

Continuation methods are a second type of steady-state calculation that offer more information than mere power flow. State of the art numerical techniques, developed for ODE systems, are extended to the DAE framework discussed in Chapter 3. The method is tested on a simple power system including a VSC.

4.2 Power Flow

The aim of the power flow calculation is to find a steady-state operating point of the power system. Note that the power flow solution is not necessarily the same as the fixed point of the dynamic system (3.3). Recognising that power system

equipment is modelled using DAEs and not pure ODEs, (3.3) can be written as:

$$\dot{\boldsymbol{X}} = F(\boldsymbol{X}, \boldsymbol{Y}, \boldsymbol{P}) \tag{4.1a}$$

$$0 = G_1(\boldsymbol{X}, \boldsymbol{Y}, \boldsymbol{P}) \tag{4.1b}$$

$$0 = G_2(\boldsymbol{X}, \boldsymbol{Y}, \boldsymbol{P}), \tag{4.1c}$$

where $G_1(\boldsymbol{X}, \boldsymbol{Y}, \boldsymbol{P})$ are the algebraic equations of the power system equipment, e.g. the generators' stator equations, and the remaining algebraic equations $G_2(\boldsymbol{X}, \boldsymbol{Y}, \boldsymbol{P})$, the network equations. Noting that the network equations do not depend on the dynamic state variables $\boldsymbol{X}$, and that a solution is sought for a constant parameter set $\boldsymbol{P} = \boldsymbol{P}_0$, the power flow equations can be written as $0 = G_2(\boldsymbol{Y}, \boldsymbol{P}_0)$. At a solution of this equation, $0 = F(\boldsymbol{X}, \boldsymbol{Y}, \boldsymbol{P})$ is not necessarily satisfied. In other words: the power flow solution does not necessarily correspond to a fixed point of the full DAE system. The AC power flow equations G_2, can be written in their general form as:

$$\boldsymbol{I} = \mathsf{Y} \cdot \boldsymbol{U} \tag{4.2a}$$

$$\boldsymbol{S} = \boldsymbol{U} \cdot \boldsymbol{I}^* \tag{4.2b}$$

4.3 Simplified Steady-State Model

4.3.1 One Converter

A generator in steady-state can be represented by a voltage source, connected to the rest of the network via a reactance (Fig. 4.1). In power flow computation, this representation is usually simplified to a PV node, i.e. a node controlling active power output and voltage. When the generator is not under voltage control, but under reactive power control, it is represented as a PQ node (Fig. 4.2). If reactive power limits are modelled in the power flow, this situation can also occur when those limits are reached: the voltage cannot be held constant, and the point of voltage control moves behind the generator's reactance. Reactive power output is then constant and at its highest value.

In section 2.4.1 it was argued that a VSC in its simplest form can be represented in steady-state by a voltage source behind a reactance (Fig. 2.4), i.e. the same as a generator. From a mathematical point of view, no distinction can be made between a VSC and a generator. It follows that VSCs can equally well be represented as PV nodes when under AC voltage control, and as PQ nodes when under reactive power control.

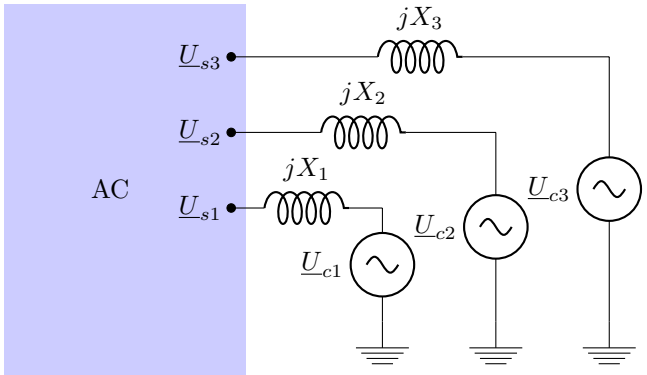

Figure 4.1: Simplified equivalent AC circuit of a generator or a VSC HVDC converter.

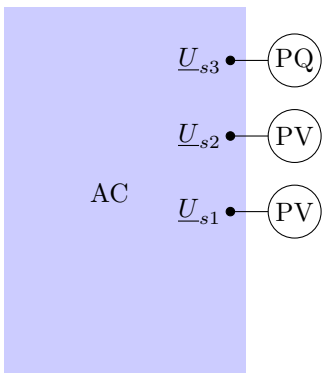

Figure 4.2: Power flow representation of a generator or a VSC HVDC converter.

4.3.2 Complete System

If a full HVDC system, comprising of more than one converter, is connected in a meshed AC system, every converter can be represented by a PV or PQ node. However, the relation between the converters, mathematically expressed by the balance of active power (2.4), needs to be taken into account (Fig. 4.3).

In practice, the active power set points of all but one converter can be chosen. The last active power set point has to be chosen such that the active power balance equation is satisfied. For a two-terminal system, the power set point of the second converter is set at: $P_{ref2} = -P_{ref1} - P_{loss}$. However, P_{loss} is not known beforehand: it depends on the active and reactive power flow through the phase reactor, only known after the power flow calculation. It depends also on

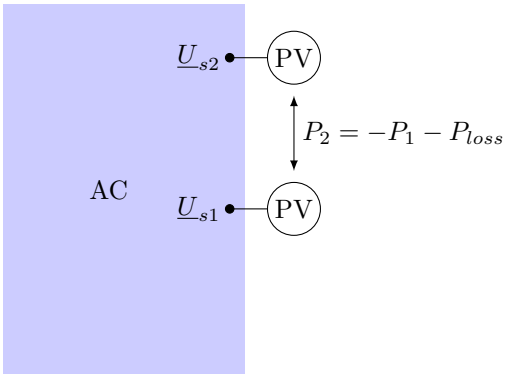

Figure 4.3: Simplified equivalent AC circuit.

the flows and parameters of the DC circuit, but as the DC circuit is not modelled at all in the simplified representation, these parameters are not known. Hence, the results obtained with this model are only as good as the estimate of P_{loss}. Especially for multi-terminal systems, obtaining a good estimate of the losses a priori can be difficult.

4.3.3 Evaluation

This simplified model is often used in power flow computations for two-terminal VSC HVDC systems. Its advantages are that it is very easy to use, and does not require detailed converter data. Furthermore, standard AC power flow software can be used. The model can be used for asynchronous infeed, two- and multi-terminal systems. However, there are some disadvantages: the internal variables are not accessible, and almost no information on the DC system is available. Also, (2.4) must be enforced at all times. If the AC/DC power flow is an underlying process for another calculation, changing the converters' active power set points, these set points must be properly adjusted so as to satisfy (2.4). It is thus worthwhile to develop a more detailed model.

4.4 Detailed Steady-State Model

The detailed model overcomes the shortcomings of the simple one. First of all, the DC system is explicitly represented, making available DC circuit information such as voltages and powers. Secondly, a more general representation of the converter's AC side is sought. In a first step, phase reactor losses are to be included. In a second step, the AC side, including transformer, filter, and phase reactor is fully

represented in the model. Lastly, it is shown how converter losses and limits are to be included in the model.

It is not the first time that more detailed models for VSC MTDC power flow are developed. However, most methods presented in the literature have shortcomings. In [33], an approximate solution is obtained by neglecting converter losses and losses in the phase reactor. In [30], converter losses are neglected, DC variables are not accessible, and the power flow set points are defined at the converter bus, not at the system bus, which simplifies the calculations, but is not in accordance with current practice in actual VSC HVDC systems. Reference [34] neglects all losses and restricts itself to two-terminal systems. Reference [32] includes a detailed converter loss model, MTDC, and DC/DC converters. However, the AC side of the converters is ignored.

4.4.1 Solution Methods

With two actual multi-terminal systems in operation, it is not surprising that much work has been done on solution methods for detailed AC/MTDC power flow for CSC HVDC systems. In some early publications, very detailed models have been proposed with solution methods, that were subsequently implemented in commercial software packages. Some difficulties make detailed AC/DC power flow computations a challenge: converter controls and mode shifting, transformer tap control and tap limits, voltage and current limits, etc. In [69], solution methods were divided into four categories: the unified method, the sequential method, the step-by-step method, and the decomposition method. A more conventional subdivision only distinguishes between unified and sequential methods. We would define unified methods as methods that change the Jacobian, and sequential ones as those that do not. With this definition, step-by-step methods [70] are essentially unified, and decomposition methods [69], [71], [72] essentially sequential.

For VSC HVDC systems, the problem is somewhat easier due to the absence of mode shifts and the easier handling of transformers in power flow. The basic solution methods are the same as for CSC systems. In this work, we opt for the sequential method, built around the AC power flow tool, MATPOWER [73].

The basic procedure goes as follows:

1. All converters are represented as PV or PQ nodes;
2. the active power set point of the slack converter is chosen such that (2.4) is satisfied with $P_{loss} = 0$;
3. the AC power flow is then solved.

So far, the procedure is exactly the same as for the simplified model, which would end here. For the detailed model, additional converter variables, and the DC network are calculated.

4. Calculate converter variables: after the AC power flow calculation, the converter bus voltage and power injections are calculated.
5. DC network calculation: the injections in the DC network are calculated from the converter injections at the AC side, and the DC network is solved.

All variables are now solved for. However, the active power of the slack converter was calculated, based on the faulty assumption that $P_{loss} = 0$. An additional iterative calculation is thus needed.

6. Slack converter iteration: lastly, the power injection of the slack converter in the system needs to be calculated from the updated values. If the difference between two successive calculations of the slack converter power is sufficiently small, the loop is terminated. If not, the updated values of the slack converter injections are used as next estimates and the calculation is repeated from step 3.

In Fig. 4.4 the basic flow diagram of the computation is shown.

4.4.2 Calculate Converter Variables

The converter buses are not included in the AC system. Hence, their voltages and power injections are not known after the AC power flow. They can be calculated by first computing the complex power injections of the converters in the system:

$$\underline{\boldsymbol{S}}_{\boldsymbol{s}} = \underline{\boldsymbol{U}}_s(\underline{\mathrm{Y}} \cdot \underline{\boldsymbol{U}}_s)^* - \underline{\boldsymbol{S}}_{bus}, \tag{4.3}$$

with $\underline{\boldsymbol{S}}_{bus}$ the standard bus injection vector, i.e. caused by loads and generators only, but without the contribution from the converter. The current flowing from the converter, through the phase reactor to the AC grid can then be calculated:

$$\underline{\boldsymbol{I}}_{\boldsymbol{pr}} = [\underline{S}_{s1}/\underline{U}_{s1}, \underline{S}_{s2}/\underline{U}_{s2}, \ldots, \underline{S}_{sn}/\underline{U}_{sn}]^*. \tag{4.4}$$

The converter voltages are:

$$\underline{\boldsymbol{U}}_{\boldsymbol{c}} = \underline{\boldsymbol{U}}_{\boldsymbol{s}} + \underline{\boldsymbol{I}}_{\boldsymbol{pr}} \cdot \underline{\boldsymbol{Z}}_{\boldsymbol{pr}}. \tag{4.5}$$

The complex power at the converter bus in the direction of the grid is:

$$\underline{\boldsymbol{S}}_{\boldsymbol{c}} = \underline{\boldsymbol{U}}_{\boldsymbol{c}}(\underline{\boldsymbol{I}}_{\boldsymbol{pr}})^*. \tag{4.6}$$

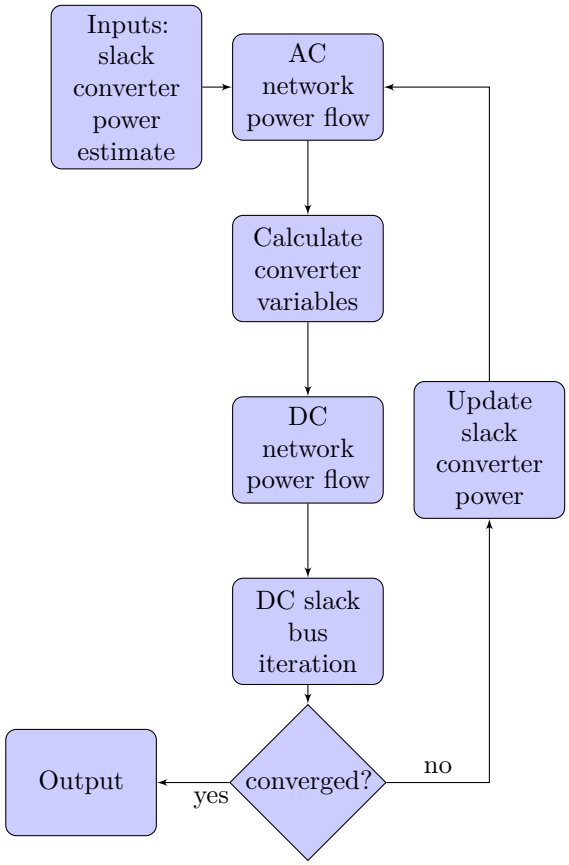

Figure 4.4: Flow chart for sequential AC/DC power flow.

If the filter is not added to the system bus in the AC model, but explicitly represented in the converter model, as we will later argue it should be, the calculation of the converter variables is slightly more involved. The single-line diagram with symbols is given for reference in Fig. 4.5.

The current through the transformer is:

$$\underline{\boldsymbol{I}}_{\boldsymbol{tr}} = [\underline{S}_{s1}/\underline{U}_1, \underline{S}_{s2}/\underline{U}_2, \ldots, \underline{S}_{sn}/\underline{U}_n]^*, \tag{4.7}$$

and the filter bus voltage by:

$$\underline{\boldsymbol{U}}_{\boldsymbol{f}} = \underline{\boldsymbol{U}} + \underline{\boldsymbol{I}}_{\boldsymbol{tr}} \cdot \underline{\boldsymbol{Z}}_{\boldsymbol{tr}}. \tag{4.8}$$

The power flowing to the grid at the filter bus is:

$$\underline{\boldsymbol{S}}_{\boldsymbol{f}} = \underline{\boldsymbol{U}}_{\boldsymbol{f}} (\underline{\boldsymbol{I}}_{\boldsymbol{tr}})^*, \tag{4.9}$$

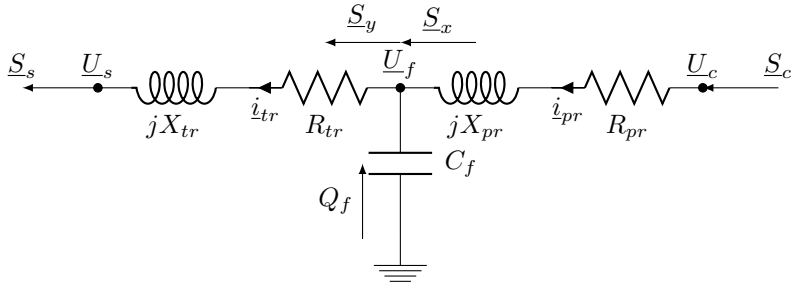

Figure 4.5: Single-line diagram of converter's AC side including filter.

and the power flowing into the filter bus is:

$$\underline{\boldsymbol{S}}_{\boldsymbol{x}} = \underline{\boldsymbol{S}}_{\boldsymbol{y}} - j\boldsymbol{Q}_{\boldsymbol{f}}, \tag{4.10}$$

with

$$\boldsymbol{Q}_{\boldsymbol{f}} = \boldsymbol{B}_{\boldsymbol{f}}\boldsymbol{U}_{\boldsymbol{f}}{}^2, \tag{4.11}$$

the reactive power injected by the filter. The current through the phase reactor can now be calculated as:

$$\underline{\boldsymbol{I}}_{\boldsymbol{pr}} = [\underline{S}_{x1}/\underline{U}_{f1}, \underline{S}_{x2}/\underline{U}_{f2}, \ldots, \underline{S}_{xn}/\underline{U}_{fn}]^*, \tag{4.12}$$

and the converter voltage as:

$$\underline{\boldsymbol{U}}_{\boldsymbol{c}} = \underline{\boldsymbol{U}}_{\boldsymbol{f}} + \underline{\boldsymbol{I}}_{\boldsymbol{pr}} \cdot \underline{\boldsymbol{Z}}_{\boldsymbol{pr}}. \tag{4.13}$$

Finally, the converter power flowing towards the grid is:

$$\underline{\boldsymbol{S}}_{\boldsymbol{c}} = \underline{\boldsymbol{U}}_{\boldsymbol{c}}(\underline{\boldsymbol{I}}_{\boldsymbol{pr}})^*. \tag{4.14}$$

4.4.3 DC Network

If the DC network is explicitly represented, the DC flows and voltages can be calculated. Also, the losses can be accurately calculated. In a two-terminal system, the flow over the DC line can be perfectly controlled. In a multi-terminal system, the DC flow distributes over the DC lines, similarly to AC networks. An additional DC power flow calculation needs to be performed to determine the power flow in the DC network. The DC power flow equations are similar to the AC power flow equations (4.2a):

$$\boldsymbol{I}_{\boldsymbol{dc}} = \mathsf{Y}_{\mathsf{dc}} \cdot \boldsymbol{U}_{\boldsymbol{dc}} \tag{4.15a}$$

$$\boldsymbol{P}_{\boldsymbol{dc}} = \boldsymbol{U}_{\boldsymbol{dc}} \cdot \boldsymbol{I}_{\boldsymbol{dc}}{}', \tag{4.15b}$$

with $\boldsymbol{U_{dc}} = [U_{dc1}, U_{dc2}, \ldots, U_{dcn}]^T$ the vector of DC voltages, and $\boldsymbol{I_{dc}} = [I_{dc1}, I_{dc2}, \ldots, I_{dcn}]^T$ the vector of DC currents. The differences between the general formulation of AC and DC power flow are that for the DC power flow:

- the bus admittance matrix of the DC network $\mathsf{Y_{dc}}$, is constructed using line resistances only;
- currents and voltages are real, and thus
- the transpose of the current vector is taken instead of the conjugate transpose;
- the power is purely active.

In the remainder of the analysis, we assume a symmetrically grounded monopolar configuration (Fig. 4.6), as it is the most common. The DC power flow equations then become:

$$\boldsymbol{I_{dc}} = \mathsf{Y_{dc}} \cdot \boldsymbol{U_{dc}} \tag{4.16a}$$

$$\boldsymbol{P_{dc}} = 2\boldsymbol{U_{dc}} \cdot \boldsymbol{I_{dc}}'. \tag{4.16b}$$

Eliminating the current vector from (4.16) leads to a system of non-linear equations:

$$0 = \mathsf{Y_{dc}}\boldsymbol{U_{dc}} - \boldsymbol{I}, \tag{4.17}$$

with

$$\boldsymbol{I} = \left[\frac{P_{dc_1}}{2U_{dc_1}}, \frac{P_{dc_2}}{2U_{dc_2}}, \ldots, \frac{P_{dc_n}}{2U_{dc_n}}\right]^T, \tag{4.18}$$

wherein the current injections $\boldsymbol{I_{dc}}$, needed to calculate $\boldsymbol{P_{dc}}$, are not known beforehand. For the other variables, distinction has to be made between slack and non-slack converters. For the slack converter, the DC voltage is known, and equal to the reference voltage of the DC grid. As for the other converters, the injected active power is known from the preceding AC power flow calculation. To simplify notation, but without loss of generality, we assume that the last converter controls the DC voltage. The vector of the unknowns is then:

$$\boldsymbol{X} = \left[\frac{\boldsymbol{X_1}}{X_2}\right] = \left[\begin{array}{c} U_{dc_1} \\ \vdots \\ \hline U_{dc_{(n-1)}} \\ P_{dc_n} \end{array}\right]. \tag{4.19}$$

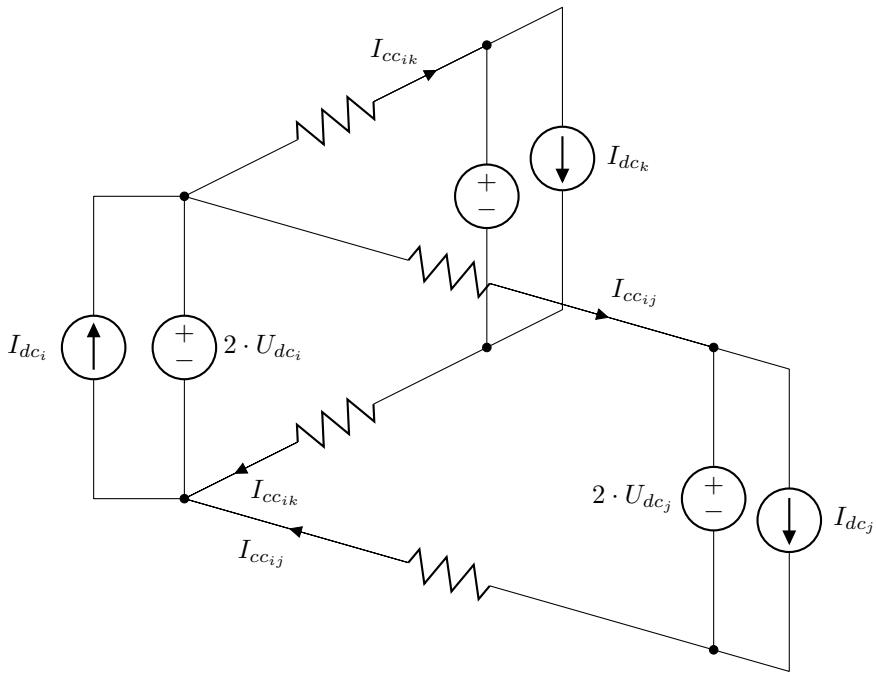

Figure 4.6: Symmetrically grounded, monopolar MTDC circuit.

The DC bus admittance matrix is partitioned as follows:

$$\mathsf{Y}_{\mathsf{dc}} = \left[\begin{array}{c|c} \mathsf{Y}_{11} & \boldsymbol{Y_{12}} \\ \hline \boldsymbol{Y_{21}} & y_{22} \end{array}\right]. \tag{4.20}$$

The matrix Y_{11} is of dimension $(n-1)$ x $(n-1)$, $\boldsymbol{Y_{12}}$ is a column vector of length $n-1$, $\boldsymbol{Y_{21}}$ a row vector of length $n-1$, and y_{22} a scalar. The problem (4.17) can now be rearranged in an equivalent form that can be conveniently solved with a Newton method:

$$\left\{\begin{array}{rl} 0 = & \mathsf{Y}_{11}\boldsymbol{X_1} + \boldsymbol{Y_{12}} \cdot u_{dcref} - \boldsymbol{T} \\ 0 = & \boldsymbol{Y_{21}}\boldsymbol{X_1} + y_{22} \cdot u_{dcref} - X_2/(2u_{dcref}) \end{array}\right. , \tag{4.21}$$

with

$$\boldsymbol{T} = \left[\frac{P_{dc_1}}{2X_1}, \frac{P_{dc_2}}{2X_2}, \ldots, \frac{P_{dc_{n-1}}}{2X_{n-1}}\right]^T. \tag{4.22}$$

Explicit representation of the DC circuit thus requires an additional iterative calculation. Solving this system, gives the DC voltages at all buses. Once the DC voltages are known, the currents between the DC buses can be obtained by

premultiplying the DC bus voltage vector by $\mathsf{Y}_{\mathsf{dcf}}$ or $\mathsf{Y}_{\mathsf{dct}}$. $\mathsf{Y}_{\mathsf{dcf}}$ is the matrix which, when multiplied by the voltage vector, gives the currents leaving the buses (4.23). Analogously, $\mathsf{Y}_{\mathsf{dct}}$ relates bus voltages and currents entering the buses (4.24).

$$\boldsymbol{I_{ccf}} = \mathsf{Y}_{\mathsf{dcf}}\boldsymbol{U_{dc}} \tag{4.23}$$

$$\boldsymbol{I_{cct}} = \mathsf{Y}_{\mathsf{dct}}\boldsymbol{U_{dc}} \tag{4.24}$$

$\mathsf{Y}_{\mathsf{dcf}}$ and $\mathsf{Y}_{\mathsf{dct}}$ are obtained as byproducts of the construction of the DC bus admittance matrix Y_{dc} and do not necessitate extra computations.

4.4.4 Slack Converter Iteration

After the DC network power flow, the converter injections P_c are known for all converters. In many papers, e.g. [30], and also in some commercially available models as discussed further, the active power flow set point is defined at the filter bus or even at the converter bus. The active power injections P_f or P_c are compared to the set point; if the difference is smaller than a specified tolerance, the calculation has converged, otherwise, the next iteration is started. However, the active power set point should be specified at the system bus, leading to an iterative calculation. The slack converter injection is used to calculate a better estimate for the slack converter injection in the system P_s. This injection can be found from the power flow equations:

$$P_c = U_c^2 G_{pr} - U_s U_c [G_{pr}\cos(\delta_c - \delta_s) + B_{pr}\sin(\delta_c - \delta_s)] \tag{4.25}$$

$$Q_c = -U_c^2 B_{pr} - U_s U_c [G_{pr}\sin(\delta_c - \delta_s) - B_{pr}\cos(\delta_c - \delta_s)] \tag{4.26}$$

or

$$P_s = -U_s^2 G_{pr} + U_s U_c [G_{pr}\cos(\delta_s - \delta_c) + B_{pr}\sin(\delta_s - \delta_c)] \tag{4.27}$$

$$Q_s = U_s^2 B_{pr} + U_s U_c [G_{pr}\sin(\delta_s - \delta_c) - B_{pr}\cos(\delta_s - \delta_c)], \tag{4.28}$$

wherein $\underline{U}_s$, and P_c are known, U_c, δ_c, Q_s, and Q_c are unknown. In order for these equations to be solved, an additional condition needs to be enforced, or another unknown needs to be assumed known. Several possibilities exist, e.g. assume Q_s or Q_c are known, or assume that the phase reactor losses are constant between iterations. We found that the last option should be avoided, as it generally leads to more iterations. Choosing Q_s is slightly better than Q_c when converter losses are included. The flow chart of the slack converter iteration is shown in Fig. 4.7. Q can be either Q_s or Q_c.

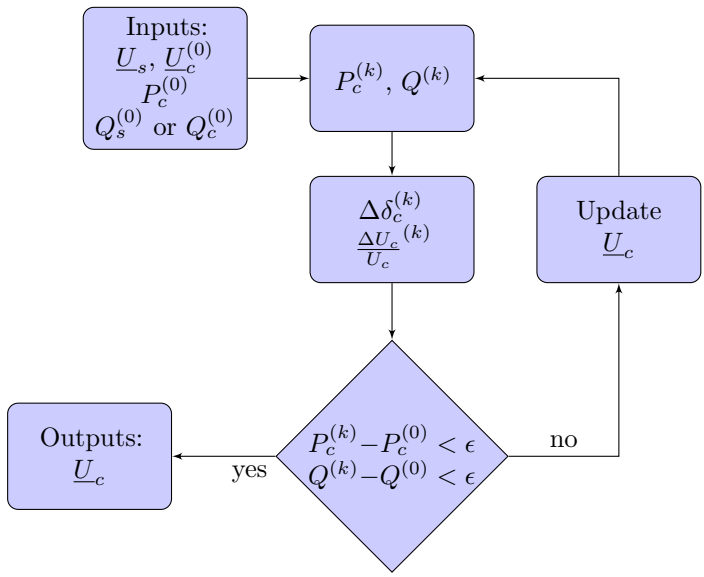

Figure 4.7: Flow chart for iterative calculation of slack bus without filter.

If the filter is included, the system of equations to be solved is:

$$0 = P_c - P_c^{(0)} \tag{4.29a}$$

$$0 = Q_c - Q_c^{(0)} \tag{4.29b}$$

$$0 = P_y - P_x \tag{4.29c}$$

$$0 = Q_y - Q_x - Q_f. \tag{4.29d}$$

The symbols are defined on Fig. 4.5. Eq. (4.29b) could be replaced by $0 = Q_s - Q_s^{(0)}$. These equations are written as power flow equations:

$$0 = U_c^2 G_{pr} - U_f U_c [G_{pr} \cos(\delta_c - \delta_f) + B_{pr} \sin(\delta_c - \delta_f)] - P_c \tag{4.30a}$$

$$0 = -U_c^2 B_{pr} - U_f U_c [G_{pr} \sin(\delta_c - \delta_f) - B_{pr} \cos(\delta_c - \delta_f)] - Q_c \tag{4.30b}$$

$$\begin{aligned} 0 = {} & U_f^2 G_{tr} - U_f U_s [G_{tr} \cos(\delta_f - \delta_s) + B_{tr} \sin(\delta_f - \delta_s)] \\ & - (-U_f^2 G_{pr} + U_f U_c [G_{pr} \cos(\delta_f - \delta_c) + B_{pr} \sin(\delta_f - \delta_c)]) \end{aligned} \tag{4.30c}$$

$$\begin{aligned} 0 = {} & -U_f^2 B_{tr} - U_f U_s [G_{tr} \sin(\delta_f - \delta_s) - B_{tr} \cos(\delta_f - \delta_s)] \\ & - (U_f^2 B_{pr} + U_f U_c [G_{pr} \sin(\delta_f - \delta_c) - B_{pr} \cos(\delta_f - \delta_c)]) - U_f^2 B_f \end{aligned} \tag{4.30d}$$

and solved with Newton-Raphson for $\underline{U}_c$ and $\underline{U}_f$, following the procedure outlined in Fig. 4.8. The active power injected into the grid by the slack converter is calculated from:

$$P_{VSC} = -U_s^2 G_{tr} + U_f U_s [G_{tr} \cos(\delta_s - \delta_f) + B_{tr} \sin(\delta_s - \delta_f)]. \tag{4.31}$$

4.4.5 Including Converter Losses

The converter loss model used is a generalised converter loss model for a $600MW$ VSC HVDC system with DC voltage of $\pm 300kV$ [74]. The converter losses are expressed as a quadratic function of reactor current:

$$P_{loss} = a + bI_{pr} + cI_{pr}^2, \tag{4.32}$$

with

$$I_{pr} = \frac{\sqrt{P_c^2 + Q_c^2}}{\sqrt{3}U_c}. \tag{4.33}$$

The loss components are further discussed in [75]. Including converter losses is straightforward for non-slack converters: after calculation of the converter voltages

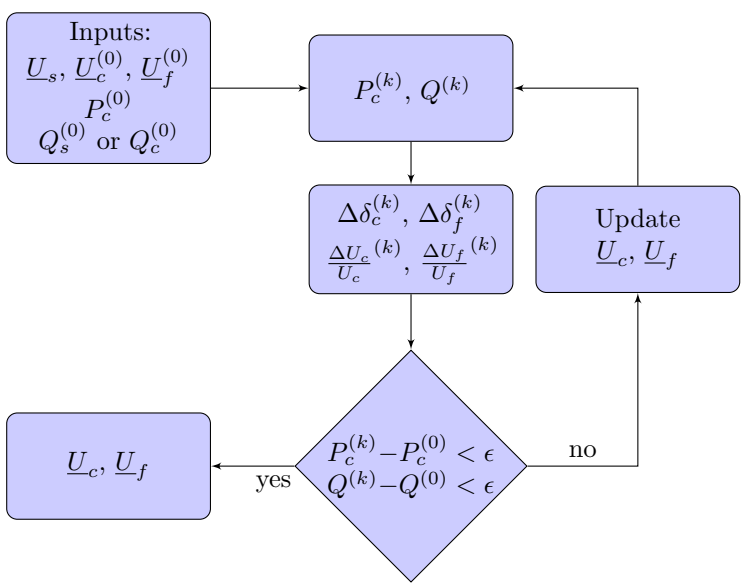

Figure 4.8: Flow chart for iterative calculation for slack bus with filter.

and power injections at the converter, the loss is calculated from these values and added to the converter active power injections to obtain the power at the DC side:

$$P_{dc} = P_c + P_{loss}. \tag{4.34}$$

The flow chart is given in Fig. 4.9.

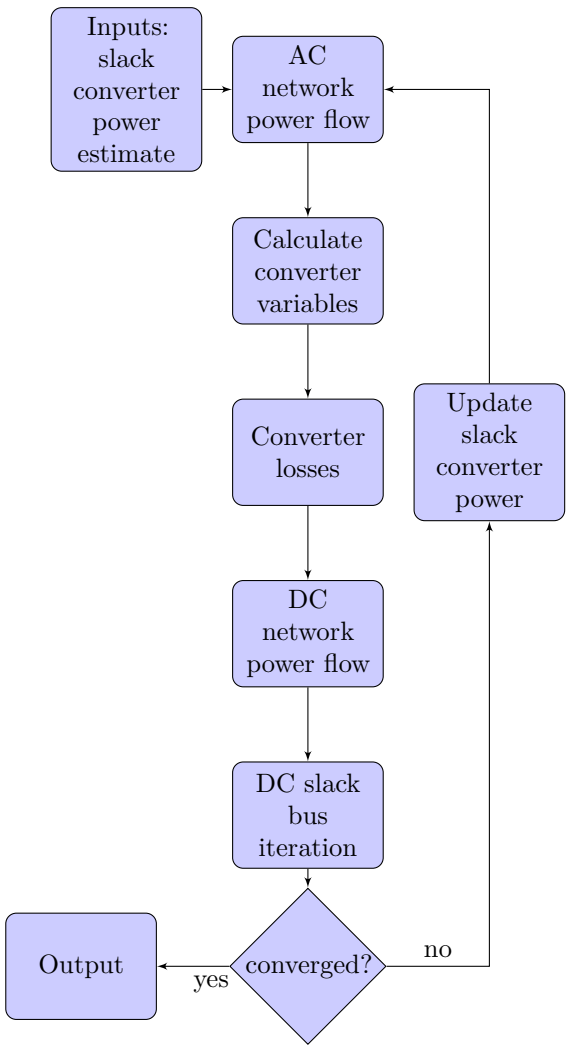

Figure 4.9: Flow chart for sequential AC/DC power flow including losses.

For the slack converters, the voltages are not known exactly as the power injection in the AC grid is not known. The converter voltage needs to be calculated iteratively, by the procedure given in Fig. 4.7. If losses are included, the converter losses are needed to perform this calculation. However, they depend on the converter voltage and the power, and are hence not known beforehand. An extra iterative calculation is thus needed. In Figs. 4.11 and 4.10 the procedure for the calculation of the slack converter's system power is given. Fig. 4.10 includes the filter, while Fig. 4.11 does not.

4.4.6 Operating Limits

In section 2.5, the locus of the limits in the PQ-plane was calculated for the lossless case. In this section, the calculation is repeated with reactor losses included. The limits are then in accordance with the rest of this chapter, wherein reactor losses are taken into account. The current limit remains the same. For the DC voltage limit, the full power flow equations have to be used. The system power in the direction to the grid is:

$$P_s = -U_s^2 G + U_s U_c [G\cos(\delta_s - \delta_c) + B\sin(\delta_s - \delta_c)], \tag{4.35}$$

which can be written as:

$$U_s U_c G\cos(\delta_s - \delta_c) + U_s U_c B\sin(\delta_s - \delta_c) = P_s + U_s^2 G \tag{4.36}$$

or

$$\cos(\delta_s - \delta_c) = \frac{P_s + U_s^2 G}{U_s U_c G} - \frac{B}{G}\sin(\delta_s - \delta_c). \tag{4.37}$$

Squaring both sides gives a quadratic equation in $\sin(\delta_s - \delta_c)$:

$$1 - \sin^2(\delta_s - \delta_c) = \left(\frac{P_s + U_s^2 G}{U_s U_c G}\right)^2 + \frac{B^2}{G^2}\sin^2(\delta_s - \delta_c) - 2\frac{P_s + U_s^2 G}{U_s U_c G}\frac{B}{G}\sin(\delta_s - \delta_c), \tag{4.38}$$

with solution

$$\sin(\delta_s - \delta_c) = \frac{\frac{B(P_s + U_s^2 \cdot G)}{U_s \cdot U_c \cdot G^2} \pm \sqrt{\frac{B^2 (P_s + U_s^2 \cdot G)^2}{(U_s \cdot U_c)^2 \cdot G^4} - \frac{B^2}{G^2 + 1}\left(\frac{(P_s + U_s^2 \cdot G)^2}{(U_s \cdot U_c \cdot G)^2} - 1\right)}}{\frac{B^2}{G^2} + 1}. \tag{4.39}$$

The solution with the plus sign should be retained, which can be verified by simply calculating $\sin(\delta_s - \delta_c)$ from δ_s and δ_c, which are in fact known. Substituting $\cos(\delta_s - \delta_c)$ and $\sin(\delta_s - \delta_c)$ in

$$Q_s = U_s^2 B + U_s U_c [G\sin(\delta_s - \delta_c) - B\cos(\delta_s - \delta_c)] \tag{4.40}$$

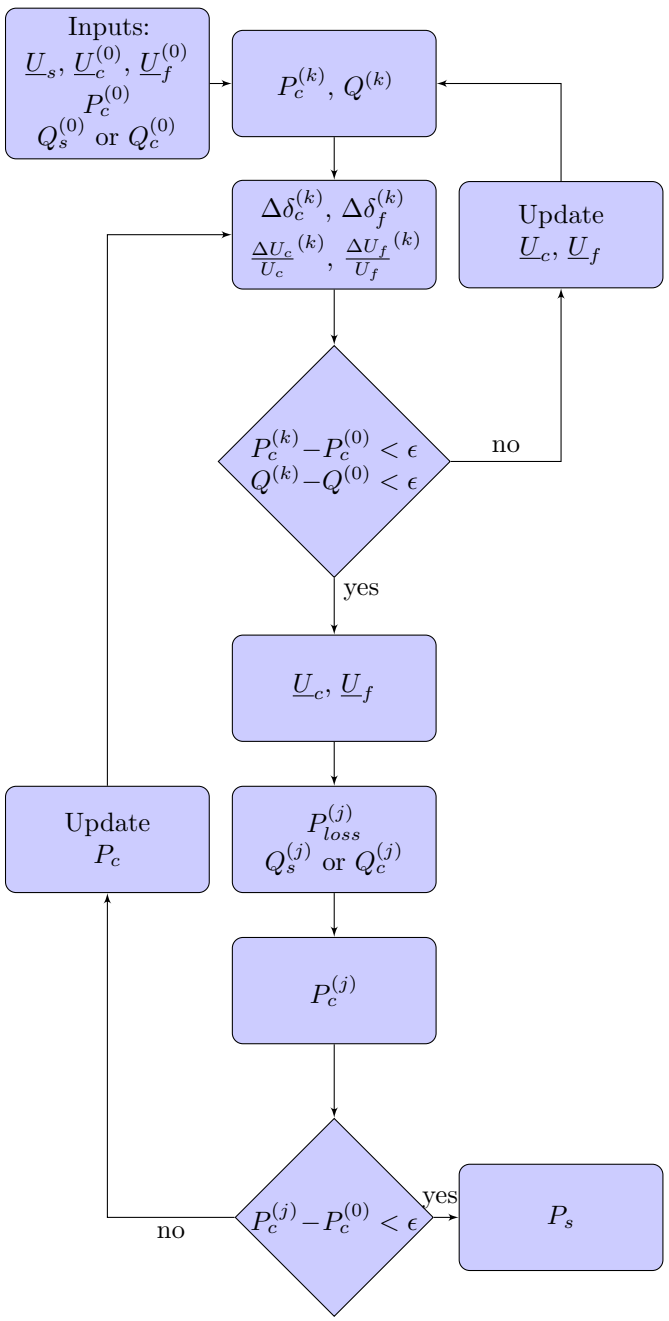

Figure 4.10: Flow chart for iterative calculation for slack bus with filter.

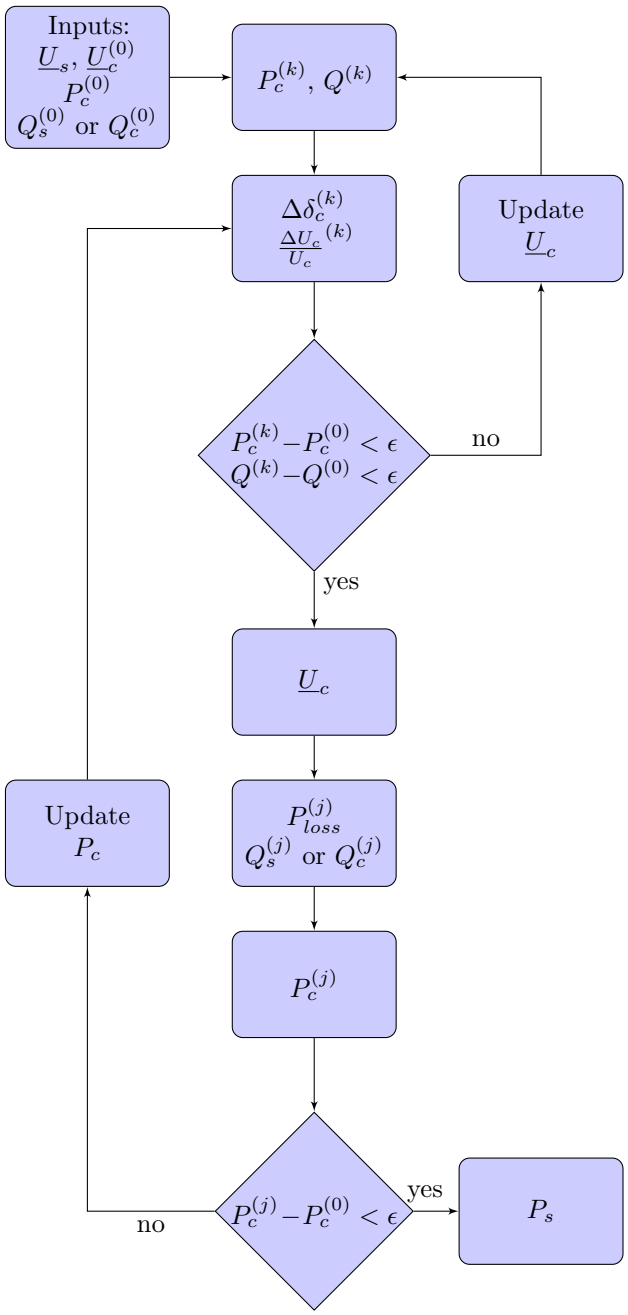

Figure 4.11: Flow chart for iterative calculation slack bus without filter.

and substituting U_c by $U_c^{(max)}$ or $U_c^{(min)}$ gives an analytical expression for the lower and upper limit of reactive power. The reactive power limit is calculated in function of varying δ_c using the exact and simplified approach and plotted for $R = 0.01$ p.u. in Fig. 4.12. If R is lower, the difference between the curves is less pronounced. Note that in a numerical computation, there is no need to solve a quadratic equation to obtain $\sin(\delta_s - \delta_c)$ as we did it here; it can be directly calculated because δ_s and δ_c are known. In HVDC systems that use PWM, the minimum reactive power corresponds to a lower limit of the modulation factor. Reducing it below the minimum value will give rise to the reappearance of harmonics. In [76], the minimum reactive power limit is a constant at -0.5 p.u. The maximum reactive power can be calculated as the minimum value of (4.40) and $Q = \sqrt{U_s \cdot I_{eq}^{max} - P^2}$, from (2.5).

When a limit is hit, the current or voltage can be brought back within bounds by reducing P or Q. In practice, priority is always given to P, and Q is tailored as much as necessary. The procedure for incorporating limits in power flow is well known from e.g. generators' reactive power limits: before starting a power flow calculation, the active power set points should not be higher than rated power, otherwise they must be reduced to their maximum value. For VSC HVDC systems it must be additionally ascertained during calculation that the slack converter's active power is within bounds. It is then checked whether a Q limit is hit. If so, the voltage controlled bus should be changed to a PQ bus with a scheduled Q. There are two ways to check for limits. The first one is checking the limits after the power flow converged. If one or more limits are hit, the most stringent one is enforced and the convergence flag is reset. The second way is to check and enforce the limits during each iteration. A variant often used in conjunction with the Newton-

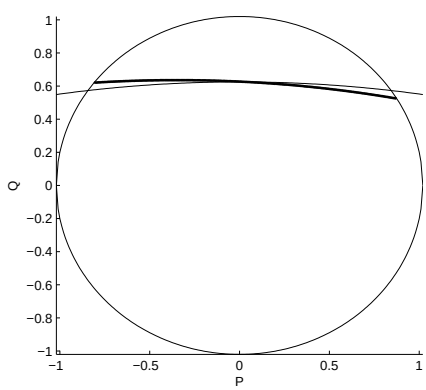

Figure 4.12: Power circle with voltage limit. The bold line represents the exact voltage limit with $R = 0.01$ p.u.

Raphson method is to iterate a few times without limit checking, before enforcing limits. Both methods proved unsatisfactory for enforcing varying Q limits, as they lead to convergence problems. The difference with enforcing generator limits is that the Q limit needs to be updated every iteration, while generator limits are usually approximated by constant values, even if this approximation becomes quite crude for modern generators with high rated power factors and high synchronous reactances [77]. We found that checking the limits after every iteration, but only updating their value every three iterations, led to convergence for the test case introduced in section 4.5.1. An option can be provided to start limit checking not from the first iteration. After convergence, the limits have to be recalculated and checked and the convergence flag may need to be reset.

4.4.7 Evaluation

The AC/MTDC power flow for VSC converters presented here, is the most detailed one available, and has an edge over other models proposed in the literature. It works for every topology of the DC grid, includes a quadratic converter loss model and an accurate representation of operating limits. The resistive component of the phase reactor and transformer are not neglected, and the filter is included. The model correctly converges to set points at the system bus, not at the filter or even converter bus.

The complexity of the method as presented here, is fairly high: there are a total of five iterative calculations: a main iteration, an AC power flow iteration, a DC power flow iteration, and a slack converter iteration with nested iteration for the determination of the losses. However, the last two iterations only involve one bus and are hence very fast.

4.5 Validation and Comparison

4.5.1 Test Case

The models and solution methods developed in this chapter are now validated by comparing the results with those obtained with two commercial models, both implemented in PSS/E. The first model comes with PSS/E, the second one, the HVDC Light model, is a manufacturer developed model.

The VSC HVDC model that comes with PSS/E consists of three modules: one DC line model (DCLINE), and two converter modules (VSCDYN), integrated as shown on Fig. 4.13. The system is connected between the filter buses: active power and voltage set point are specified with respect to the filter bus. Transformers and

filters connected to the filter bus should be modelled explicitly by a transformer record and a fixed or switched capacitive shunt record. The converter bus is not accessible by the user, and any information about the phase reactor, such as its impedance, or current is absent. In the DCLINE record, the line resistance must be specified. In the VSCDYN record it must be specified whether the converter controls active power or DC voltage, and whether it controls AC voltage or maintains a fixed power factor. Actually, the model does not distinguish between a converter controlling active power and a converter controlling DC voltage. The converters are both controlling active power: the slave converter calculates its power set point from the master controller's power set point. Such a set-up is never used in practice, but is acceptable for power flow calculations. The model includes operating limits, and a linear loss model, consisting of fixed losses [kW] and losses linearly dependent on the DC current [kW/A]. The model does not support multi-terminal calculations [78]. Actually, the model is of the simplified type, with a few additions such as operating limits and a loss model.

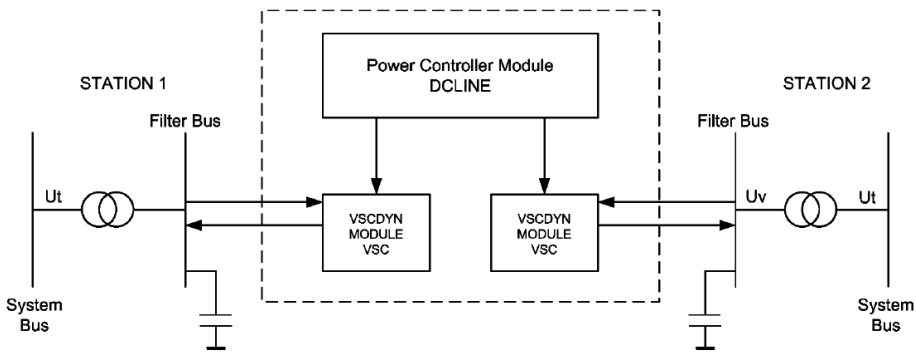

Figure 4.13: PSS/E model [78].

In the HVDC Light model, shown in Fig. 4.14, the converters are modelled as generators and no DC line is modelled. The model is thus also of the simplified type. The model is designed with dynamic simulations in mind. The power flow has to be merely seen as a means of obtaining a starting point for the dynamic analysis. Filters and transformers are added separately. As is the case in the PSS/E model, the filter bus is not accessible. However, the impedance of the phase reactor, which should be purely inductive, can be added as parameter XSORCE in the generator record. It is not used in power flow calculations, but becomes available for use in fault analysis and dynamic analysis after the generators have been converted by the PSS/E activity CONG. The model could in principle be used for multi-terminal power flow calculations, but in dynamic simulations, MTDC is not supported.

The features of the three models are compared in Table 4.1.

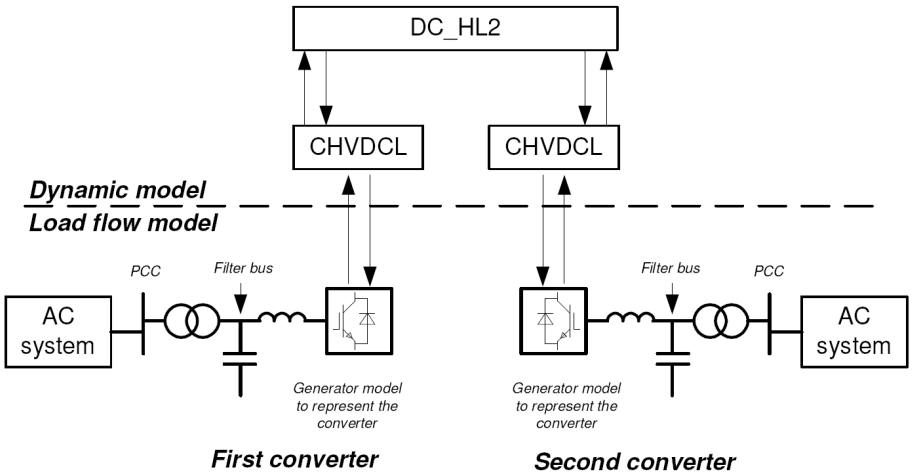

Figure 4.14: HVDC Light model [76].

Table 4.1: Comparison between models.

	PSS/E model	HVDC Light model	Detailed model
converter bus	not accessible	not modelled	accessible
phase reactor	not accessible	accessible	accessible
filter	part of AC grid	part of AC grid	part of VSC
transformer	part of AC grid	part of AC grid	part of VSC
losses	linear in I_{dc}	not modelled	quadratic in I_{pr}
limits	not in PF	not modelled	exact I and U limits
DC network	two-terminal	not modelled	multi-terminal
MTDC	not supported	supported	supported

For the comparison between the models, a simple but not trivial 7 bus test network with 2 generators is used (Fig. 4.15). The data is given in Table 4.2. For the VSC HVDC system, actual data are provided by the manufacturer. The data of this HVDC Light 'M1' system, valid for 50 Hz systems, is given in Table 4.3 [76]. One change had to be made: the filters provide 10 MVar instead of 15.15 MVar, as otherwise the PSS/E model converged to a filter bus voltage that deviated slightly from the set point. The data can be directly added in the HVDC Light model. In the PSS/E model, both converters are set to voltage control. All parameters can be directly inserted except the DC line resistance which has to be transformed to its actual value expressed in Ω.

Table 4.2: Test network data.

bus	data
2	P = -50 MW
	Q = -10 MVar
3	$\delta = 0$
	U = 1 p.u.
4	P = 50 MW
	U = 1 p.u.
5	P = -200 MW
	Q = -30 MVar

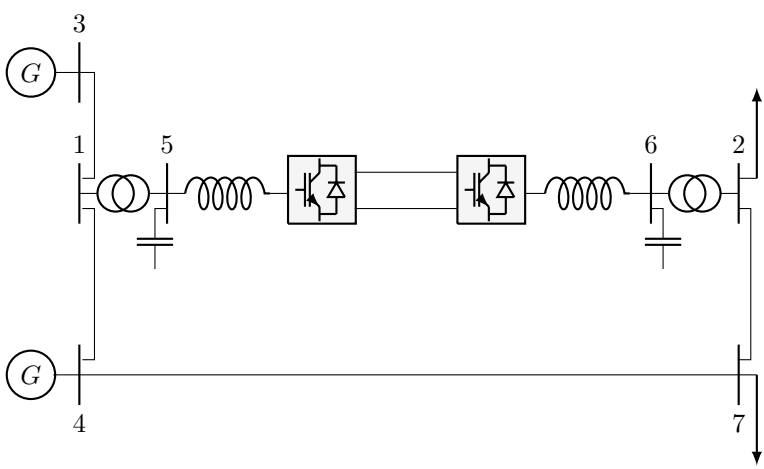

Figure 4.15: Single-line diagram of the test network.

Table 4.3: HVDC Light 'M1' data sheet.

Converter	
Base MVA	101
Base kV	80
X_{pr} [p.u.]	0.16428
R_{pr} [p.u.]	0
P_{max} [MW]	98.7
P_{min} [MW]	-102
Filter	
MVar	15.15
Voltage [kV]	104
Transformer	
Base MVA	107
X_{tr} [p.u.]	0.12
R_{tr} [p.u.]	0
DC line	
Resistance [p.u.]	0.001

4.5.2 Calculations

The simplified model is validated by comparing it with the HVDC Light model. The detailed model is validated in different steps. In a first step, losses are neglected. Subsequently, constant and linear losses are added. Lastly, the effect of including the filter bus is shown by comparing the detailed model including filter bus with the PSS/E model.

Simplified Model

The simplified model, implemented in MATPOWER is compared with the HVDC Light and PSS/E model. The converters' active power set points are -102 MW and 93 MW. The results are the same for the three models, and are shown in Tables 4.4 and 4.5

Table 4.4: Results simplified model: bus voltages.

bus	U [p.u.]	δ [deg]
1	0.999	-1.21
2	0.994	-2.46
3	1.000	0.00
4	1.000	-1.84
5	1.000	-8.25
6	1.000	3.99
7	0.994	-2.72

Table 4.5: Results simplified model: branch flows.

bus		from bus injection		to bus injection	
from	to	P [MW]	Q [MVar]	P [MW]	Q [MVar]
3	1	209.8	-9.5	-209.4	13.9
1	4	107.4	-19.4	-107.3	20.6
2	7	43.0	-10.00	-43	10.20
4	7	157.3	42.8	-157.0	-40.1
1	5	102.00	5.5	-102.00	7.0
6	2	93.00	10.5	-93.00	0.00
5	6	102.0	3.0	-93.0	-0.5

Detailed Model Without Losses

The detailed model is compared with the PSS/E, the HVDC Light, and the simplified model. All losses are neglected. The filter bus is not modelled as part of the converter in the detailed model so that the set points in all models are defined with respect to the same bus. The DC resistance is set to a very low value, but not to zero since this would lead to a singular matrix. The four models give exactly the same results up to the accuracy displayed in Tables 4.6 and 4.7.

Table 4.6: Results detailed model without losses: bus voltages.

bus	U [p.u.]	δ [deg]
1	0.999	-1.16
2	0.994	-2.25
3	1.000	0.00
4	1.000	-1.73
5	1.000	-8.19
6	1.000	4.82
7	0.994	-2.56

Table 4.7: Results detailed model without losses: branch flows.

bus		from bus injection		to bus injection	
from	to	P [MW]	Q [MVar]	P [MW]	Q [MVar]
3	1	200.8	-8.9	-200.4	12.9
1	4	98.4	-18.5	-98.3	19.5
2	7	52.0	-11.0	-52.0	11.3
4	7	148.3	43.7	-148.0	-41.3
1	5	102.0	5.5	-102.0	7.0
6	2	102.0	11.6	-102.0	1.0
5	6	102.0	3.0	-102.0	-1.6

Detailed Model with Constant Converter Losses and DC Line Losses

The converter loss coefficients of the Södra Länken project, defined on a base of 300 kV and 600 MVA, are used (Table 4.8) [75].

Table 4.8: Converter loss coefficients Södra Länken.

	constant [MW]	linear [kV]	quadratic [Ω]
	a	b	c
rectifier	6.62	1.8	1.98
inverter	6.62	1.8	3.00

The constant loss coefficient is scaled down to the appropriate MVA base. The results are shown in Tables 4.9 and 4.10. The results obtained with the detailed model exactly match those obtained with the PSS/E model and the HVDC Light model.

Table 4.9: Results detailed model with constant converter losses and DC line losses: bus voltages.

bus	U [p.u.]	δ [deg]
1	0.999	-1.17
2	0.994	-2.31
3	1.000	0.00
4	1.000	-1.76
5	1.000	-8.21
6	1.000	4.61
7	0.994	-2.60

Table 4.10: Results detailed model with constant converter losses and DC line losses: branch flows.

bus		from bus injection		to bus injection	
from	to	P [MW]	Q [MVar]	P [MW]	Q [MVar]
3	1	203.1	-9.1	-202.7	13.2
1	4	100.7	-18.7	-100.6	19.8
2	7	49.7	-10.8	-49.7	11.0
4	7	150.6	43.5	-150.3	-41.0
1	5	102.0	5.5	-102.0	7.0
6	2	99.7	11.3	-99.7	0.8
5	6	102.0	-3.0	-99.7	1.3

Detailed Model with Linear Loss Model

The previous simulation is augmented by adding linear loss coefficients. In PSS/E, this coefficient is entered in kW/A. It is calculated by multiplying the p.u. value by the base kVA and dividing by the base current. The results are shown in Tables 4.11 and 4.12 for the PSS/E model, and Tables 4.13 and 4.14 for the detailed model. The results do not match perfectly as the losses in the PSS/E model linearly depend on DC current, not on phase reactor current. No comparison with the HVDC Light model is given, because the linear losses are hard to estimate a priori.

Table 4.11: Results PSS/E model with linear loss model: bus voltages.

bus	U [p.u.]	δ [deg]
1	0.999	-1.18
2	0.994	-2.34
3	1.000	0.00
4	1.000	-1.78
5	1.000	-8.22
6	1.000	4.46
7	0.994	-2.63

Table 4.12: Results PSS/E model with linear loss model: branch flows.

bus		from bus injection		to bus injection	
from	to	P [MW]	Q [MVar]	P [MW]	Q [MVar]
3	1	204.7	-9.2	-204.3	13.4
1	4	102.3	-18.9	-102.2	19.9
2	7	48.1	-10.6	-48.1	10.8
4	7	152.2	43.6	-151.9	-40.8
1	5	102.0	5.5	-102.0	7.0
6	2	98.1	11.1	-98.1	0.6
5	6	102.0	3.0	-98.1	-1.1

Table 4.13: Results detailed model with linear loss model: bus voltages.

bus	U [p.u.]	δ [deg]
1	0.999	-1.17
2	0.994	-2.32
3	1.000	0.00
4	1.000	-1.76
5	1.000	-8.21
6	1.000	4.57
7	0.994	-2.61

Table 4.14: Results detailed model with linear loss model: branch flows.

bus		from bus injection		to bus injection	
from	to	P [MW]	Q [MVar]	P [MW]	Q [MVar]
3	1	203.5	-9.1	-203.1	13.2
1	4	101.1	-18.7	-101.0	19.8
2	7	49.3	-10.7	-49.3	11.0
4	7	151.0	43.5	-150.7	-41.0
1	5	102.0	5.5	-102.0	7.0
6	2	99.3	11.3	-99.3	0.7
5	6	102.0	3.0	-99.3	-1.3

Full Model vs PSS/E and HVDC Light Model

Finally, the detailed sequential model, that includes the filter buses, is compared with the PSS/E and HVDC Light models. DC conductor losses are taken into account. The converter losses are represented by a constant loss only, as the linear loss component is calculated differently in the PSS/E model and the quadratic loss coefficient not present. By doing so, the influence of explicitly modelling the filter bus, is isolated. The transformer resistance is 0.002 p.u. In Tables 4.15 and 4.16, the results for the PSS/E model and HVDC Light model are shown. The results match, except on branch 2-7 where the HVDC Light model gives -12.1 instead of -12.2 MVar. This is probably due to the truncation of the active power set point of the HVDC Light model's second converter.

Table 4.15: Results PSS/E and HVDC Light model: bus voltages.

bus	U [p.u.]	δ [deg]
1	0.999	-1.17
2	0.993	-2.31
3	1.000	0.00
4	1.000	-1.76
5	1.000	-8.22
6	1.000	4.60
7	0.994	-2.60

Table 4.16: Results PSS/E and HVDC Light model: branch flows.

bus		from bus injection		to bus injection	
from	to	P [MW]	Q [MVar]	P [MW]	Q [MVar]
3	1	203.5	-9.9	-203.1	14.0
1	4	100.9	-17.9	-100.8	19.0
2	7	49.5	-12.2	-49.5	12.4
4	7	150.8	44.9	-150.5	-42.4
1	5	102.2	3.9	-102.0	8.7
6	2	99.7	9.9	-99.5	2.2
5	6	102.0	1.3	-99.7	0.1

The results of the detailed model are shown in Tables 4.17 and 4.18. The susceptance of the filter is chosen such that the reactive power is 10 MVar at a filter bus voltage of 1 p.u. From these results it is seen that the scheduled power of 102 MW correctly appears on bus 1, and that the voltage is exactly 1 p.u. at the system buses 1 and 2, not at the filter buses.

Table 4.17: Results detailed model: bus voltages.

bus	U [p.u.]	δ [deg]
1	1.000	-1.18
2	1.000	-2.35
3	1.000	0.00
4	1.000	-1.76
5	1.021	-8.12
6	1.046	4.18
7	0.997	-2.62

Table 4.18: Results detailed model: branch flows.

bus		from bus injection		to bus injection	
from	to	P [MW]	Q [MVar]	P [MW]	Q [MVar]
3	1	203.5	-18.2	-203.1	22.4
1	4	101.1	-9.6	-101.0	10.6
2	7	49.3	20.9	-49.2	-20.6
4	7	151.0	11.7	-150.8	-9.4
1	2	102.0	-12.83	-99.26	-30.87

4.6 Continuation Methods

The Newton-Raphson algorithm can fail due to a number of reason such as an initial guess outside a solution's region of attraction, oscillation around the solution, or overflow. Another common cause is a singular or nearly-singular Jacobian. In the context of power systems this can occur when the system is heavily loaded. Continuation methods allow tracing a solution curve through points where the conventional power flow Newton-Raphson would fail. Often,

such points contain important information about the system. An example is the point of maximum loadability on the PV curve for constant power loads. Usually, continuation methods are applied to the system G_2. The method is then called continuation power flow, but they can be also applied to the full DAE system. The analysis then gives far more information and insight about the system. In this work we focus on the most general case, i.e. the full DAE system.

4.6.1 Numerical Aspects of Continuation Methods

Predictor-Corrector Continuation Algorithms

A continuation problem can be seen as the numerical equivalent of the Implicit Function Theorem. According to this theorem, applied to the map

$$(\boldsymbol{x}, \alpha) \mapsto F(\boldsymbol{x}, \alpha), \boldsymbol{x} \in \mathbb{R}^n, \alpha \in \mathbb{R}, \tag{4.41}$$

there exists a unique continuum of solutions near the equilibrium point, if the Jacobian of F is invertible. The continuation method finds this continuum numerically by for instance a predictor-corrector method. The predictor step finds a point close to the curve in a given search direction. The corrector calculates a point on the curve by applying a Newton method. If the point obtained from the predictor step is outside the region of attraction of the Newton method, the predictor step is repeated with a smaller step size from a previous solution. Note that an extra scalar equation $H(\boldsymbol{Z})$, with $\boldsymbol{Z} = [\boldsymbol{X}, \boldsymbol{Y}, \alpha]$ has to be appended to (3.3) in order to apply a Newton method:

$$\Sigma_C : \begin{cases} F(\boldsymbol{Z}) = 0 \\ G(\boldsymbol{Z}) = 0 \\ H(\boldsymbol{Z}) = 0 \end{cases} \tag{4.42}$$

Most functions have natural parameters, for instance power system loading. When such a parameter is chosen as continuation parameter, the method is referred to as natural parameter continuation. In the corrector step, a Newton method calculates the point that lies on the curve and in a hyperplane orthogonal to the natural parameter's coordinate axis and containing the predictor point. This method is straightforward and computationally light. However, when the curve is folding with respect to the selected coordinate axis, the method fails. At such points, the Jacobian is singular which means that the conditions of the Implicit Function Theorem are no longer satisfied. For the calculation of PV curves, P can be selected as the natural parameter, but the method still fails. A solution is to check at each step the components of the direction vector and select the one with the maximum absolute value.

An alternative method uses a parametrisation by arclength [79]. It can be shown to converge for a sufficiently small step size. Suppose a starting point $\boldsymbol{Z_0} = [\boldsymbol{X_0}, \boldsymbol{Y_0}, \alpha_0]$ and the tangent vector in this point $\boldsymbol{v_0}$, are known. A predictor point $\tilde{\boldsymbol{Z}}$ is found by

$$\tilde{\boldsymbol{Z}} = \boldsymbol{Z_0} + \Delta s \cdot \boldsymbol{v_0}, \tag{4.43}$$

with Δs the step size. In this so-called pseudo-arclength method, $H(\boldsymbol{Z})$ is the equation of a hyperplane through $\tilde{\boldsymbol{Z}}$, orthogonal to $\boldsymbol{v^0}$:

$$H(\boldsymbol{Z}) = \langle \boldsymbol{Z} - \tilde{\boldsymbol{Z}}, \boldsymbol{v} \rangle. \tag{4.44}$$

The corrector step calculates the nonlinear system Σ_C by a Newton method. The Newton steps are:

$$\boldsymbol{Z}^{k+1} = \boldsymbol{Z}^k - \begin{bmatrix} \mathsf{J}_\mathsf{Z}(\boldsymbol{Z}^k) \\ \boldsymbol{v_i}^T \end{bmatrix}^{-1} \begin{bmatrix} F(\boldsymbol{Z}^k) \\ 0 \end{bmatrix}, \tag{4.45}$$

with

$$\mathsf{J}_\mathsf{Z} = \begin{bmatrix} \frac{\partial F}{\partial \boldsymbol{X}} & \frac{\partial F}{\partial \boldsymbol{Y}} & \frac{\partial F}{\partial \alpha} \\ \frac{\partial G}{\partial \boldsymbol{X}} & \frac{\partial G}{\partial \boldsymbol{Y}} & \frac{\partial G}{\partial \alpha} \end{bmatrix}. \tag{4.46}$$

The next direction vector can be calculated by solving

$$\begin{bmatrix} \mathsf{J}_\mathsf{Z} \\ \boldsymbol{v_i}^T \end{bmatrix} \boldsymbol{v_{i+1}} = \begin{bmatrix} \boldsymbol{0} \\ 1 \end{bmatrix}. \tag{4.47}$$

This follows directly from (4.44) and from the requirement that tangent vectors be normalised. It follows from the above that two linear systems have to be solved to obtain the next point on the curve and its corresponding direction vector:

$$\begin{bmatrix} \mathsf{J}_\mathsf{Z}(\boldsymbol{Z_i}) \\ \boldsymbol{v_i}^T \end{bmatrix} \boldsymbol{\Delta Z} = \begin{bmatrix} -F(\boldsymbol{Z_i}) \\ 0 \end{bmatrix}, \tag{4.48}$$

$$\begin{bmatrix} \mathsf{J}_\mathsf{Z}(\boldsymbol{Z_i}) \\ \boldsymbol{v_i}^T \end{bmatrix} \boldsymbol{v_{i+1}} = \begin{bmatrix} \boldsymbol{0} \\ 1 \end{bmatrix}. \tag{4.49}$$

Eqs. (4.48) and (4.49) can be written as a single matrix equation:

$$\begin{bmatrix} \mathsf{J}_\mathsf{Z}(\boldsymbol{Z_i}) \\ \boldsymbol{v_i}^T \end{bmatrix} \begin{bmatrix} \boldsymbol{\Delta Z} & \boldsymbol{v_{i+1}} \end{bmatrix} = \begin{bmatrix} -F(\boldsymbol{Z_i}) & \boldsymbol{0} \\ \boldsymbol{0} & 1 \end{bmatrix}. \tag{4.50}$$

Detecting and Locating Singular Points

To detect a bifurcation point, a test function is evaluated at each step of the continuation algorithm. The test function is zero at the bifurcation point and changes sign if the bifurcation point is located between two steps. Formally, a bifurcation point is detected between points $\boldsymbol{Z}^k$ and $\boldsymbol{Z}^{k+1}$ by the test function $H(\boldsymbol{Z})$ if:

$$H(\boldsymbol{Z}^k)H(\boldsymbol{Z}^{k+1}) < 0. \tag{4.51}$$

A condition for the fold bifurcation is that the system Jacobian is singular, or alternatively that it has a zero eigenvalue λ. Hence, two suitable test functions for the fold bifurcation are:

$$H_F = det \begin{pmatrix} \frac{\partial F}{\partial \boldsymbol{X}} & \frac{\partial F}{\partial \boldsymbol{Y}} \\ \frac{\partial G}{\partial \boldsymbol{X}} & \frac{\partial G}{\partial \boldsymbol{Y}} \end{pmatrix}, \tag{4.52}$$

and

$$H_F = \lambda_1 \cdot \lambda_2 \cdots \lambda_n. \tag{4.53}$$

Additionally, some transversality conditions must hold.

The Hopf bifurcation is characterised by a pair of complex eigenvalues crossing the imaginary axis. It can be verified that the test function

$$H_H = \prod_{i>j} (\lambda_i + \lambda_j), \tag{4.54}$$

is zero when this happens [80].

A Singularity Induced Bifurcation (SIB) arises when $\partial G/\partial \boldsymbol{Y}$ is singular. A test function for the SIB is thus:

$$H_S = det \left(\frac{\partial G}{\partial \boldsymbol{Y}} \right). \tag{4.55}$$

To derive a test function for the Limit Induced Bifurcation (LIB), the standard DAE formulation is rewritten in a form that allows direct application of the Complementary Limit Induced Bifurcation Theorem [81]:

$$F(\boldsymbol{X}, \boldsymbol{Y}, z_1, z_2, p) = 0 \tag{4.56}$$

$$G(\boldsymbol{X}, \boldsymbol{Y}, z_1, z_2, p) = 0 \tag{4.57}$$

$$z_1 \cdot z_2 = 0, \tag{4.58}$$

with z_1 and z_2 the output of a limiter. The test function then follows directly from the Complementary Limit Induced Bifurcation Theorem:

$$H_L = \begin{bmatrix} z_1 \\ z_2 \end{bmatrix}. \tag{4.59}$$

Note that the condition

$$det \begin{bmatrix} \frac{\partial F}{\partial \boldsymbol{X}} & \frac{\partial F}{\partial \boldsymbol{Y}} & \frac{\partial F}{\partial z_1} \\ \frac{\partial G}{\partial \boldsymbol{X}} & \frac{\partial G}{\partial \boldsymbol{Y}} & \frac{\partial G}{\partial z_1} \end{bmatrix} \Bigg|_{(\boldsymbol{X_0},\boldsymbol{Y_0},0,0,p)} \cdot det \begin{bmatrix} \frac{\partial F}{\partial \boldsymbol{X}} & \frac{\partial F}{\partial \boldsymbol{Y}} & \frac{\partial F}{\partial z_2} \\ \frac{\partial G}{\partial \boldsymbol{X}} & \frac{\partial G}{\partial \boldsymbol{Y}} & \frac{\partial G}{\partial z_2} \end{bmatrix} \Bigg|_{(\boldsymbol{X_0},\boldsymbol{Y_0},0,0,p)} > 0 \tag{4.60}$$

states that the stability changes at the point $(\boldsymbol{X}, \boldsymbol{Y}, 0, 0, p_0)$. If it is not satisfied, the point cannot be called a bifurcation point. However, this condition is not enforced, as points not satisfying (4.60) are important points nevertheless.

After a singular point has been detected, it can be located accurately by solving system Σ_c (4.42), with appropriate H function for every type of singular point.

Two Parameter Continuation of Singular Points

An additional parameter α_2 can be freed, $\boldsymbol{Z}$ and the tangent vector $\boldsymbol{v}$ then have one extra dimension. The same continuation methods that were used for the continuation of equilibrium points can be used. One additional equation is needed for the Newton corrector steps. Such an equation could be a test function H for a singular point. In a first step, use equilibrium continuation to detect singular points. Then a second parameter is freed and a chosen singular point is continued. On the obtained curve, codimension two bifurcations can be detected. For instance on a fold curve in a pure ODE system, Bogdanov-Takens, Zero-Hopf, Cusp, and Branch bifurcations can be detected. Such codimension two singular points are of limited importance in power systems, and are not further discussed.

For the localisation and continuation of singular points, the system Σ_C must be solved. As this system is nonlinear, a Newton method is used, which requires building the Jacobian

$$\begin{bmatrix} \frac{\partial F}{\partial \boldsymbol{X}} & \frac{\partial F}{\partial \boldsymbol{Y}} & \frac{\partial F}{\partial \alpha_1} & \frac{\partial F}{\partial \alpha_2} \\ \frac{\partial G}{\partial \boldsymbol{X}} & \frac{\partial G}{\partial \boldsymbol{Y}} & \frac{\partial G}{\partial \alpha_1} & \frac{\partial G}{\partial \alpha_2} \\ \frac{\partial H}{\partial \boldsymbol{X}} & \frac{\partial H}{\partial \boldsymbol{Y}} & \frac{\partial H}{\partial \alpha_1} & \frac{\partial H}{\partial \alpha_2} \end{bmatrix}. \tag{4.61}$$

For $H = H_L$, the calculation of the Jacobian is straightforward. However, for folds, SIBs, and Hopf points, H contains either all eigenvalues of the system Jacobian, or its determinant. This means that for each point on the continuation curve, either all eigenvalues of the system Jacobian, or its determinant must be calculated, which is very costly for large systems. Furthermore, the Jacobian of H must be

calculated as well at each point. It is clear that this is not viable in practice. Recent developments in the field of numerical mathematics provide means to efficiently calculate Σ_C using bordered matrices.

Bordered Matrices

A system Σ_C is solved for continuation of equilibria, and localisation and continuation of singular points. It is thus of great importance in continuation methods to solve Σ_C efficiently, with a robust method. The solution of Σ_C may run into problems close to singular points. At singular points, the Jacobian is singular. However, by appending elements to the Jacobian, it can be made nonsingular. In general, the bordered matrix M of a matrix A is:

$$\mathsf{M} = \begin{bmatrix} \mathsf{A} & \boldsymbol{b} \\ \boldsymbol{c}^T & d \end{bmatrix}, \tag{4.62}$$

where $\mathsf{A} \in \mathbb{R}^{nxn}$, $\boldsymbol{b}, \boldsymbol{c} \in \mathbb{R}^n, d \in \mathbb{R}$. It can be shown that $\boldsymbol{b}, \boldsymbol{c}$ and d can be chosen such that M is nonsingular. In practice d can be chosen zero and $\boldsymbol{c}$ and $\boldsymbol{b}$ are the eigenvectors of A and A^t respectively [80, p.502]. The system

$$\mathsf{M} \begin{bmatrix} \boldsymbol{v} \\ s \end{bmatrix} = \begin{bmatrix} \boldsymbol{0} \\ 1 \end{bmatrix}, \tag{4.63}$$

can then be solved, where $v \in \mathbb{R}^n, s \in \mathbb{R}$. By applying Cramer's rule, s can be calculated as

$$s = \frac{det(\mathsf{A})}{det(\mathsf{M})}. \tag{4.64}$$

As $det(\mathsf{M}) \neq 0$, an equivalent condition for $det(\mathsf{A}) = 0$ is $s = 0$. This conditions does not require the calculation of the determinant of A. Furthermore, if the transposed system,

$$\mathsf{M}^T \begin{bmatrix} \boldsymbol{w} \\ s \end{bmatrix} = \begin{bmatrix} \boldsymbol{0} \\ 1 \end{bmatrix}, \tag{4.65}$$

which has the same solution for s as (4.63), is also solved, the derivatives of s can be calculated in function of the derivatives of A as [82]:

$$\frac{\partial s}{\partial \boldsymbol{Z}} = -\boldsymbol{w}^T \frac{\partial \mathsf{A}}{\partial \boldsymbol{Z}} \boldsymbol{v}. \tag{4.66}$$

Bordered matrix systems can be solved by standard linear solvers. However, for large systems it is advantageous to use special purpose solvers. First of all, a

solver that exploits the sparsity of M should be used. When the number of state variables is high, A is usually sparse. M is also sparse, but the sparsity structure is different. Some manipulation on the system can be performed to exploit the sparsity of M. Also, there exist algorithms that can solve bordered systems using solvers for A and A^T only. The bordering algorithm requires solving $m+1$ linear systems. A stable algorithm for solving bordered systems is provided in [82].

This theory is now applied to the localisation and continuation of singular points. For fold and Hopf points, it is well described in the literature [80] how to proceed. For Hopf points the method is slightly involved because it requires the bialternate product. For SIBs, which do not occur in ODEs, no method using bordered matrices is provided in the literature yet. It is shown here that the system Σ_C for SIBs can be solved in a similar way as for fold points because H_F and H_S both involve the evaluation of the determinant of a Jacobian matrix. It was shown that it is sufficient to solve $s=0$. For the system Σ_C, $\mathsf{A}=[F,G,H]^T$ is defined and the bordered matrix system:

$$\begin{bmatrix} \mathsf{J} & \boldsymbol{w_{bor}} \\ \boldsymbol{v}_{bor}^T & 0 \end{bmatrix} \begin{bmatrix} \boldsymbol{v} \\ s \end{bmatrix} = \begin{bmatrix} \mathbf{0} \\ 1 \end{bmatrix}, \tag{4.67}$$

with

$$\mathsf{J} = \begin{bmatrix} \frac{\partial F}{\partial \boldsymbol{X}} & \frac{\partial F}{\partial \boldsymbol{Y}} & \frac{\partial F}{\partial \alpha_1} & \frac{\partial F}{\partial \alpha_2} \\ \frac{\partial G}{\partial \boldsymbol{X}} & \frac{\partial G}{\partial \boldsymbol{Y}} & \frac{\partial G}{\partial \alpha_1} & \frac{\partial G}{\partial \alpha_2} \\ \frac{\partial H}{\partial \boldsymbol{X}} & \frac{\partial H}{\partial \boldsymbol{Y}} & \frac{\partial H}{\partial \alpha_1} & \frac{\partial H}{\partial \alpha_2} \end{bmatrix}, \tag{4.68}$$

is solved. The system

$$\begin{bmatrix} \mathsf{J}^T & \boldsymbol{v_{bor}} \\ \boldsymbol{w_{bor}}^T & 0 \end{bmatrix} \begin{bmatrix} \boldsymbol{w} \\ s \end{bmatrix} = \begin{bmatrix} \mathbf{0} \\ 1 \end{bmatrix}, \tag{4.69}$$

is solved as well.

The derivatives $\partial H/\partial \boldsymbol{Z}$ can then be calculated as:

$$\frac{\partial H}{\partial \boldsymbol{Z}} = -\boldsymbol{w}^T \frac{\partial}{\partial \boldsymbol{Z}} \begin{pmatrix} \frac{\partial F}{\partial \boldsymbol{X}} & \frac{\partial G}{\partial \boldsymbol{Y}} \\ \frac{\partial G}{\partial \boldsymbol{X}} & \frac{\partial G}{\partial \boldsymbol{Y}} \end{pmatrix} \boldsymbol{v} \tag{4.70}$$

for folds and

$$\frac{\partial H}{\partial \boldsymbol{Z}} = -\boldsymbol{w}^T \frac{\partial}{\partial \boldsymbol{Z}} \left(\frac{\partial G}{\partial \boldsymbol{Y}} \right) \boldsymbol{v} \tag{4.71}$$

for SIBs, that is, in function of the derivatives of F and G only.

4.6.2 Continuation Methods: Example

Non-limited Case

We continue with the system of example 3.2. With the load active power P_l as continuation parameter, an equilibrium point is continued and singular points are detected and located. To obtain a PV curve, U_2 is plotted versus P_l. The PV curve thus obtained, is derived from the full system. Fig. 4.16 shows the PV curve. Even though no limits are present, still a fold occurs, which is in this case also a maximum loadability point. The fold and SIB are plotted as well as the determinant of $\partial G/\partial \boldsymbol{Y}$ and of J. It can be verified that they are zero at the SIB[1] and fold respectively.

The state space, projected on the most interesting dimensions, load voltage and the converter's reactive power, is plotted in Fig. 4.17. The equilibrium points and trajectories for a certain value of P_l are shown. Both equilibrium points are stable, which can be verified by either calculating the eigenvalues of the system Jacobian or by plotting the trajectories in function of time. For small changes of P_l, state space remains homeomorph, as no bifurcations are encountered. For larger variations, the equilibrium points become unstable after crossing the singular surface, then coalesce in a fold, and finally disappear. It is not apparent from the PV curve that there are two solutions. A three-dimensional PV curve is shown in (Fig. 4.18). Now it is clear that there are indeed two solutions, that coalesce in the folds.

Limited Case

In practice the converter's reactive power output is limited. If the converter is limited for every value of load power, the PV curve of a non-controlled PQ bus appears. If the converter is limited for some values of load power, the PV curve has a constant voltage section (Fig. 4.19). State space is restricted and all equilibria and singular points lie on the manifold of constant or maximum reactive power. A LIB occurs on the intersection of those two manifolds (Fig. 4.20).

[1] From the remark in Chapter 3 that the power system model can always be written as a DAE system of index 1, it follows that all SIBs can be removed from the model.

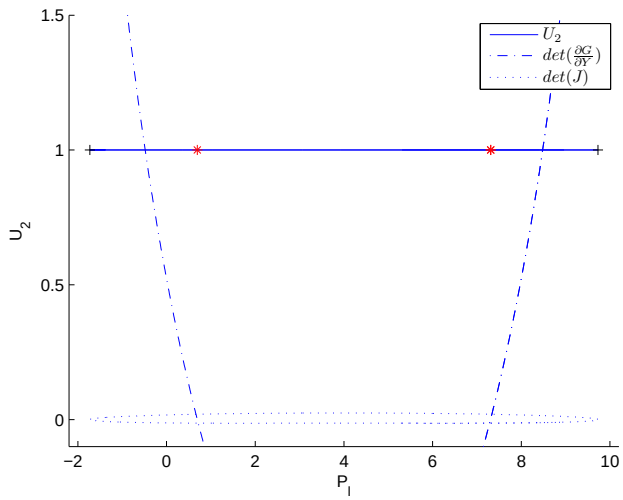

Figure 4.16: PV curve for the non-limited case. + denotes a fold, $*$ a SIB.

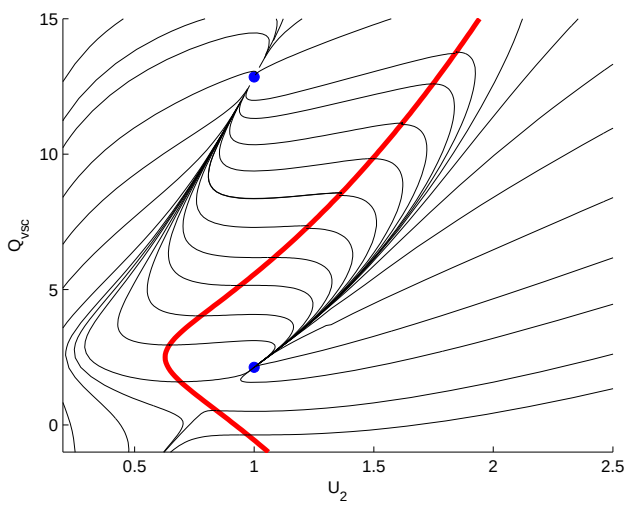

Figure 4.17: Trajectories in projection of state space for the non-limited case. • denotes an equilibrium point. The bold line represents the singular manifold S.

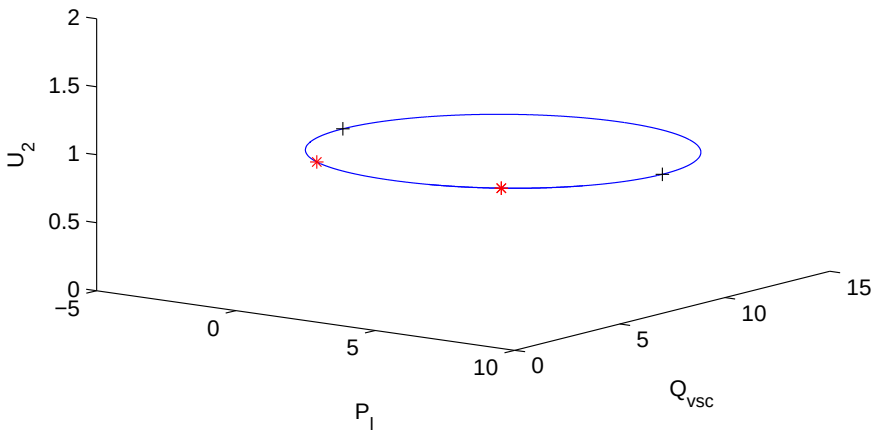

Figure 4.18: Three-dimensional PV curve for the non-limited case. + denotes a fold, ∗ a SIB.

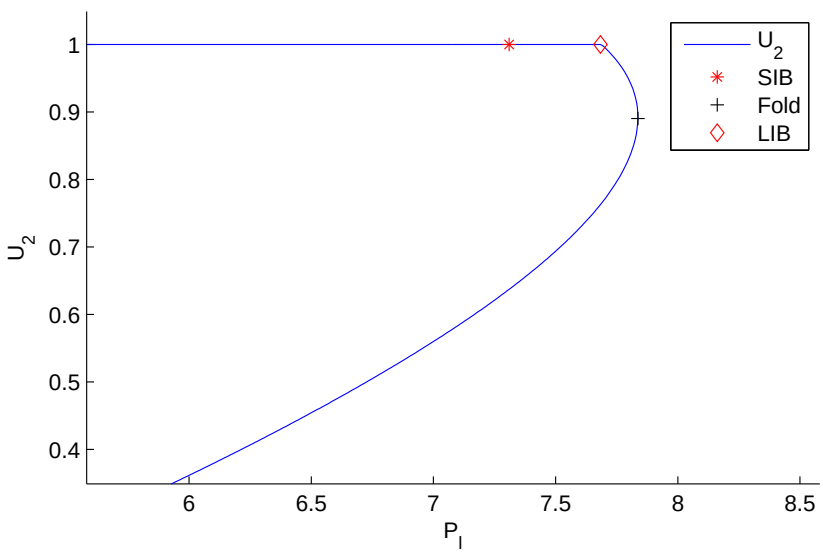

Figure 4.19: PV curve for the limited case.

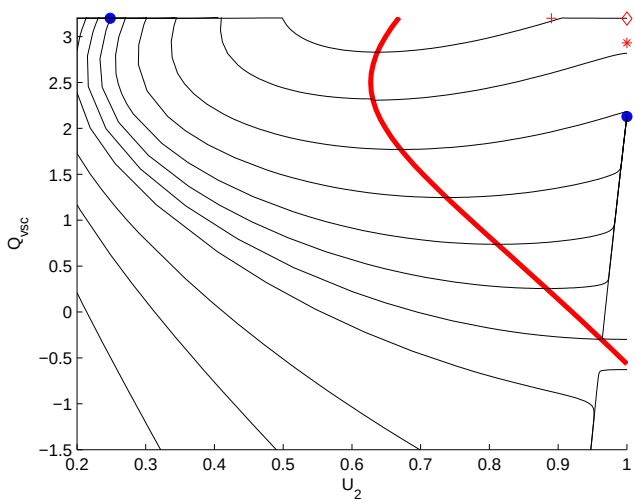

Figure 4.20: Trajectories in projection of state space for the limited case. • denotes an equilibrium point, + a fold, ∗ a SIB, and ⋄ a LIB. The bold line represents the singular manifold S.

Two-parameter Continuation

The continuation of LIB points is the set of points satisfying system Σ_c, with

$$H = \begin{bmatrix} U_2 - U_{ref} \\ Q_{vsc} - Q_{max} \end{bmatrix}. \tag{4.72}$$

Two logical choices for the second free parameter are Q_l and P_{VSC}. For $\alpha_2 = Q_l$, the relevant projection of parameter space is plotted in Fig. 4.21. This figure contains the information of all PV curves for all values of Q_l, as well as the stability of each operating point for every combination of P_l and Q_l. For high values of Q_l, no singular points are detected, because simply no equilibrium points exist. For lower Q_l, e.g. $Q_l = 3.7$ (Fig. 4.22), there are SIB and fold points, but no LIBs, meaning that the system is viable, but cannot maintain the desired voltage. If Q_l is even lower, e.g. $Q_l = 2.8$ (Fig. 4.23), the converter can maintain voltage up to a certain loading, then the voltage drops. For $Q_l = 2.3$ (Fig. 4.24), a SIB occurs before a LIB, however without changing the system's behaviour. It looks tempting to say that Q_l should be as low as possible, because loadability increases with decreasing Q_l. The problem is that below a certain value, the fold ceases to exist. This phenomenon of course does not occur when no limits are taken into account. At $Q_l = 2.0$ for instance (Fig. 4.25), two equilibrium points coalesce in a LIB, not a fold, under continuous change of P_l. Operation in this region is potentially dangerous: the voltage remains at 1 p.u. up to the LIB point. Passing the LIB point results in immediate collapse without warning. The power system then operates on the lower half of the curve, which is theoretically stable. Sustained operation in this region is not possible: it results in practice in voltage collapse.

The stability of equilibrium points can be directly seen from Fig. 4.26. The equilibrium is unstable between the SIB and fold continuation. For the parameter values in the shaded area, the equilibrium is stable. The region above the fold continuation is infeasible.

Parameter space is plotted for $\alpha_2 = P_{VSC}$ in Fig. 4.27. The graph can be interpreted in the same way as Fig. 4.26. The seemingly obvious reasoning, that it suffices to increase P_{VSC} to increase the loadability, confirmed by Fig. 4.27, is proven wrong if the reactive power limit is calculated exactly, i.e. taking into account both voltage and current limit [83].

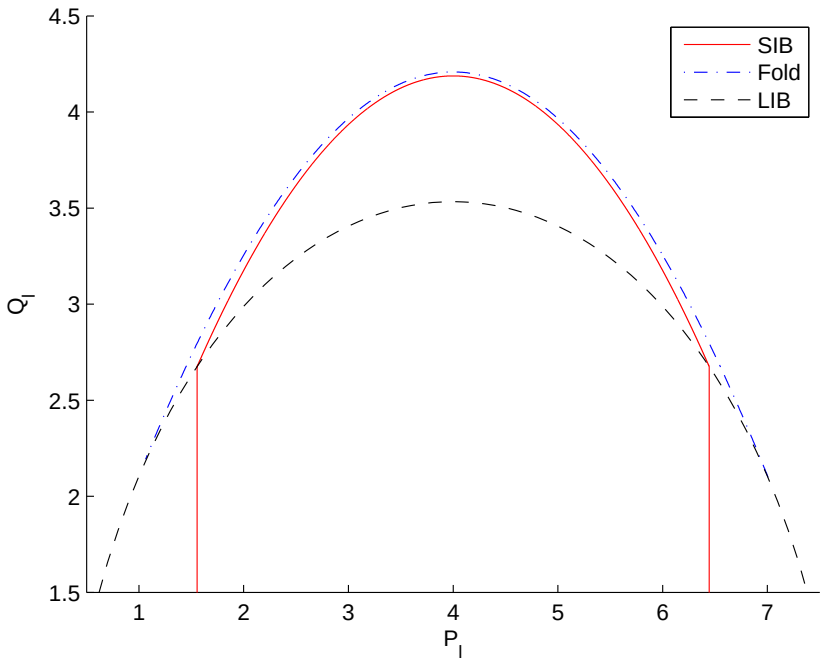

Figure 4.21: Parameter space.

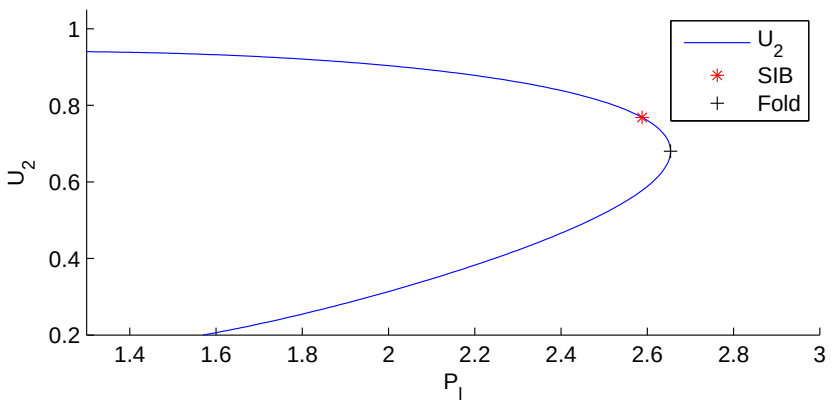

Figure 4.22: PV curve ($Q_l = 3.7$).

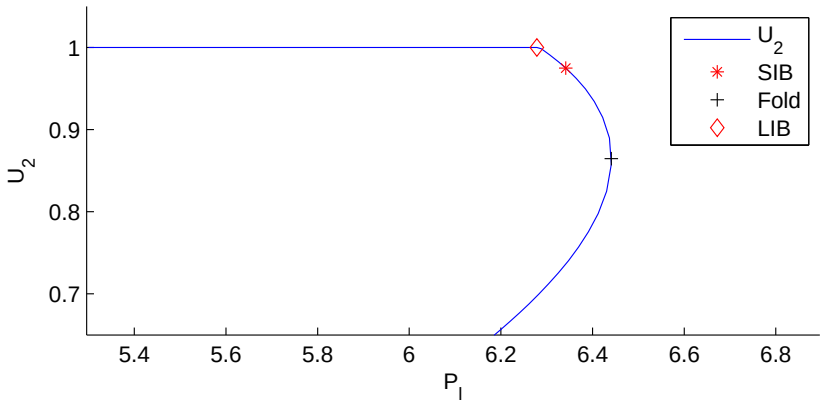

Figure 4.23: PV curve before discontinuity ($Q_l = 2.8$).

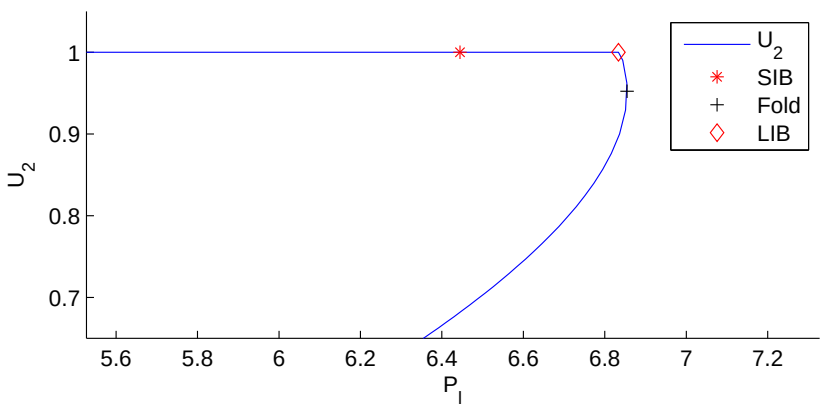

Figure 4.24: PV curve after discontinuity ($Q_l = 2.3$).

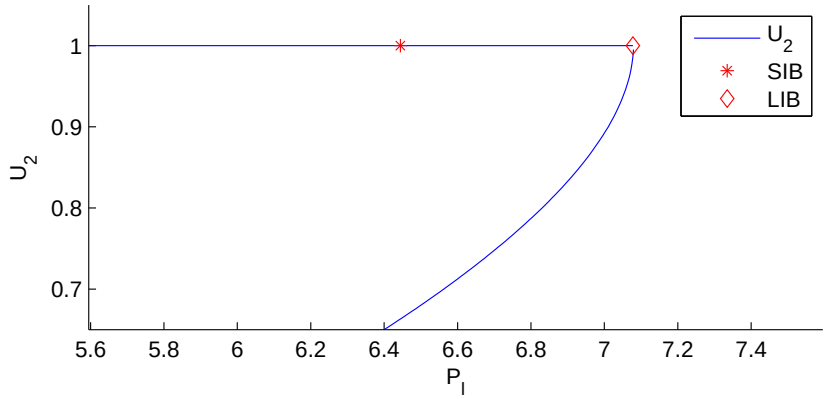

Figure 4.25: PV curve after discontinuity ($Q_l = 2.0$).

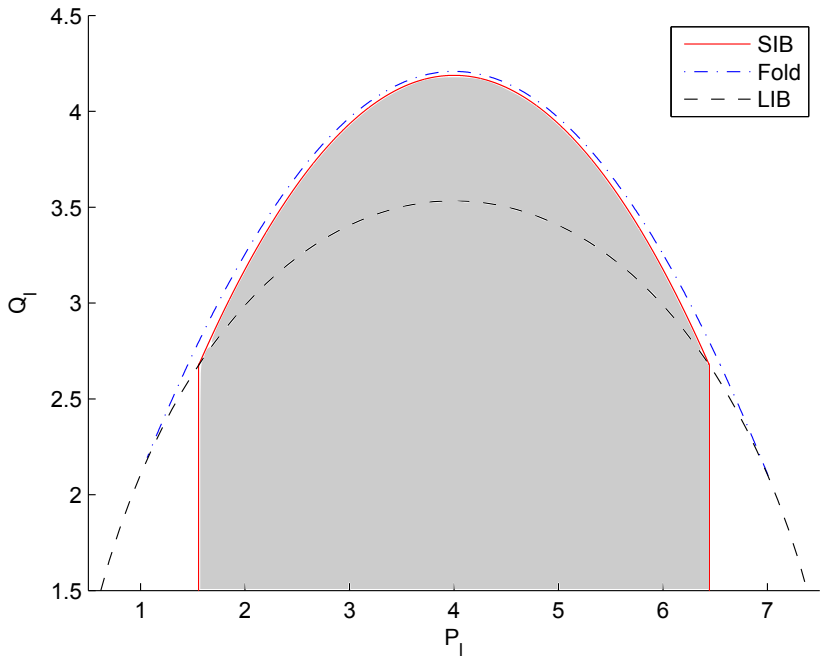

Figure 4.26: Stability in parameter space. The shaded surface represents the stable region.

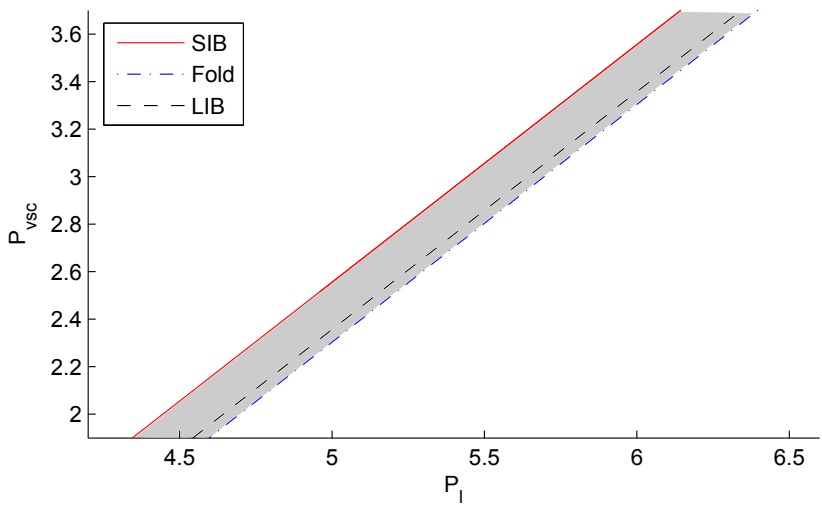

Figure 4.27: Stability in parameter space. The shaded surface represents the stable region.

4.7 Conclusions

In this chapter steady-state VSC HVDC models are developed. A simplified power flow model, that represents converters as PV or PQ nodes, has been first presented. The HVDC Light and PSS/E models are basically of this type. Simulations showed that these three models provide the same results. Next a detailed model has been proposed with much more detail than those present in commercial grade software and even manufacturer delivered models. Most notably, the model supports MTDC systems, takes into account accurate limits, filters, converter losses and correctly defines set points with respect to the system bus. The model has been thoroughly validated by comparing with a manufacturer delivered model and a model that comes with PSS/E. Finally, continuation methods are treated. It is shown how state of the art numerical techniques for continuation in ODE systems can be extended to DAE systems. An example illustrated the application of continuation methods to power systems with VSCs.

Chapter 5

Time-domain Simulation

5.1 Introduction

Time-domain simulation can be seen as an implementation of the solution of (3.3) in function of time, under the conditions established in Chapter 3. Time-domain simulation software is a commonly used tool for dynamic analysis of power systems, for instance angle or voltage stability assessment. Many such tools exist, but do not allow implementing multi-terminal VSC HVDC models in an easy way. A basic time-domain simulation tool should therefore be developed. For this work's research purposes, it is imperative that it be capable of simulating the dynamic behaviour of large AC power systems in a reliable way, and be easily extended to AC/DC system simulation. The tool can then act as a platform for testing and implementing dynamic VSC MTDC models.

Such a time-domain simulation tool, called $MatDyn$, is here developed. It is designed specifically to enable the extension to integrated AC/DC systems. The actual extension to AC/DC grids is discussed in the next chapter, where the dynamic models are derived. In this chapter, the rationale behind the development of the $MatDyn$ software is presented, and its functioning and implementation explained in detail. It is validated by comparing its results with those obtained by the commercial grade software PSS/E.

5.2 Rationale

Several commercial software programs for power system analysis are available, characterised by a high computational efficiency, a wide range of available models

and they are reliable, robust and precise. It is decided to develop a new dynamic simulation program from scratch. This is certainly a time consuming task, and no mean feat to do. Notwithstanding the advantages of commercial grade software, it is generally recognised by academia that commercial programs are not very well suited for research and educational purposes. They have a steep learning curve, and implementation aspects, such as integration algorithms, power flow solvers, and the implementation of models remain hidden from the user and are very hard to modify, if at all possible. Several programs, that are more oriented towards education and research, e.g.: Power System Toolbox (PST) [84], Power Analysis Toolbox (PAT) [85], Power System Analysis Toolbox (PSAT) [86], Voltage Stability Toolbox (VST) [87], and ObjectStab [88], have been developed at universities to address these issues. While commercial programs are often coded in low-level languages such as C/C++ or Fortran, the aforementioned programs tend to use high-level programming languages. One popular choice is Matlab. Matlab is available at many universities and is used extensively in many undergraduate and graduate engineering courses. The salient features of Matlab include a wide range of high-level mathematical functions, a high-level programming language, and impressive, easy to use plotting features. It should come at no surprise that quite some non-commercial power system software packages are developed using Matlab. Apart from PST, PAT and PSAT, already mentioned, MATPOWER [89] can be added to the list of power system software that is developed using Matlab.

MatDyn, the software presented in this chapter, is a new Matlab-based toolbox for power system stability analysis. It is Open Source Software (OSS), freely downloadable from [90], and comes with full documentation [91]. It is listed by the IEEE Task Force on Open Source Software for Power Systems and boasts several unique features, explained in this chapter.

With the development of *MatDyn*, the aim is to extend the use of MATPOWER, limited to power flow and optimal power flow only, to dynamic analysis, while strictly adhering to the latter's philosophy: "It is intended as a simulation tool for researchers and educators that is easy to use and modify. MATPOWER is designed to give the best performance possible while keeping the code simple to understand and modify." [73, p.3]. Furthermore, care has been taken to make *MatDyn* integrate seamlessly with MATPOWER, so that MATPOWER's large user base can easily familiarise itself with *MatDyn*. In this way, a synergy is obtained between MATPOWER and *MatDyn*, in line with the objective identified by the 'IEEE Task Force on Open Source Software for Power Systems' [92].

The main requirement of *MatDyn* is the capability to include in an easy way general multi-terminal VSC HVDC models. The models presented in the next chapter, would be very difficult, or even impossible, to implement in block-diagram editors of commercial power system software. *MatDyn*'s ease of use, flexibility, easy customisation, and access to every part of the code all contribute to making it a suitable platform for integration of VSC HVDC models. Although a difficult

and time-consuming task, developing *MatDyn* is an effort well spent.

5.3 Program Flow

In *MatDyn*, the set of differential equations F consists of the dynamic equations of the equipment such as generators, exciters, and governors, while the algebraic equations contain the power flow equations and the stator current equations of the generators. The task of the simulation tool is to solve this system of DAEs. In the literature, two methods have been proposed to solve this system: a simultaneous approach, and a partitioned approach. Both have been implemented in commercial applications. In the simultaneous approach ([93], [94]), the differential and algebraic equations are solved at once. Coding such a method can be quite a hassle: the full system Jacobian needs to be constructed, resulting in a large and intricate matrix that makes the code hard to understand. This is unacceptable in view of the design criteria of *MatDyn*. Consequently, the partitioned approach is used, whereby F is solved for the algebraic variables, and subsequently G for the dynamic variables. *MatDyn* fully utilizes the matrix handling capabilities of Matlab: all the generators' state variables are grouped in a matrix `Xgen`, the exciters' state variables in `Xexc`, and the governors' state variables in `Xgov`. The exciters, generators and governors are solved sequentially, by feeding the matrices `Xgen`, `Xexc`, and `Xgov` into the integration subroutine. This resulted in a high readability of the code, which in turn helps to integrate VSC HVDC models.

The program flow is represented schematically in Fig. 5.1. Starting from the power flow solution, *MatDyn* constructs and factorises the augmented bus admittance matrix and proceeds with calculating the initial conditions of the generators, exciters, and governors. If the system is in steady-state, the main loop is started. The set of differential equations F is integrated, and the set of algebraic equations G solved. If an event occurs, the augmented bus admittance matrix is refactorised and the algebraic equations G, consisting of the network equations and stator current equations, are recalculated. The variables of interest are saved and time is advanced with the optimal step size for methods with step size control or with fixed step size for the fixed step size methods.

5.4 Initial Conditions

The bulk of the algebraic variables can be solved for by a power flow computation. *MatDyn* uses MATPOWER to obtain a power flow solution and proceeds with calculating the dynamic variables and the remaining algebraic variables at $t = 0$

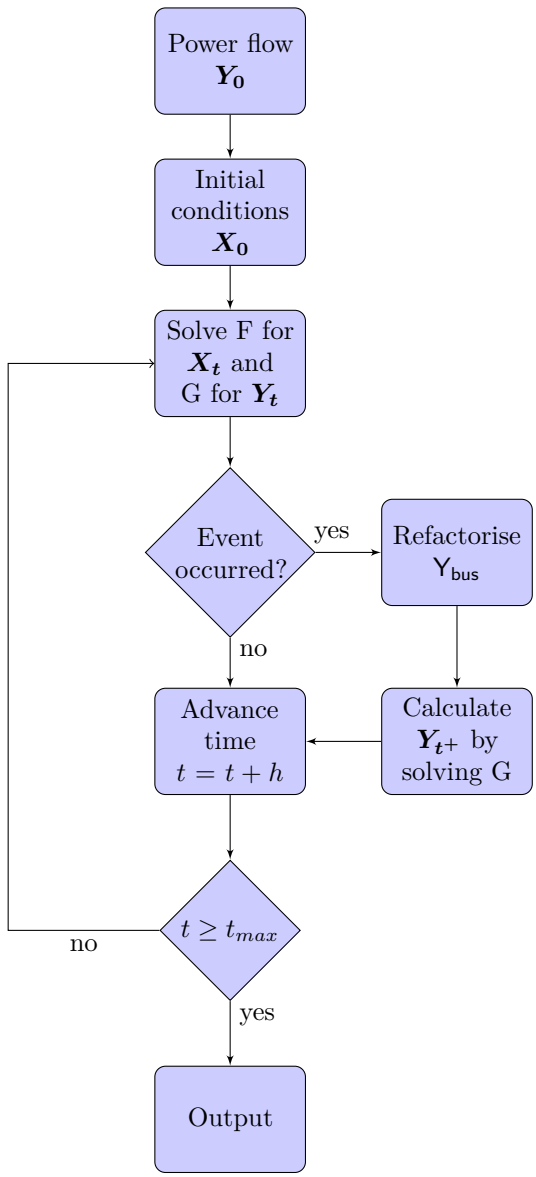

Figure 5.1: *MatDyn* flowchart.

by solving:

$$0 = F(\boldsymbol{X}, \boldsymbol{Y}, \boldsymbol{P}). \tag{5.1}$$

This set consists of equations for the generators, exciters, and governors defined in `GeneratorInit`, `ExciterInit` and `GovernorInit`. Before the main loop is started, it is checked whether the calculated initial conditions represent a steady-state situation. If this is not the case, the user is notified and the program is stopped.

5.5 Solving the Differential Equations

MATLAB is known to have a powerful ODE suite [95]. Its ODE solvers are however not well suited for solving the power system dynamic equations. First of all, most of the MATLAB's ODE suite's methods are designed for ODEs and not for DAEs. Even in the sequential approach, where differential and algebraic equations are solved separately, ODE solvers cannot be directly used because not only after every step, but also after every stage of the integration, the algebraic equations have to be solved. Secondly, discontinuities, which arise frequently in the power system, e.g. three-phase faults, need special attention. Therefore, custom ODE solvers have been developed. *MatDyn* comes with a number of ODE solvers. The first one is a second order Modified Euler method. The second is the well-known fourth order Runge-Kutta method. The third and fourth methods are variations of the standard Runge-Kutta method: the Runge-Kutta Fehlberg method is a 6 stage embedded method of order 4(5) with step size control, the Runge-Kutta method of Higham and Hall is a variable step size, 7 stage embedded method of order 6(5) with local extrapolation. The Modified Euler method and fourth order Runge-Kutta method are implemented with a fixed step size. However, they could be modified to accommodate variable step sizes. All methods are explicit integration methods. Explicit methods are recognised not to work well for stiff systems [53, p.841]. The reason explicit methods perform acceptably is that the stiffness of power systems is moderate. It is however imperative that step size remain low. For fixed step size solvers, a step size has to be chosen that is smaller than the smallest time constant of the system. For variable step size solvers, step size is automatically chosen such as to guarantee a certain accuracy. If due to more and more detailed models, the stiffness further increases, explicit methods are not acceptable anymore. At that point, the question should be raised whether it would not be better to move to electromagnetic simulation. The real drawback of explicit methods in power system analysis appears in long-term simulation. Even when fast dynamics are not excited any more, and the system is governed by slow dynamics, the step size has to remain low, thus leading to very long simulation times. Programs that rely on explicit integration algorithms are therefore not well suited for long-term simulations.

5.5.1 Modified Euler

Two Stage Method

The modified Euler method is a two-stage method, often used in power system analysis computer programs [96]. The forward Euler method is used to obtain a first approximation ${\boldsymbol{y_{n+1}}}^{(0)}$. In the second stage, a better approximation ${\boldsymbol{y_{n+1}}}^{(1)}$ is found by using the average of the derivatives in the beginning and at the end of the interval using the first approximation.

$$ {\boldsymbol{y_{n+1}}}^{(0)} = \boldsymbol{y_n} + hf(\boldsymbol{y_n}) \tag{5.2} $$

$$ {\boldsymbol{y_{n+1}}}^{(1)} = \boldsymbol{y_n} + \frac{h}{2}(f(\boldsymbol{y_n}) + f({\boldsymbol{y_{n+1}}}^{(0)})) \tag{5.3} $$

Modified Euler with Interface Error Control

The modified Euler method with interface error control checks after the second stage whether the interface errors are within bounds. If not, more stages are calculated until the desired tolerance is met.

$$ {\boldsymbol{y_{n+1}}}^{(0)} = \boldsymbol{y_n} + hf(\boldsymbol{y_n}) \tag{5.4a} $$

$$ {\boldsymbol{y_{n+1}}}^{(1)} = \boldsymbol{y_n} + \frac{h}{2}(f(\boldsymbol{y_n}) + f({\boldsymbol{y_{n+1}}}^{(0)})) \tag{5.4b} $$

$$ {\boldsymbol{y_{n+1}}}^{(2)} = \boldsymbol{y_n} + \frac{h}{2}(f(\boldsymbol{y_n}) + f({\boldsymbol{y_{n+1}}}^{(1)})) \tag{5.4c} $$

$$ \vdots $$

$$ {\boldsymbol{y_{n+1}}}^{(i)} = \boldsymbol{y_n} + \frac{h}{2}(f(\boldsymbol{y_n}) + f({\boldsymbol{y_{n+1}}}^{(i-1)})) \tag{5.4d} $$

In section 5.9.3, the problem of interface errors is explained.

5.5.2 Runge-Kutta

An s-stage explicit Runge-Kutta method can be defined as:

$$ k_i = f(\boldsymbol{x_n} + c_i h, \boldsymbol{y_n} + \sum_{j=1}^{i-1} a_{i,j-1} k_j), \quad i = 1, \ldots, s \tag{5.5} $$

$$\boldsymbol{y_{n+1}} = \boldsymbol{y_n} + h \sum_{i=1}^{s} b_i k_i, \tag{5.6}$$

with the coefficients given by a Butcher tableau:

$$\begin{array}{c|cccc|c} 0 & & & & & \\ c_2 & a_{21} & & & & \\ c_3 & a_{31} & a_{32} & & & \\ \vdots & \vdots & \vdots & \ddots & & \\ c_s & a_{s1} & a_{s2} & \cdots & a_{s,s-1} & \\ \hline & b_1 & b_2 & \cdots & b_{s-1} & b_s \end{array}$$

The most well-known Runge-Kutta method is the fourth order, four-stage method defined by the following Butcher tableau:

$$\begin{array}{c|cccc} 0 & & & & \\ \frac{1}{2} & \frac{1}{2} & & & \\ \frac{1}{2} & 0 & \frac{1}{2} & & \\ 1 & 0 & 0 & 1 & \\ \hline & \frac{1}{6} & \frac{2}{6} & \frac{2}{6} & -\frac{1}{6} \end{array}$$

The power system's differential equations are autonomous, i.e. time is implicit. The constants $c_0, \ldots, c_s$ are therefore not used.

5.5.3 Runge-Kutta Fehlberg

The Runge-Kutta Fehlberg method is given by the following Butcher tableau:

0						
$\frac{1}{4}$	$\frac{1}{4}$					
$\frac{3}{8}$	$\frac{3}{32}$	$\frac{9}{32}$				
$\frac{12}{13}$	$\frac{1932}{2197}$	$-\frac{7200}{2197}$	$\frac{7296}{2197}$			
1	$\frac{439}{216}$	-8	$\frac{3680}{513}$	$-\frac{845}{4104}$		
$\frac{1}{2}$	$-\frac{8}{27}$	2	$-\frac{3544}{2565}$	$\frac{1859}{4104}$	$-\frac{11}{40}$	
y_1	$\frac{25}{216}$	0	$\frac{1408}{2565}$	$\frac{2197}{4104}$	$-\frac{1}{5}$	0
$\hat{y}_1$	$\frac{16}{135}$	0	$\frac{6656}{12825}$	$\frac{28561}{56430}$	$-\frac{9}{50}$	$\frac{2}{55}$

The idea is to calculate two approximations of the solution for every step: one fourth order and one fifth order approximation. The difference between both solutions is a measure for the local error of the lower order result. This error can be used to determine the optimal step size. If the local error is within specified bounds, the step is accepted and the step size enlarged. If the local error is too large, the step is rejected, the step size is reduced and the calculation is repeated with a smaller step size. The coefficients are optimised to minimise the error of the lower order result [97, p.178], used in the further calculations. It is thus a fourth order method.

The new step size is calculated as

$$h^{new} = hq, \tag{5.7}$$

with q usually

$$q = 0.84 \left(\frac{tol}{|\boldsymbol{y_n} - \boldsymbol{y_{n-1}}|} \right)^{1/4}. \tag{5.8}$$

To ensure that the step size does not change too fast, $h^{new} = hq$ is replaced by [97, p.168]:

$$h^{new} = h \cdot min(facmax, max(facmin, q)). \tag{5.9}$$

5.5.4 Higham and Hall

For stiff systems such as the power system, the evolution of the step size is oscillatory and lots of steps are rejected, wasting computing time. Higham and Hall sought a method with smooth step size changes for stiff systems. The method of Higham and Hall is of order five. The coefficients seek "reasonable size of the stability domain, large parts of SC-stability and a small sixth order error constant."

[98, p.27]. For the selection of the optimal step size, the method explained in section 5.5.3 is used. The Butcher tableau is:

0							
$\frac{2}{9}$	$\frac{2}{9}$						
$\frac{1}{3}$	$\frac{1}{12}$	$\frac{1}{4}$					
$\frac{1}{2}$	$\frac{1}{8}$	0	$\frac{3}{8}$				
$\frac{3}{5}$	$\frac{91}{500}$	$-\frac{27}{100}$	$\frac{78}{125}$	$\frac{8}{125}$			
1	$-\frac{11}{20}$	$\frac{27}{20}$	$\frac{12}{5}$	$-\frac{36}{5}$	5		
1	$\frac{1}{12}$	0	$\frac{27}{32}$	$-\frac{4}{3}$	$\frac{125}{96}$	$\frac{5}{48}$	
y_1	$\frac{1}{12}$	0	$\frac{27}{32}$	$-\frac{4}{3}$	$\frac{125}{96}$	$\frac{5}{48}$	0
$\hat{y}_1$	$\frac{2}{15}$	0	$\frac{27}{80}$	$-\frac{2}{15}$	$\frac{25}{48}$	$\frac{1}{24}$	$\frac{1}{10}$

5.6 Solving the Algebraic Equations

All equipment injecting into, or taking out current at a network node, such as generators, loads, and converters, are converted to Norton equivalents. For generators and converters modelled in the *dq*-frame, Kron's transformation (3.44) is applied so that all variables are expressed in the network's reference frame. The Norton equivalents can then be connected to the network. The bus admittance matrix is augmented by including the Norton admittances. This matrix, sometimes called 'reduced admittance matrix', is in *MatDyn* referred to as the 'augmented admittance matrix'. The bus voltages can then be solved for by solving the following nonlinear matrix equation:

$$\boldsymbol{I} = \mathsf{Y}_{\mathsf{bus}}\boldsymbol{U}, \tag{5.10}$$

wherein $\boldsymbol{I}$ is the vector of positive or negative current injections by equipment such as generators, converters, and loads. It is obtained by calculating the equipment's differential and algebraic equations. The matrix $\mathsf{Y}_{\mathsf{bus}}$ is the augmented bus matrix. This equation is only valid in steady-state, but it is shown in [99, pp.370-372] that it is exact for transient conditions if transformer and speed voltages are neglected.

After every event and after every step and stage of the integration algorithm, these network equations have to be solved, leading to great computational effort. In many commercial programs, several tweaks are implemented in order to reduce this effort: the Jacobian can be held constant during the Newton steps (dishonest Newton), or even during several time steps (very dishonest Newton) [100]. *MatDyn* does not use extrapolation and computes the $\boldsymbol{Y}$ variables after

every step and after every stage, but retains computational simplicity by imposing two conditions:

- generators do not exhibit transient saliency;
- loads are represented by a constant admittance only.

The first condition assures that the generators' Norton admittance is time invariant, the second implies that the currents injected by the loads are zero. Under these two conditions, the network equations are all linear and the voltages can be solved for by solving a linear system of equations, which can be done efficiently in Matlab by LU-factorisation of the augmented $\mathsf{Y}_{\mathsf{bus}}$ matrix.

In commercial programs, where it is of the utmost importance to achieve accurate results, such an approach would not be justified. However, for a program, geared towards eduction and research, it is acceptable to impose these two modelling restrictions.

5.7 Handling Events

A wide variety of events (disturbances) can be applied. Events give rise to discontinuities in the DAE system and require special attention. They are detected at the end of the main loop, after the state at time t is calculated (Fig. 5.1). If an event is detected, the calculated values are to be considered as the system state at t^-. The $\mathsf{Y}_{\mathsf{bus}}$ matrix is reconstructed and refactorised, and the network equations solved to obtain a second solution, valid at t^+. As discontinuities can never occur in the $\boldsymbol{X}$ variables, because their dynamics are governed by the F set, it is not needed to integrate the differential equations a second time.

Special care must be taken for variable step size solvers, as they can jump over discontinuities as their step size increases. Therefore, after every step it is checked whether the optimal step size for the next step has not jumped over an event. If this is indeed the case, the step size is reduced.

5.8 Models

In *MatDyn* it is possible to include user defined models. It is this functionality that is used to incorporate dynamic VSC HVDC models. For every model, two routines are defined: one that calculates its initial conditions, and one that contains its differential equations. Every model also has three matrices: X contains the model's state variables, P its constant parameters, and V variables that are

not state variables of the model, for instance another model's state variables or bus voltages. The exciter's initial conditions and differential equations, for instance, can then be evaluated by calling: `ExciterInit(Xexc, Pexc, Vexc)` and `Exciter(Xexc, Pexc, Vexc)`. The generator model needs its own state variables X_{gen}, parameters P_{gen} and variables V_{gen}, but also needs the exciter's state variable E_{fd} and the governor's state variable P_m. The model is thus called as `Generator(Xgen, Xexc, Xgov, Pgen, Vgen)`.

Example 5.1. *As an example it is shown how to include a simplified IEEE AC4A exciter in MatDyn. Only two files,* `Exciter.m` *and* `ExciterInit.m`*, must be changed. This example is for illustrative purposes only: the limiters are neglected here, which is wrong, but simplifies the example. For realistic results, limiters should be modelled, as done for the IEEE DC1A exciter model, which comes with MatDyn. The block diagram of the simplified IEEE AC4A exciter is shown in Fig. 5.2.*

Step 1: *Differential equations*

It is easier to write down the equations when the block diagram is transformed to the equivalent block diagram shown in Fig. 5.3. The following three equations describe the dynamic behaviour of the exciter:

$$\dot{x} = \frac{1}{T_B}(U_{ref} - U - x), \tag{5.11}$$

$$U_r = x + \dot{x}T_C, \tag{5.12}$$

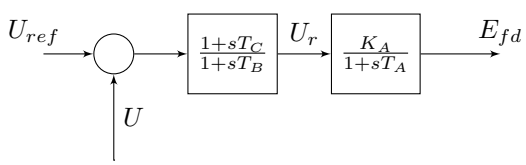

Figure 5.2: Simplified IEEE type AC4A excitation system.

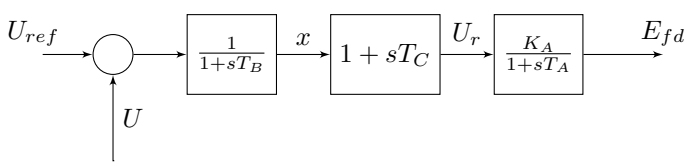

Figure 5.3: Simplified IEEE type AC4A excitation system: equivalent.

$$\dot{E_{fd}} = \frac{1}{T_A}(K_A U_r - E_{fd}). \tag{5.13}$$

Substituting (5.11) in (5.12) and the result thereof in (5.13) leads to the following two differential equations, that completely describe the system:

$$\dot{x} = \frac{1}{T_B}(U_{ref} - U - x), \tag{5.14}$$

$$\dot{E_{fd}} = \frac{1}{T_A}(K_A(x + \frac{T_C}{T_B}(U_{ref} - U - x)) - E_{fd}). \tag{5.15}$$

Step 2: *Initial conditions*

The initial conditions can be found by solving the equations obtained when the right-hand side of (5.14) and (5.15) are set to zero:

$$0 = \frac{1}{T_B}(U_{ref} - U - x), \tag{5.16}$$

$$0 = \frac{1}{T_A}(K_A(x + \frac{T_C}{T_B}(U_{ref} - U - x)) - E_{fd}). \tag{5.17}$$

Solving for x and U_{ref} gives:

$$x = \frac{E_{fd}}{K_A}, \tag{5.18}$$

$$U_{ref} = U + x. \tag{5.19}$$

Step 3: *Insert initial conditions in MatDyn*

Open `ExciterInit.m` *and add a third exciter model:*

```
%% Define exciter types
...
type3 = d(exctype==3);
```

The model has two state variables, E_{fd} and x, and four parameters, K_A, T_A, T_B, and T_C. The reference voltage U_{ref} is not a state variable nor a parameter, but needs to be accessible. It must therefore be appended to the parameter matrix.

```
%% Exciter type 3: IEEE AC4A
Efd0 = Xexc(type3,1);

Ka = Pexc(type3,2);
Ta = Pexc(type3,3);
Tb = Pexc(type3,4);
Tc = Pexc(type3,5);

U = Vexc(type3,1);

x = Efd0./Ka;
Uref = U + x;

Xexc0(type3,1:2) = [Efd0, x];
Pexc0(type3,1:6) = [Pexc(type3,1), Ka, Ta, Tb, Tc, Uref];
```

Step 4: *Insert dynamic equations in MatDyn*

Open `Exciter.m` *and add a third exciter model:*

```
%% Define exciter types
...
type3 = d(exctype==3);
```

The dynamic equations are then inserted:

```
%% Exciter type 3: IEEE AC4A
Efd = Xexc(type3,1);
x = Xexc(type3,2);

Ka = Pexc(type3,2);
Ta = Pexc(type3,3);
Tb = Pexc(type3,4);
Tc = Pexc(type3,5);
Uref = Pexc(type3,6);

U = Vexc(type3,1);

dx = 1./Tb.*(Uref - U - x);
dEfd = 1./Ta .* ( Ka .* (x + Tc./Tb.*(Uref - U - x)) - Efd);

F(type3,1:2) = [dEfd dx];
```

Step 5: *Insert parameter values in the dynamic data file*

The parameters of the IEEE DC1A model are entered by appending the row `[gen Ka Ta Tb Tc]` *to the exc matrix in the dynamic data file. Suppose the first and third generator are equipped with the IEEE DC1A exciter and the second one with the IEEE AC4A exciter. The exc matrix is then defined as follows:*

```
exc=[1 Ka Ta Ke Te Kf Tf Aex Bex Urmin Urmax;
     2 Ka Ta Tb Tc 0  0  0   0   0     0;
     3 Ka Ta Ke Te Kf Tf Aex Bex Urmin Urmax]
```

New governor models can be added similarly. Adding generator models or HVDC converters requires more changes as they contain algebraic equations. It is explained in Chapter 6 how to change the program to include converters.

5.9 Validation

If VSC HVDC models are to be validated, it is a prerequisite that the simulation tool, in this case *MatDyn* provide correct results. The validation of the software is therefore extremely important, and is discussed at some length. First the influence of speed voltages, frequency dependency of network parameters, and interface errors are researched, next *MatDyn* is compared to the well-established, commercial grade software tool, PSS/E.

5.9.1 Speed Voltages

In *MatDyn*, speed voltages are neglected, as are transformer voltages. The effects of both phenomena counteract each other. In [53], it is proven that for small deviations, the error introduced by neglecting speed voltages completely counteracts the error introduced by neglecting transformer voltages. It is therefore recommended in the same work to either take them both into account or either neglect them both. However, whether speed voltages should be taken into account or not, is still debated: in PSS/E and Eurostag for instance, speed voltages are taken into account, in Simpow, the choice is left to the user. According to our simulations with a test version of *MatDyn*, modified to include speed voltages, the difference is very small. When taking into account speed voltages, the solution is slightly underdamped. It is thus conservative to include the speed voltages.

5.9.2 Frequency Dependency of Network Parameters

Theoretically, frequency is not defined during transients. However, the notion of a 'dynamic frequency' can be introduced:

$$\omega_i = \omega_s + \frac{d\theta_i}{dt}, \qquad i = 1 \dots n. \tag{5.20}$$

It has the property of being equivalent to frequency at steady-state [101, p.156]. A frequency can then be assigned to every bus voltage and line current during transients. Line parameters depend on this dynamic frequency, and should hence be recalculated at every time step. As the frequency deviation is very limited, the influence on line parameters is negligible. This was verified with *MatDyn*. In most commercial power system analysis software, such as PSS/E, the choice is left to the user whether to include frequency dependence of the line parameters. It should be understood that including frequency dependence of line parameters comes at a huge penalty: the admittance matrix has to be refactorised every time step.

5.9.3 Interface Errors

In the sequential solution method, care has to be taken to avoid interface errors. Interface errors can arise because F and G are not solved simultaneously: when solving F for $\boldsymbol{X}$, $\boldsymbol{Y}$ has to be known, and when solving G for $\boldsymbol{Y}$, $\boldsymbol{X}$ has to be known. Interface errors can be avoided by checking after the last stage of the integration whether the error on $\boldsymbol{X}$ and $\boldsymbol{Y}$ is within bounds, and by computing more approximations if it is not. This procedure was implemented in `ModifiedEuler2.m` to quantify *MatDyn*'s interface errors. A system (60 Hz) is solved with the standard Modified Euler method, and with Modified Euler 2. To eliminate interface errors, the required tolerance is set to 1e-8. Results are plotted in Fig. 5.4, for a step size of 0.02s, and in Fig. 5.5, for a step size of 0.01s. It appears that the interface errors are negligible, especially when a small step size is chosen. A contributing factor to this good performance is the fact that the algebraic equations are solved after every step and every stage of the integration in *MatDyn*.

5.9.4 Comparison with Commercial Grade Software

MatDyn is validated by comparing its results with those obtained using the commercial power system software PSS/E and the open source software package PSAT [86]. A five bus network, two generator network has been simulated. The full description of the system, including one-line diagram, system data, and the results

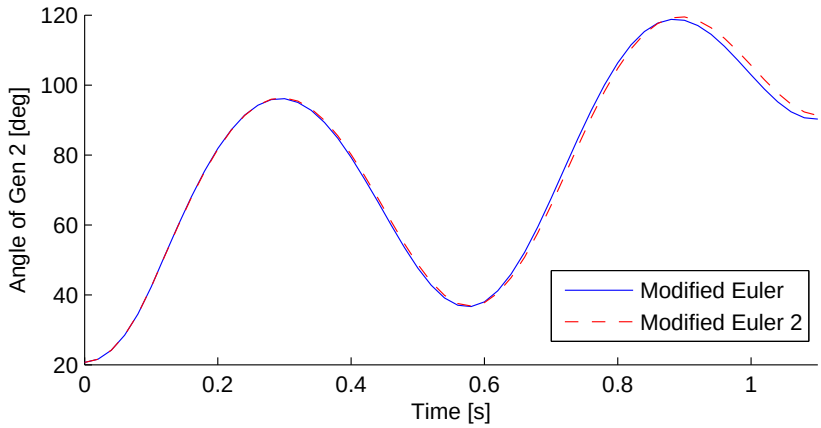

Figure 5.4: Comparison between Modified Euler (with interface errors) and Modified Euler 2 (without interface errors) for a step size of 0.02s (60 Hz).

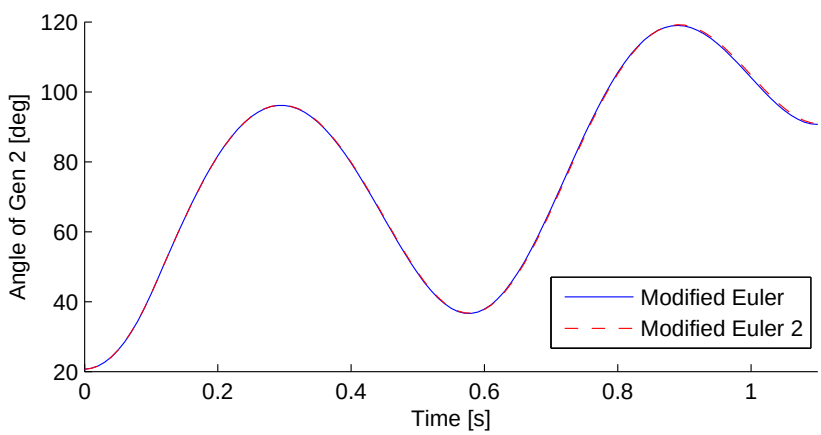

Figure 5.5: Comparison between Modified Euler (with interface errors) and Modified Euler 2 (without interface errors) for a step size of 0.01s (60 Hz).

can be found in [96]. The three software packages show a very good correspondence. The results do however differ very slightly. This is due to some design decisions. For instance: in PSS/E, speed voltages are taken into account, in *MatDyn* and in PSAT, they are not (Figs. 5.6 and 5.7).

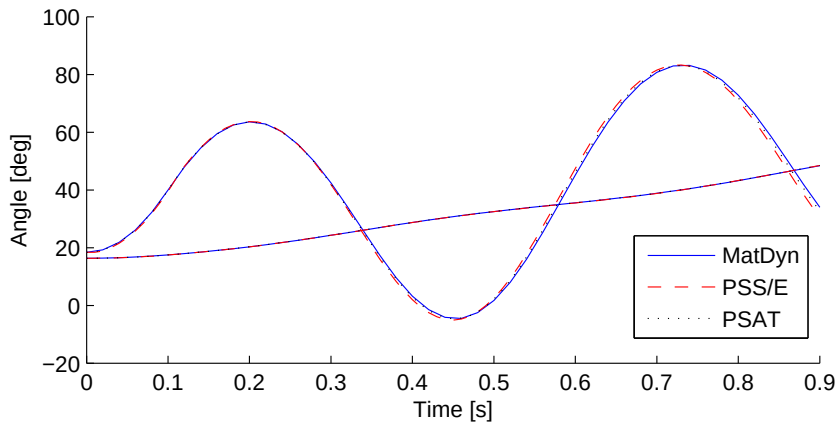

Figure 5.6: Comparison between *MatDyn*, PSS/E, and PSAT: generator angles.

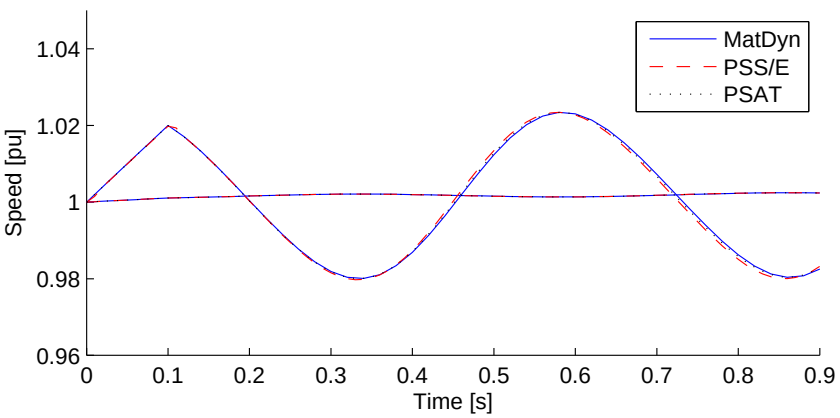

Figure 5.7: Comparison between *MatDyn*, PSS/E, and PSAT: generator speeds.

5.9.5 Validating the ODE Solvers

In order to test and compare *MatDyn*'s different ODE solvers, two scripts `Test1.m` and `Test2.m` are developed. They are included in *MatDyn* in order for the reader to repeat and verify the simulations.

In `Test1.m`, a case is solved with the different ODE solvers that come with *MatDyn*. The generator angles are plotted in Fig. 5.8. As seen, all solvers provide accurate results, that differ marginally from one another. Fig. 5.9 shows the step sizes of the ODE solvers. Note that at $t = 0$ (fault on) and $t = 0.1$ (fault off), the step size is reduced because discontinuities in the algebraic variables appear. The Modified Euler and fourth-order Runge-Kutta methods are implemented with fixed step size (here 10 ms). The Runge-Kutta Fehlberg and Higham-Hall methods allow for larger step sizes.

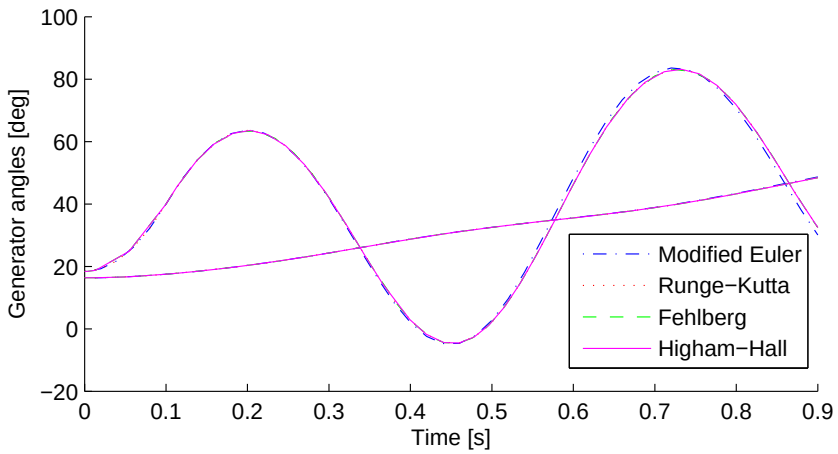

Figure 5.8: Generator angles for different ODE solvers (tol = 1e-4).

The same calculation is repeated with the Fehlberg method, for different error tolerances. The results show that a solution obtained with low error tolerance deviates from the more accurate solution (Fig. 5.10). On the other hand, the simulation is faster as larger step sizes are possible (Fig. 5.11).

5.9.6 Anderson and Fouad's Benchmark Case

Finally, the nine bus, three generator test case from Anderson and Fouad's *Power System control and Stability* is simulated in *MatDyn*. A full description of this case, with complete system data can be found in [99, pp.37-45]. The single-line

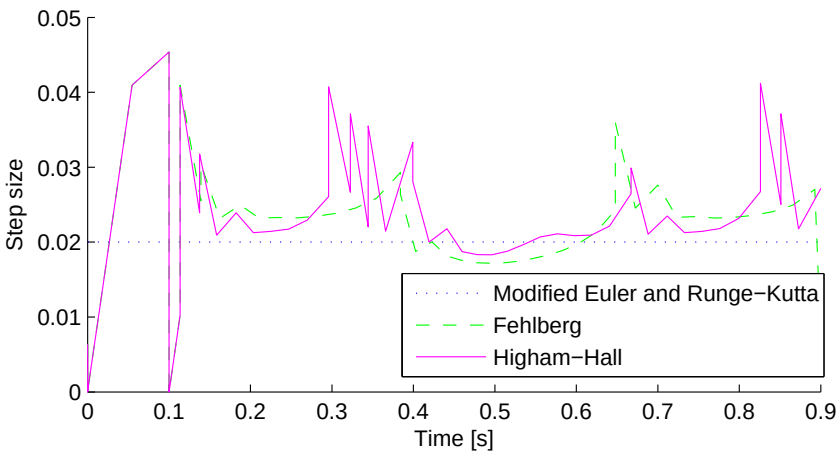

Figure 5.9: Step sizes for different ODE solvers.

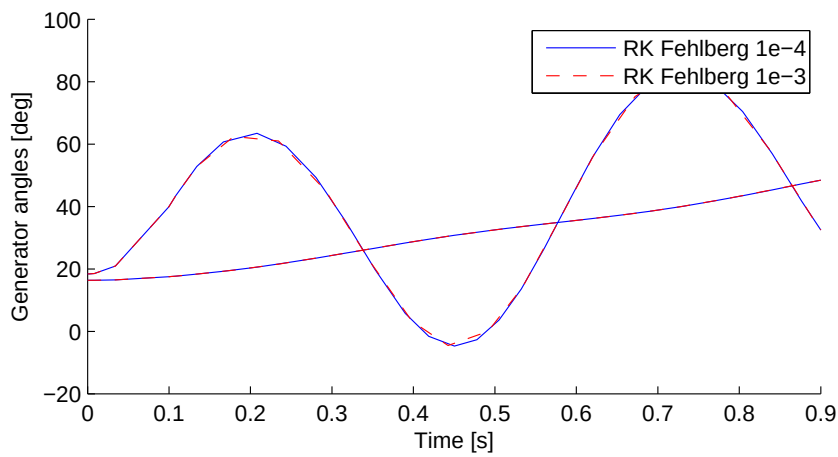

Figure 5.10: Generator angles for different error tolerance.

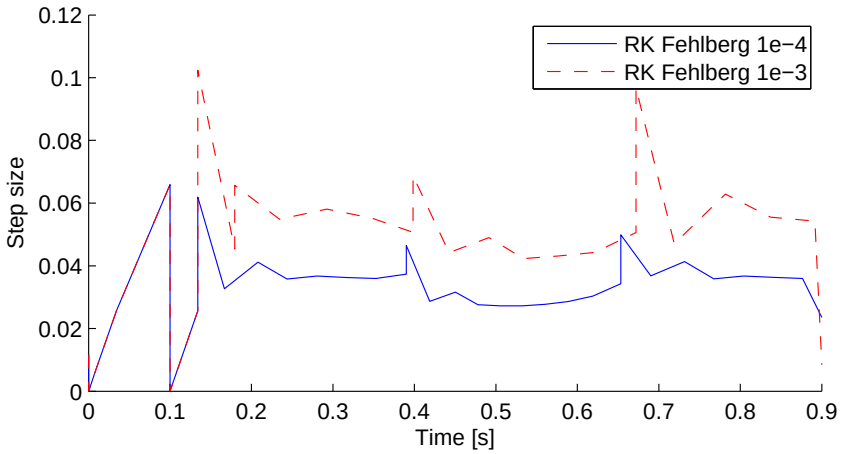

Figure 5.11: Step sizes for different error tolerance of the Fehlberg ODE solver.

diagram is given in Fig. 5.12. The results are plotted in Figs. 5.13 and 5.14 and very closely match the plots in [99].

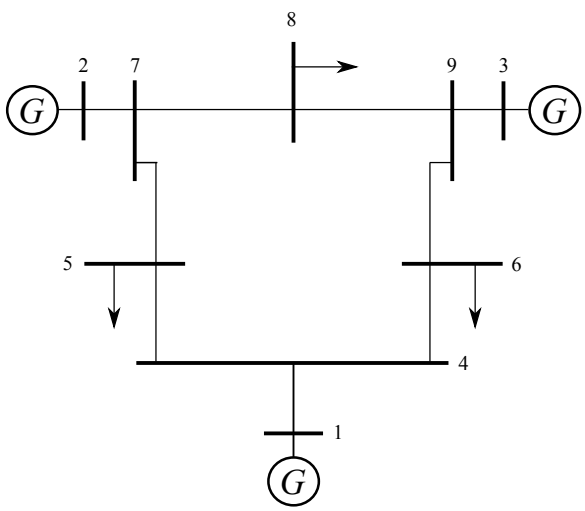

Figure 5.12: Single-line diagram of Anderson and Fouad's nine bus network.

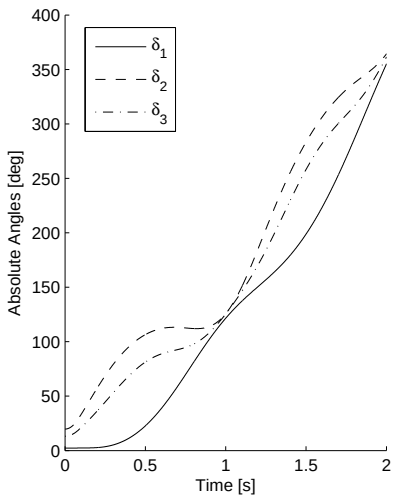

Figure 5.13: Absolute generator angles.

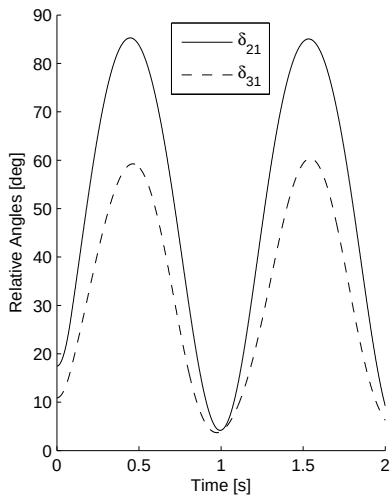

Figure 5.14: Relative generator angles.

5.10 Conclusions

MatDyn is a new Matlab based software for dynamic analysis of power systems, that uses a well-structured sequential solution method to solve (3.3). The software is shown to provide accurate results, by comparing its results with those obtained by the commercial grade software package PSS/E. *MatDyn*'s most salient features include a wide range of integration routines, the ease of use, flexibility, and the very well structured code, that is easy to understand and can be easily modified. It has been explained why minor concessions, such as disallowing transient saliency and dynamic loads, had to be made in order to comply with the design philosophy. Nevertheless, *MatDyn* retains an impressive overall flexibility, allowing user defined models and the provision to accommodate additional user provided ODE solvers. As such, it is an excellent tool for integrating multi-terminal VSC HVDC system models.

Chapter 6

Dynamic Modelling

6.1 Introduction

The principal aim of this chapter is to develop dynamic models for multi-terminal VSC HVDC systems, valid for every topology of the DC grid, and regardless of converter topology. Both detailed and reduced order models are developed. The basic differential equations of the AC and DC circuits are the start, to which controller and coupling equations are appended, taking care not to rely on any topology-specific information. Control loop design, influence of filter and PLL modelling are treated. Reduced order models, usually developed *ad hoc*, are to be derived from the full model in a mathematically sound way. The models should be validated by comparison with a manufacturer provided model.

Additionally, the aim is to research how power system analysis programs, such as *MatDyn* presented in Chapter 5, must be changed in order to accommodate for dynamic VSC HVDC models, and how the models can be implemented efficiently. This is a key point if the models are to be of any practical relevance. Finally, a number of examples is provided to illustrate the model's capability.

6.2 Modelling Philosophy

In the early days of power system modelling, the demarcation between electromechanical and electromagnetic models was very clear. With the advent of fast-switching FACTS devices and HVDC systems, this demarcation has become blurred. It was chosen to represented the dynamic model, derived in this chapter, in more detail as customary in electromechanical modelling. It is thus not a

strictly quasi-stationary model. However, it is not a very detailed electromagnetic model either. It still holds that the model is only valid for small deviations from fundamental frequency. A full electromagnetic model, valid for a broad frequency range, would require representing the AC filter in much detail, as well as DC filters, the valves, etc. Modelling the VSC HVDC systems in detail, does not lead to inconsistencies with the AC network model. The VSC HVDC system is connected to the AC network at certain buses. As seen from the AC network, the VSC system is a black box. All calculations performed within the black box ultimately lead to a complex current to be injected into the system at the buses where the converters are connected. This current is a quasi-stationary phasor, and thus the model is still consistent with the AC network model.

6.3 AC Side

Some models proposed in the literature explicitly rely on PWM to derive the model, e.g. [102], [103], [19], and [21]. In that case, the modulation index can be used to provide a relation between AC and DC side voltages. Here the aim is to develop a generic model, also valid for VSC HVDC systems that do not use PWM.

VSC HVDC converters are connected to the system through a phase reactor and a transformer (Fig. 6.1). The basic equation of this circuit,

$$u_c(t) - u_s(t) = L_{pr}\frac{di_{pr}(t)}{dt} + R_{pr}i_{pr}(t), \tag{6.1}$$

is transformed to a rotating dq-reference frame, using the power invariant Park transformation:

$$\frac{d(i_{pr}^d e^{j\omega t})}{dt} = -\frac{R_{pr}}{L_{pr}}i_{pr}^d e^{j\omega t} + \omega i_{pr}^q e^{j\omega t} + \frac{1}{L_{pr}}(u_c^d - u_s^d)e^{j\omega t}, \tag{6.2a}$$

$$\frac{d(i_{pr}^q e^{j\omega t})}{dt} = -\frac{R_{pr}}{L_{pr}}i_{pr}^q e^{j\omega t} - \omega i_{pr}^d e^{j\omega t} + \frac{1}{L_{pr}}(u_c^q - u_s^q)e^{j\omega t}. \tag{6.2b}$$

The angle ωt is provided by the PLL, arbitrarily assumed here to align system voltage with the q-axis. Dividing by $e^{j\omega t}$, the dynamic equations of the AC circuit

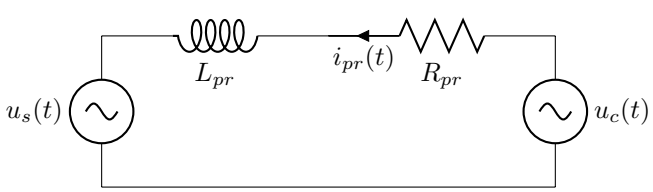

Figure 6.1: Single-line diagram of the AC Circuit without filter.

in the dq-frame are obtained:

$$\frac{di_{pr}^d}{dt} = -\frac{R_{pr}}{L_{pr}} i_{pr}^d + \omega i_{pr}^q + \frac{1}{L_{pr}}(u_c^d - u_s^d), \tag{6.3a}$$

$$\frac{di_{pr}^q}{dt} = -\frac{R_{pr}}{L_{pr}} i_{pr}^q - \omega i_{pr}^d + \frac{1}{L_{pr}}(u_c^q - u_s^q). \tag{6.3b}$$

6.4 DC Circuit Modelling

The DC circuit of a VSC HVDC system consists of a large capacitor at the converter station and a DC cable. Fig. 6.2 represents the DC side of a two-terminal VSC HVDC system with two cables of opposite voltage. The basic equations are:

$$C_{dc}\frac{du_{dc_1}}{dt} = i_{dc_1} - i_{cc}, \tag{6.4}$$

$$C_{dc}\frac{du_{dc_2}}{dt} = i_{dc_2} + i_{cc}, \tag{6.5}$$

$$L_{dc}\frac{di_{cc}}{dt} = u_{dc_1} - u_{dc_2} - R_{dc} i_{cc}. \tag{6.6}$$

A converter of a MTDC system can be connected to a number of other converters. A node of a generalised, symmetrically grounded monopolar DC system is shown in Fig. 4.6, and reproduced as Fig. 6.3 for reference. The current directions in the

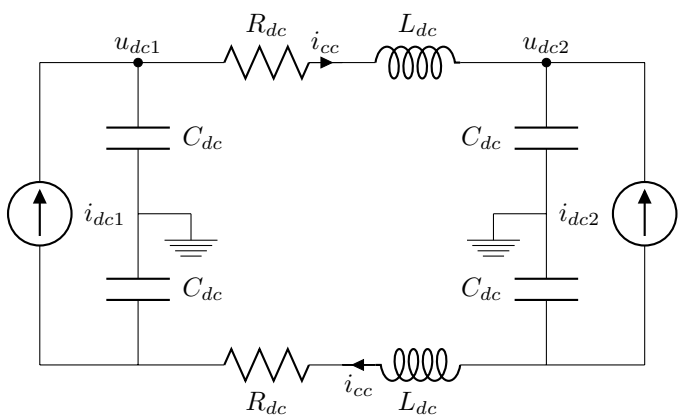

Figure 6.2: DC circuit.

DC lines are fixed such that the current from converter i to converter j is positive if i is smaller than j. Converter 1 has thus only incoming currents, and converter n only outgoing currents. For every other converter i, there are $n-1$ incoming, and $n-i$ outgoing currents. The generalised dynamic equations of any DC circuit can then be written as:

$$C_{dc_i}\frac{du_{dc_i}}{dt} = i_{dc_i} - \sum_{j=i+1}^{n} i_{cc_{ij}}, \quad i = 1 \tag{6.7a}$$

$$C_{dc_i}\frac{du_{dc_i}}{dt} = i_{dc_i} + \sum_{j=1}^{i-1} i_{cc_{ji}} - \sum_{j=i+1}^{n} i_{cc_{ij}}, \quad i = 2, \ldots, n-1 \tag{6.7b}$$

$$C_{dc_i}\frac{du_{dc_i}}{dt} = i_{dc_i} + \sum_{j=1}^{i-1} i_{cc_{ji}}, \quad i = n \tag{6.7c}$$

and

$$L_{dc_{ij}}\frac{di_{cc_{ij}}}{dt} = u_{dc_i} - u_{dc_j} - R_{dc_{ij}} i_{cc_{ij}} \quad \forall j < n, \forall i < j. \tag{6.8}$$

The DC voltage control equations have to be appended to the above equations.

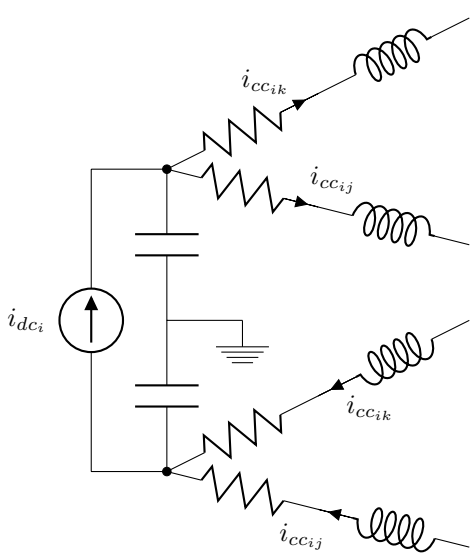

Figure 6.3: Node in a MTDC Circuit.

6.5 Coupling Equations

Finally, the AC and DC circuit equations have to be coupled. The coupling equations follow from the active power balance between AC and DC side of the converter. They allow to calculate the q-axis reference current of the slack converter, and the DC currents of the other converters:

$$i^q_{pr_n^{ref}} = \frac{2i_{dc_n} \cdot u_{dc_n} - i^d_{pr_n} \cdot u^d_{c_n}}{u^q_{c_n}}, \tag{6.9}$$

$$i_{dc_i} = \frac{u^d_{c_i} \cdot i^d_{pr_i} + u^q_{c_i} \cdot i^q_{pr_i}}{2u_{dc_i}}, \quad \forall i \leq n-1. \tag{6.10}$$

6.6 Control Systems

Developing new control strategies is one of the most popular research activities in the field of VSC HVDC. A variety of controllers have been proposed in the literature: internal model control in [104], H_∞ controllers in [104] and [105], a combination of genetic algorithms and H_∞ in [106], a combination of Linear-Quadratic-Gaussian (LQG) control and genetic algorithms in [107], a control strategy based on Lyapunov functions in [108], and optimal coordinated control of VSC and AC line in parallel [109]. While it is commendable to try to improve VSC HVDC systems performance by innovative control strategies, such new control strategies are often very specific and therefore not very suitable for a standard model. Furthermore, more conservative control strategies are used in real applications. The control strategy most used is vector control [105], which will be adopted here too, in conjunction with PI controllers.

6.6.1 Current Controller Design

The converter equations (6.3a) and (6.3b), obtained in the previous section, can be controlled by two parallel control loops, using PI controllers. The cross-coupling terms Δu^d_c and Δu^q_c compensate for the cross coupling between the two control loops, introduced by the transformation to a rotating reference frame. The reference voltage in d- and q-components are then:

$$u^d_{c^{ref}} = u^d_s + \Delta u^d_c + \left(K^d_{p,i} + \frac{K^d_{i,i}}{s}\right)(i^d_{pr^{ref}} - i^d_{pr}) \tag{6.11a}$$

$$u^q_{c^{ref}} = u^q_s + \Delta u^q_c + \left(K^q_{p,i} + \frac{K^q_{i,i}}{s}\right)(i^q_{pr^{ref}} - i^q_{pr}), \tag{6.11b}$$

with

$$\Delta u_c^d = -\omega L_{pr} i_{pr}^q \tag{6.12}$$

$$\Delta u_c^q = \omega L_{pr} i_{pr}^d, \tag{6.13}$$

the cross-coupling terms. After introducing two additional state variables, M_d and M_q, such that:

$$\frac{dM_d}{dt} = K_{i,i}^d (i_{pr^{ref}}^d - i_{pr}^d) \tag{6.14a}$$

$$\frac{dM_q}{dt} = K_{i,i}^q (i_{pr^{ref}}^q - i_{pr}^q), \tag{6.14b}$$

the reference voltages can be expressed as algebraic equations:

$$u_{c^{ref}}^d = u_s^d + \Delta u_c^d + K_{p,i}^d (i_{pr^{ref}}^d - i_{pr}^d) + M_d \tag{6.15a}$$

$$u_{c^{ref}}^q = u_s^q + \Delta u_c^q + K_{p,i}^q (i_{pr^{ref}}^q - i_{pr}^q) + M_q. \tag{6.15b}$$

The actual converter voltages are only equal to the reference voltages in steady-state. During transients, the fast current controller provides a reference value. The actual value of the voltage lags the reference due to the time-lag introduced by the converter's power electronics and digital control circuitry. The relation between the actual and the reference value can be approximated by a time delay with time constant T_σ [110]:

$$\frac{du_c^d}{dt} = \frac{1}{T_\sigma} u_{c^{ref}}^d - \frac{1}{T_\sigma} u_c^d, \tag{6.16a}$$

$$\frac{du_c^q}{dt} = \frac{1}{T_\sigma} u_{c^{ref}}^q - \frac{1}{T_\sigma} u_c^q. \tag{6.16b}$$

The expression for the reference voltages (6.15a) and (6.15b) can be substituted in these equations:

$$\frac{du_c^d}{dt} = -\frac{K_{p,i}^d}{T_\sigma} i_{pr}^d - \omega \frac{L_{pr}}{T_\sigma} i_{pr}^q - \frac{1}{T_\sigma} u_c^d + \frac{1}{T_\sigma} M_d + \frac{K_{p,i}^d}{T_\sigma} i_{pr^{ref}}^d + \frac{1}{T_\sigma} u_s^d, \tag{6.17a}$$

$$\frac{du_c^q}{dt} = -\frac{K_{p,i}^q}{T_\sigma} i_{pr}^q + \omega \frac{L_{pr}}{T_\sigma} i_{pr}^d - \frac{1}{T_\sigma} u_c^q + \frac{1}{T_\sigma} M_q + \frac{K_{p,i}^q}{T_\sigma} i_{pr^{ref}}^q + \frac{1}{T_\sigma} u_s^q. \tag{6.17b}$$

A block diagram of the current control loop is given in Fig. 6.4. Following the discussion on operating limits in section 2.5, the d- and q-axis voltages and currents need to be limited. This is achieved in dynamic simulation by setting the right hand side of the differential equation, associated with the limited variable, to zero, and by setting the limited variable to its minimum or maximum value.

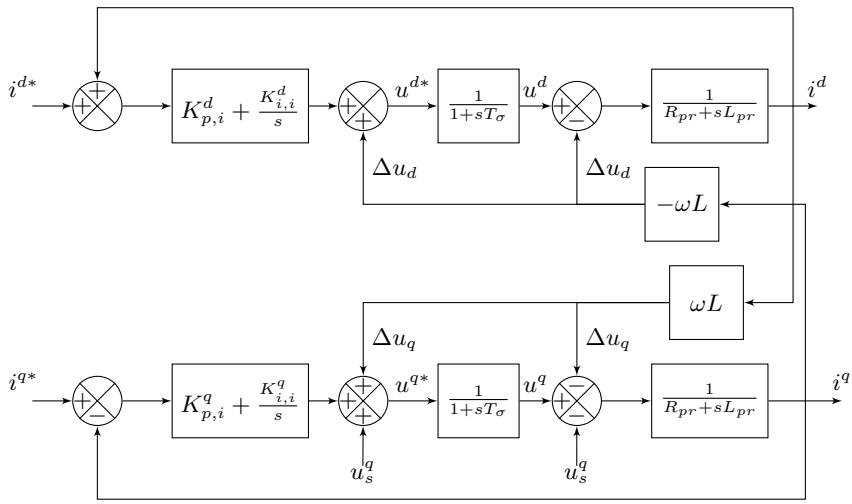

Figure 6.4: Current control loop of VSC HVDC system. Variables with asterisk represent reference values.

6.6.2 Tuning the Current Controller

All well-known methods can be used for the current controller tuning. Here, section 5.4 in [111] is followed, that cites [112] as its main reference. This method allows to specify the desired rise time of the controller. For current controllers a fast rise time is key. The transfer function of the PI controller is:

$$G_{PI} = \frac{U^{dq}_{c^{ref}}}{I^{dq}_{pr^{ref}}} = K_p + \frac{K_i}{s} = K_p\Big(1 + \frac{1}{T_i s}\Big). \tag{6.18}$$

The closed loop transfer function of a first order transfer function $G(s) = \frac{1}{a+bs}$ is:

$$G_{cl}(s) = \frac{\alpha}{s+\alpha} \tag{6.19}$$

for a certain choice of K_p and K_i, with α the bandwidth. The closed loop transfer function of the system, including the controller is:

$$G_{cl} = \frac{G_{PI}(s)G(s)}{1 + G_{PI}(s)G(s)}. \tag{6.20}$$

Equating the right-hand sides of (6.19) and (6.20) gives:

$$G_{PI}(s)G(s) = \frac{\alpha}{s}, \tag{6.21}$$

or

$$G_{PI}(s) = \frac{\alpha}{s} G(s)^{-1} = \frac{\alpha}{s}(a + bs) = \alpha b + \frac{\alpha a}{s}. \tag{6.22}$$

The controller parameters can be calculated directly from (6.22) in function of the bandwidth:

$$K_p = \alpha b, \tag{6.23}$$

$$K_i = \alpha a. \tag{6.24}$$

For a first order system, the relation between rise time T and bandwidth is [111]:

$$\alpha T = ln(9). \tag{6.25}$$

The control parameters can then be expressed in function of rise time as:

$$K_p = \frac{\ln(9)}{T} b, \tag{6.26}$$

$$K_i = \frac{\ln(9)}{T} a. \tag{6.27}$$

These expressions are only valid if $G(s)$ is a first order transfer function.

6.6.3 Outer Controllers

Reactive Power Control and Voltage Control

In a VSC HVDC system, every converter can independently control its reactive power injection in the power system. When the system voltage is aligned with the q-axis, the reactive power Q can be calculated as

$$Q = u_s^q i_{pr}^d. \tag{6.28}$$

The d-axis current setpoint, $i_{pr^{ref}}^d$, is thus calculated from the reactive power setpoint Q_{ref}. A combination of an open loop and a PI controller is used to drive reactive power to its desired value, leading to [25]:

$$i_{pr^{ref}}^d = \frac{Q_{ref}}{u_s^q} + \left(K_{p,q}^d + \frac{K_{i,q}^d}{s}\right)(Q_{ref} - Q). \tag{6.29}$$

Finally state variable N^d is introduced, resulting in an additional differential equation for the PI controller,

$$\frac{dN^d}{dt} = K_{i,q}^d (Q_{ref} - u_s^q i_{pr}^d), \tag{6.30}$$

such that substitution of (6.28) and (6.30) in (6.29) leads to an algebraic expression for the d-axis current reference:

$$i^d_{pr^{ref}} = \frac{Q_{ref}}{u^q_s} + N^d + K^d_{p,q}(Q_{ref} - u^q_s i^d_{pr}), \tag{6.31}$$

which can be substituted in (6.17a). Alternatively, the AC system voltage can be controlled instead of the reactive power. In practice, an extra control loop provides the reactive power reference to the reactive power control loop. In computer models, the d-axis current reference can be calculated directly from the voltage reference using a PI controller:

$$i^d_{pr^{ref}} = \left(K^d_{p,u} + \frac{K^d_{i,u}}{s}\right)(U_{s^{ref}} - U_s), \tag{6.32}$$

with

$$U_s = \sqrt{(u^q_s)^2 + (u^d_s)^2} = u^q_s. \tag{6.33}$$

After introducing state variable N^d, the following equations can be written:

$$\frac{dN^d}{dt} = K^d_{i,u}\left(U_{ref} - u^q_s\right), \tag{6.34}$$

$$i^d_{pr^{ref}} = N^d + K^d_{p,u}\left(U_{ref} - u^q_s\right). \tag{6.35}$$

Equation (6.35) can be substituted in (6.17a).

Active Power Control

In a two-terminal VSC HVDC system, one converter sets the active power, while the other converter controls the DC voltage. In general, an n converter VSC HVDC system has $n-1$ converters controlling active power, and one controlling the DC voltage. The variable $i^q_{pr^{ref}}$ is calculated from the active power setpoint of all converters except the slack converter. One must therefore differentiate between the slack converter and the other converters for the calculation of the q-axis current setpoint. The slack converter's q-axis reference current can be obtained from its DC voltage control equation.

Again using a combination of an open loop and a PI controller, the q-axis reference current can be expressed as:

$$i^q_{pr^{ref}} = \frac{P_{ref}}{u^q_s} + \left(K^q_{p,p} + \frac{K^q_{i,p}}{s}\right)(P_{ref} - P), \tag{6.36}$$

with

$$P = u_s^q i_{pr}^q. \tag{6.37}$$

Introducing a new state variable N^q leads to an extra equation

$$\frac{dN^q}{dt} = K_{i,p}^q (P_{ref} - u_s^q i_{pr}^q). \tag{6.38}$$

After substitution of (6.38) and (6.37) in (6.36), the expression of the q-axis reference current to be substituted in (6.17b) becomes:

$$i_{pr^{ref}}^q = \frac{P_{ref}}{u_s^q} + N^q + K_{p,p}^q (P_{ref} - u_s^q i_{pr}^q). \tag{6.39}$$

DC Voltage Control

The remaining q-axis reference current can be obtained from the slack converter's DC voltage control equation. When a PI controller is used, the reference DC current of the slack converter can be expressed as:

$$i_{dc_n^{ref}} = \left(K_{p,dc} + \frac{K_{i,dc}}{s} \right) \cdot (u_{dcref} - u_{dc_n}). \tag{6.40}$$

This current cannot be delivered instantly due to the converter delay, that is approximated here by a time constant T_{dc}:

$$\frac{di_{dc_n}}{dt} = \frac{1}{T_{dc}} i_{dc_n^{ref}} - \frac{1}{T_{dc}} i_{dc_n}. \tag{6.41}$$

Combining (6.41) and (6.40), and introducing

$$\frac{dM_{dc}}{dt} = K_{i,dc}(u_{dcref} - u_{dc_n}), \tag{6.42}$$

yields the following control equation:

$$\frac{di_{dc_n}}{dt} = \frac{1}{T_{dc}} \left(-i_{dc_n} + K_{p,dc}(u_{dcref} - u_{dc_n}) + M_{dc} \right). \tag{6.43}$$

The next step is the design of the DC voltage controller for a two-terminal system. All well-known techniques such as pole placement and the ones proposed for the current controller, can be used. Here, root locus design is chosen. The following expression can be found for the open loop transfer function from $I_{dc2}(s)$ to $U_{dc2}(s)$ (Fig. 6.2):

$$\frac{U_{dc2}}{I_{dc2}} = \frac{1}{sC_{dc}} \frac{s^2 L_{dc} C_{dc} + sR_{dc} C_{dc} + 1}{s^2 L_{dc} C_{dc} + sR_{dc} C_{dc} + 2}. \tag{6.44}$$

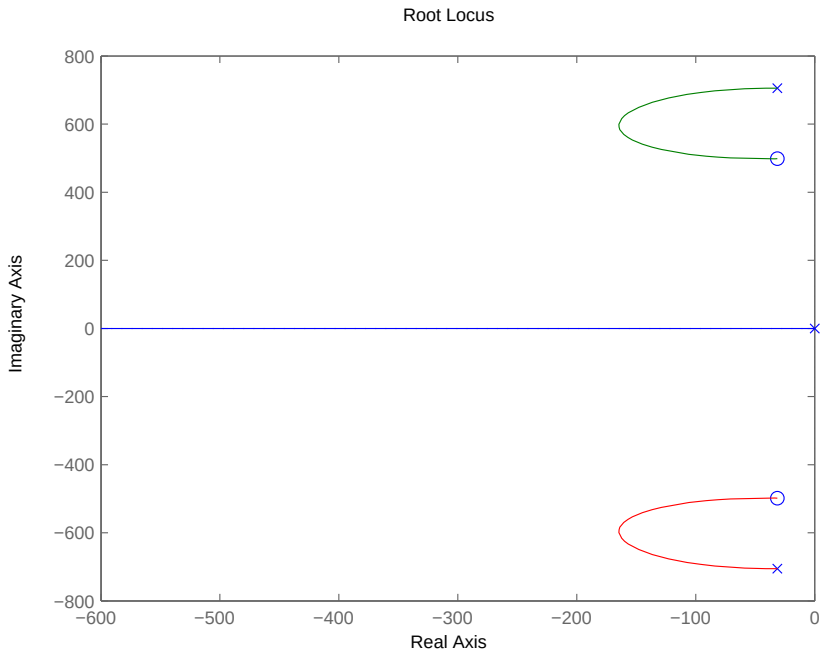

Figure 6.5: Root locus of DC circuit's open loop transfer function.

Its root locus is plotted in Fig. 6.5. The transfer function has a zero pole and two complex conjugate zeros and poles. After some easy but tedious manipulations, the following expression is obtained for the closed loop transfer function:

$$\frac{U_{dc2}}{U_{dc2^{ref}}} = \frac{(K_{i,dc} + K_{p,dc}s)(s^2 L_{dc}C_{dc} + sR_{dc}C_{dc} + 1)}{(s^3 C_{dc}T_{dc})(s^2 L_{dc}C_{dc} + sR_{dc}C_{dc} + 2) + (K^{dc}_{i,dc} + K_{p,dc}s)(s^2 L_{dc}C_{dc} + sR_{dc}C_{dc} + 1)}. \tag{6.45}$$

The PI controller allows to place a zero, and select a gain. In Fig. 6.6 root loci for different zero locations are shown. In Fig. 6.7, a close-up is shown for a zero at -15 and -10. Lines of constant damping and constant natural frequency are plotted to help select a suitable gain and a good location for the zero. Strictly speaking, these lines are only valid for second order systems, and must be treated as rough

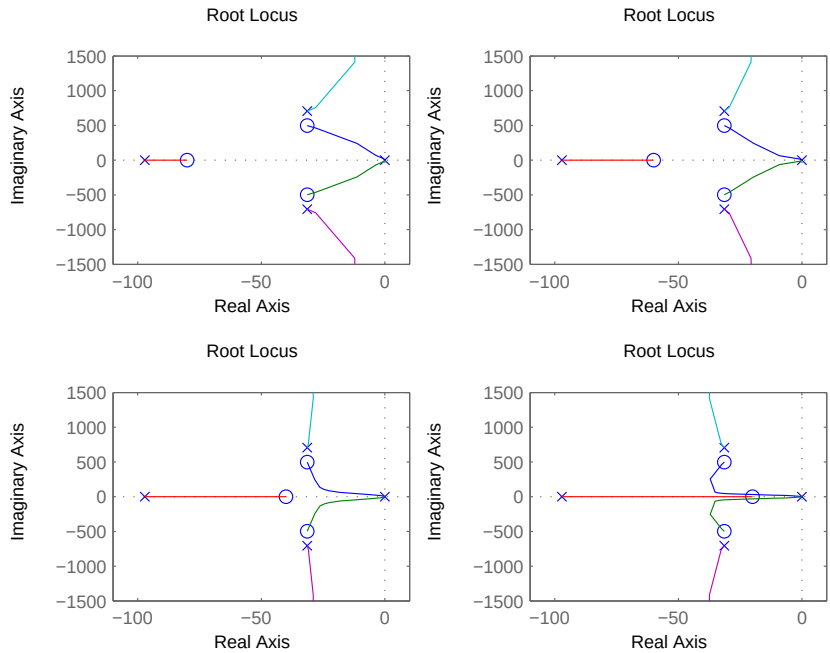

Figure 6.6: Root loci for different zero locations. From top left to bottom right: zero at -80, -60 and at -40, -20.

approximations for higher order systems [113, p.145]. The zero is placed at -10, close to the natural frequency in accordance with the recommendations in [113, p.313]. The gain is determined such that the poles are as far to the left as possible. The step response is plotted in Fig. 6.8.

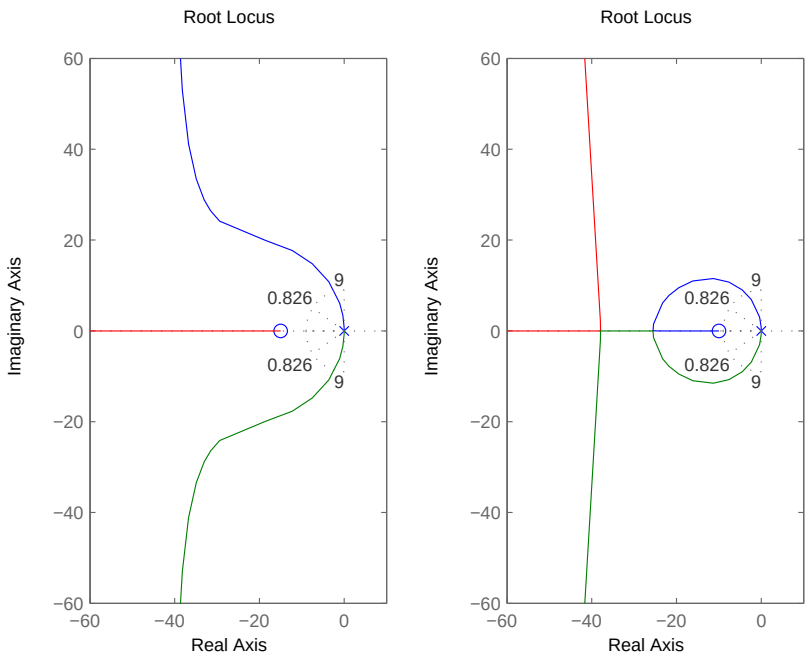

Figure 6.7: Close up of root loci for zero location -15 and -10.

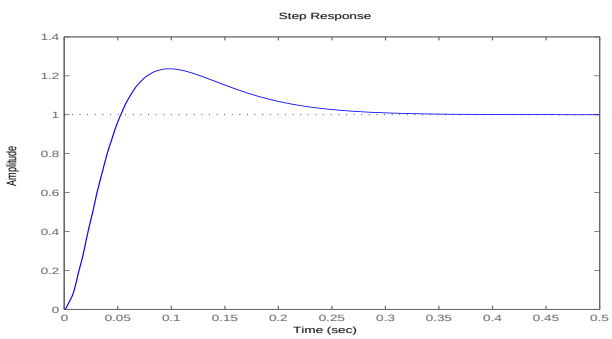

Figure 6.8: Step response of the DC voltage controller, designed with root locus method.

6.7 Phase-Locked Loop

In general, a PLL is "a circuit synchronizing an output signal (generated by an oscillator) with a reference or input signal in frequency as well as in phase." [114, p.1] It is a control system that acts on the phase difference between the reference signal and the output, such that the phase of the output is locked to the phase of the reference. [114, p.1] All PLLs consist of three basic components: a phase detector (PD), a loop filter (LF), and a voltage controlled oscillator (VCO) (Fig. 6.9). The phase detector compares the phase of the input or reference signal with the phase of the output signal, produced by the voltage controlled oscillator. The voltage controlled oscillator produces an oscillating signal with a frequency determined by the output signal of the loop filter. The loop filter removes noise and high frequency signals, and is responsible for the control of the PLL.

Here the circuit of Fig. 6.10 is used. It is a type 2 loop, most prevalent in phase-locked loops [115, p.16]. The differential equations of the system are:

$$\dot{x} = \frac{K_{pd}}{b}(\theta_i - \theta_o), \tag{6.46}$$

$$\dot{\theta_o} = K_{vco}\left(\frac{K_{pd}}{b}(\theta_i - \theta_o) + ax\right). \tag{6.47}$$

The design of the PLL can have a major influence on the dynamic behaviour of the system. Therefore, it is now common practice to include a detailed PLL model in electromagnetic programs. In phasor modelling it is less common to model the PLL. However, it has been shown in some contributions that the PLL has an influence on stability. A PLL introduces a small delay, between 10-100 ms according to [20, p.5]. In [116], it has been shown that the PLL delay can

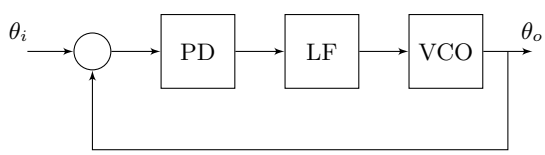

Figure 6.9: General structure of a PLL circuit.

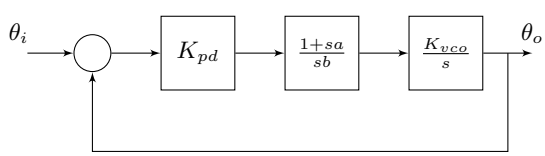

Figure 6.10: PLL implementation.

cause undesired power exchange. To investigate the influence of the PLL on power system stability, simulations are performed with and without PLL using modified versions of MATPOWER [89] and *MatDyn* [90]. At $t = 0.2$, a large load with P and Q component is switched in. Fig. 6.11 shows a close up around $t = 0.2$ of the converter's reactive power output. If a PLL is modelled, its time delay causes the reactive power output to drop first, in accordance to the results obtained in [116]. Without PLL, this behaviour is not present. When looking at overall reactive power output (Fig. 6.12), it can be seen that the difference is very small and does not significantly impact the other state variables, and thus can be safely neglected in power system stability studies.

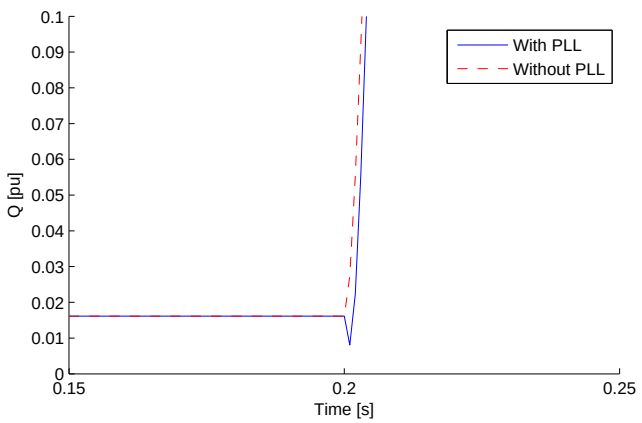

Figure 6.11: Converter reactive power with and without PLL (close up).

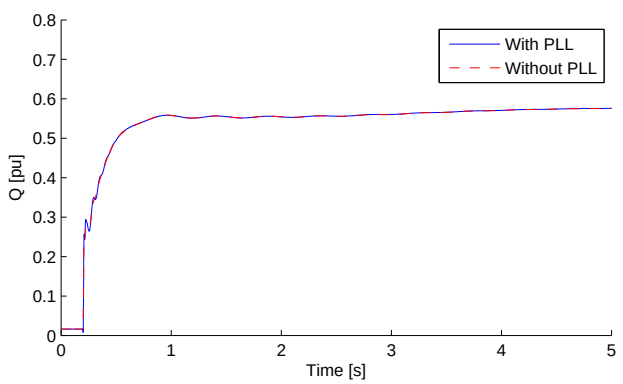

Figure 6.12: Converter reactive power with and without PLL.

6.8 Filter

Many models proposed in the literature do not take into account the filter bus, e.g.: [103], [117], [118], [119]. However, it can be included as shown in Fig. 6.13. It was shown in [120] that the filter behaves as a pure capacitor at system frequency. The equations of this system are:

$$u_c(t) - u_f(t) = L_{pr}\frac{di_{pr}(t)}{dt} + R_{pr}i_{pr}(t), \tag{6.48}$$

$$u_f(t) - u_s(t) = L_{tr}\frac{di_{tr}(t)}{dt} + R_{tr}i_{tr}(t), \tag{6.49}$$

$$i_{pr}(t) = i_{tr}(t) + C_f\frac{du_f(t)}{dt}. \tag{6.50}$$

In Figs. 6.14 and 6.15 the response of the converter voltage to a step in d-axis reference current is shown for different values of the filter capacitance in p.u. A slightly higher or lower value of the filter capacitance has a large influence on the magnitude of the converter voltage. However, from a system perspective, quantities such as active and reactive power injected in the network are more important. The effect on active and reactive power output is less pronounced (Figs. 6.16 and 6.17). If voltage limiters are implemented, the converter voltage reaches its operating limits at different instants depending on the value of the filter capacitance. This has a small influence on the power output (Fig. 6.18). It can be concluded that neglecting the filter for power system stability studies leads to slightly different results. The advantage of neglecting filters is that four state variables and associated equations are eliminated per converter.

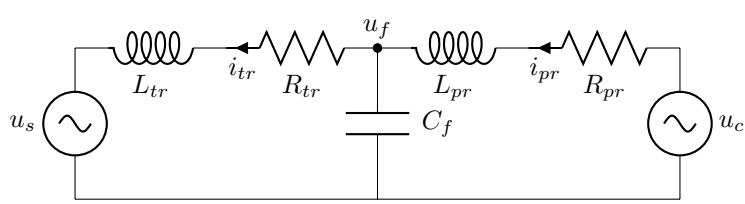

Figure 6.13: Single-line diagram of the AC Circuit with filter. u_s is the system voltage, u_c the converter voltage.

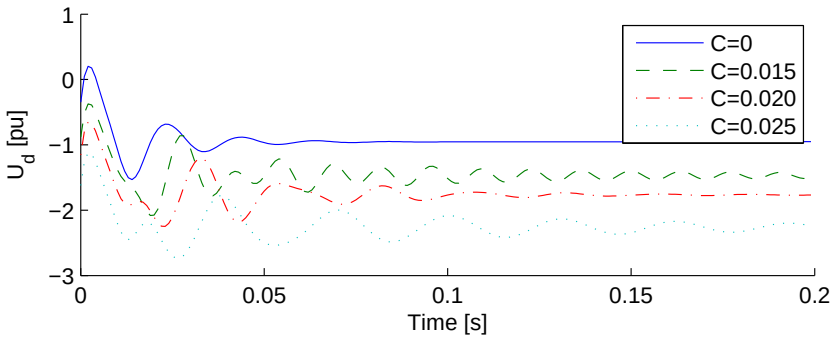

Figure 6.14: *d*-axis converter voltage for different values of filter capacitance in p.u.

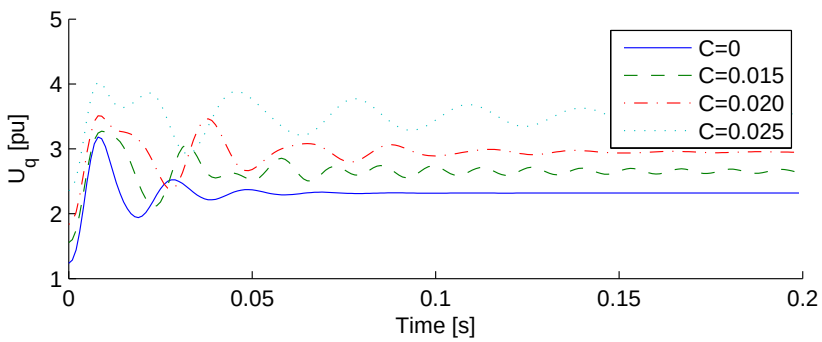

Figure 6.15: *q*-axis converter voltage for different values of filter capacitance in p.u.

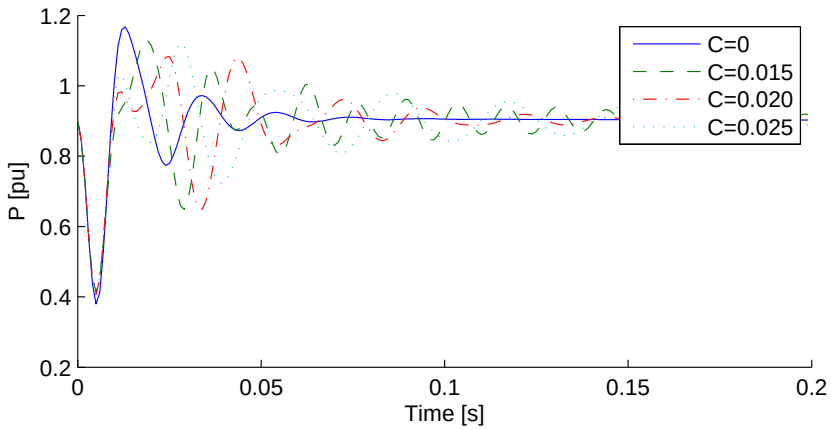

Figure 6.16: Converter active power for different values of filter capacitance in p.u.

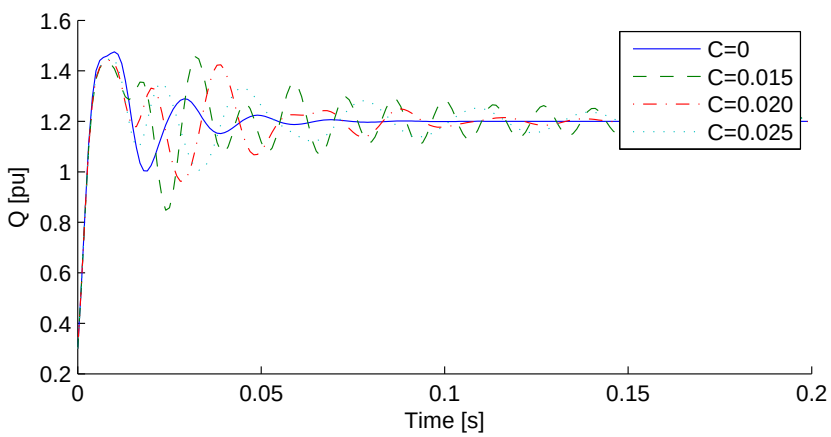

Figure 6.17: Converter reactive power for different values of filter capacitance in p.u.

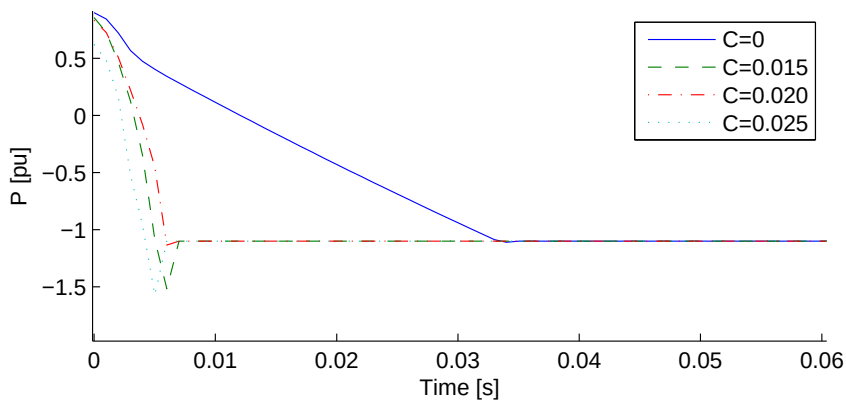

Figure 6.18: Converter active power with converter voltage limits.

6.9 Reduced Order Models

A set of new models is now derived that are simplifications of the full model. A correct way of deriving simplified models is eliminating very small time constants. This is equivalent to making the assumption that very fast dynamics are infinitely fast compared to slower phenomena. The full model has five time constants. For the AC side: T_σ, the time constant of the power electronics, and the time constant associated with the phase reactor. For the DC circuit: the time constant T_{dc}, and the time constants related to L_{dc}, and C_{dc}. Each of the time constants are analysed now.

- AC current dynamics

  By removing the phase reactor from the AC circuit ($L_{pr} = 0$), the AC current responds instantaneously to variations in the voltage difference between the AC system and the converter. The differential equations describing the current dynamics (6.48) to (6.50) or (6.3a) and (6.3b) disappear. This simplification is only of theoretical interest, as the phase reactor is the most important element at the converter's AC side.

- AC Voltage dynamics

  The AC voltage dynamics can be neglected formally by assuming that the voltage is equal to the voltage reference, or $T_\sigma = 0$. The equations describing the voltage dynamics (6.17a) and (6.17b) disappear. The time delay of power electronics is then neglected.

- DC line current (i_{cc}) dynamics

  By removing the inductor from the DC circuit, L_{dc} is set to zero and the dynamics of the DC line currents disappear from the model.

- DC voltage dynamics

  By removing the capacitors from the DC circuit, C_{dc} is set to zero and the dynamics of the DC voltage disappear from the model. This is also of theoretical interest only, as the DC capacitors are the most important element in the DC circuit.

- DC current (i_{dc}) dynamics

  Lastly, the assumption $T_{dc} = 0$, removes the DC current dynamics. It assumes that the DC current required by the DC voltage controller is provided by the converter without delay.

The five simplifications can be implemented separately or combined. In total, 31 simplified models can be constructed, corresponding to $2^5 - 1 = 31$ combinations.

The advantage of the simplifications is a reduction of the number of differential equations. Furthermore, less data is needed which can be hard to collect for practical systems. Even more advantageous is the possibility to speed up calculations significantly by using a larger integration step size, if the overall systems dominant time constant is removed. An intelligent way to simplify the full model is thus to remove one or more of the smallest time constants. The difficulty in proposing a standard simplified model lies in the fact that the smallest time constants depend on the parameters, which can vary considerably between different systems. The following generalities can nevertheless be agreed upon:

- the DC capacitors are the dominant elements in the DC circuit and their corresponding time constants should be maintained;
- the phase reactor is the dominant element in the converter AC side and its corresponding time constant should be maintained.

The three time constants that can be removed, are: T_σ, and those related with L_{dc}, and T_{dc}. We suggest to neglect them all because it cannot be determined which one is the smallest. The remaining dynamics are those associated with the outer controllers, the phase reactor and the DC capacitors. Compared to the full model, the order of the model is reduced by $2n + m + 1$, for a n converter system with m DC lines. Furthermore, a larger step size can be selected.

To validate this last claim, the full and reduced order models are solved using a variable step size solver. It is expected that the full order system requires a smaller step size, and hence more steps. Step sizes are plotted in Fig. 6.19. Contrary to what is expected, the reduced order systems actually require a smaller step size than the full order system. The full order model is solved in 340 steps, the reduced order model in 1296.

To further analyse the discordant results, the DC system of a two-terminal VSC HVDC connection is simulated. The full system equations are given by the DC circuit equations (6.4), (6.5), and (6.6), and the control equations (6.42), and (6.43). The reduced system equations are obtained by setting $L_{dc} = 0$ in (6.6), and $T_{dc} = 0$ in (6.43). A step response in DC voltage order is applied. The full system is first solved with an explicit method. In this case, Matlab's ode45[1] solver is used. The solver uses a variable step size. The result and evolution of the step size for the full system is given in Figs. 6.20 and 6.21. The adaptive step size algorithm needs 785 steps to solve the system. The same simulation has been repeated for the reduced order system. The solution is plotted in Fig. 6.22. This time, the adaptive step size algorithm needs a very small, oscillating step size (Fig. 6.23), and requires a staggering 150725 steps. It seems that the reduced

[1]Ode45 is a Runge-Kutta Dormand-Prince solver from the Matlab ODE suite, suited for non-stiff systems [95]. It is similar to the Fehlberg method used in *MatDyn*.

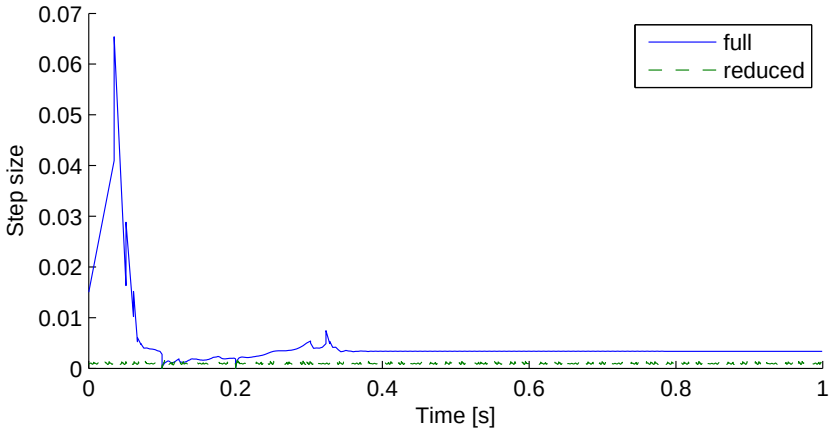

Figure 6.19: Comparison of the step size of full and reduced order models (Fehlberg, tolerance = 1e-4).

order model is seriously disadvantaged as compared to the full order model, which is counterintuitive. The simulations for the full and reduced order systems are now repeated with a different solver, here Matlab's ode15s[2], which uses an implicit integration method. The result is obtained in 597 steps (Figs. 6.24 and 6.25), which is less than the required 785 steps for the explicit method. The reduced order model is solved in just 41 steps (Figs. 6.26 and 6.27), which is not only less than the 150725 steps needed by the explicit method, but is, more importantly, also less than the 597 steps needed by the implicit method to solve the full order model. The expected behaviour that the reduced order model can be solved with larger step size, is thus confirmed for implicit methods. The conclusion is that an implicit method should be used to solve the reduced order model.

[2]Ode15s is a solver from the Matlab ODE suite based on the Numerical Differentiation Formulas (NDF), particularly suited for stiff systems [95].

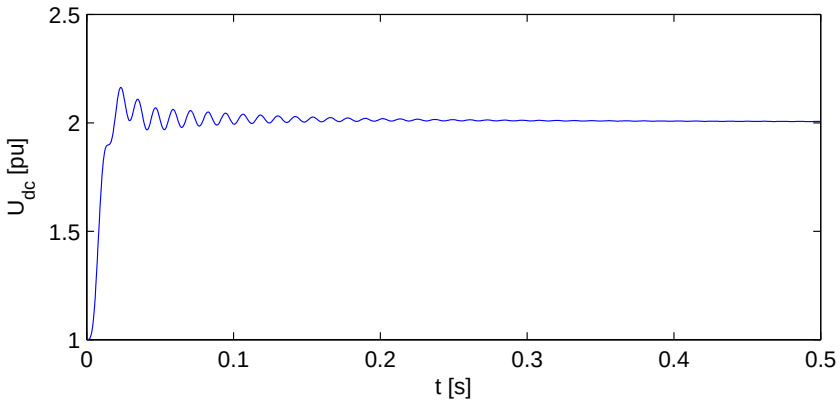

Figure 6.20: Full system, solved in 785 steps by explicit solver: DC voltage.

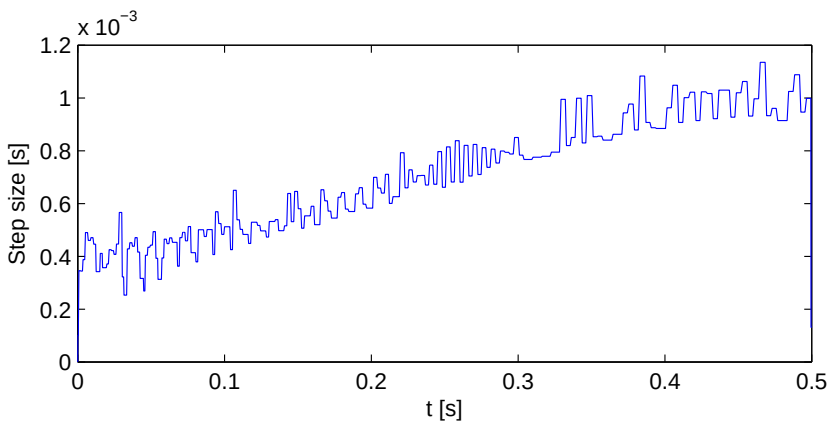

Figure 6.21: Full system, solved in 785 steps by explicit solver: step size.

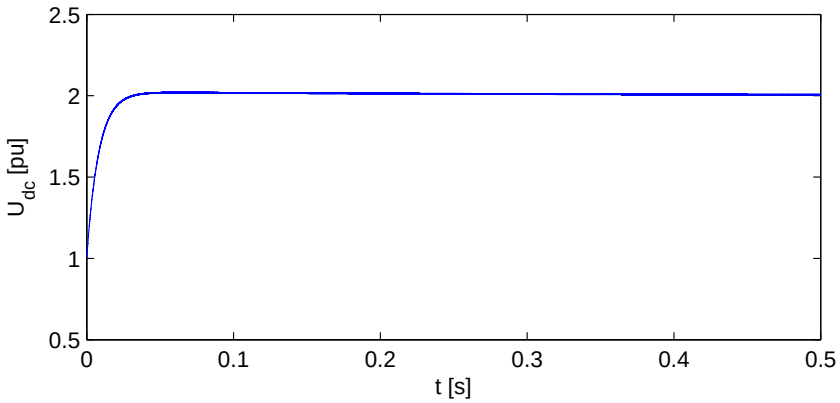

Figure 6.22: Reduced system, solved in 150725 steps by explicit solver: DC voltage.

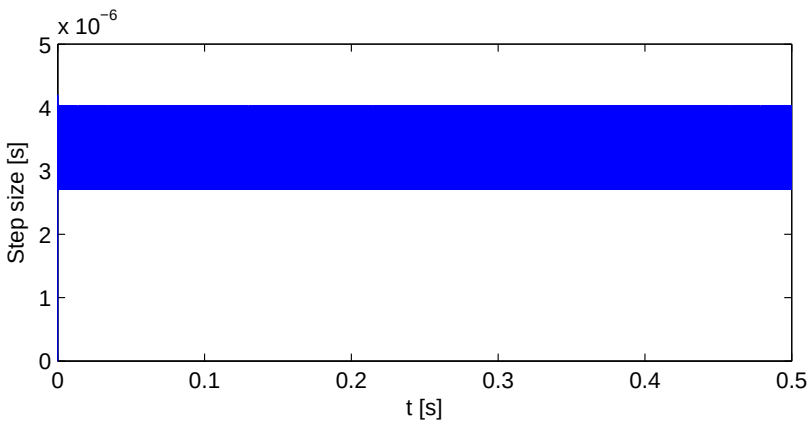

Figure 6.23: Reduced system solved in 150725 steps by explicit solver: step size. The step size oscillates between approximately $3 \cdot 10^{-6}$ and $4 \cdot 10^{-5}$.

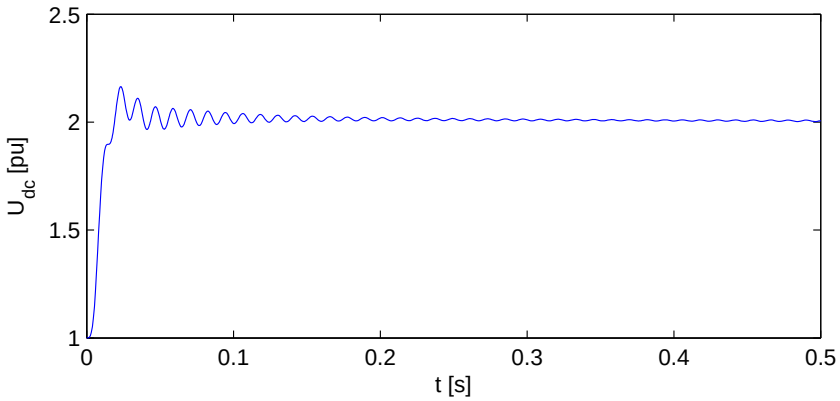

Figure 6.24: Full system, solved in 597 steps by implicit solver: DC voltage.

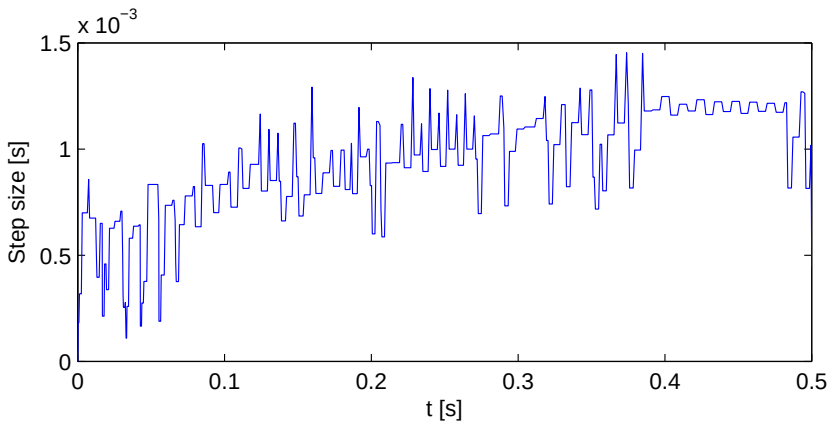

Figure 6.25: Full system, solved in 597 steps by implicit solver: step size.

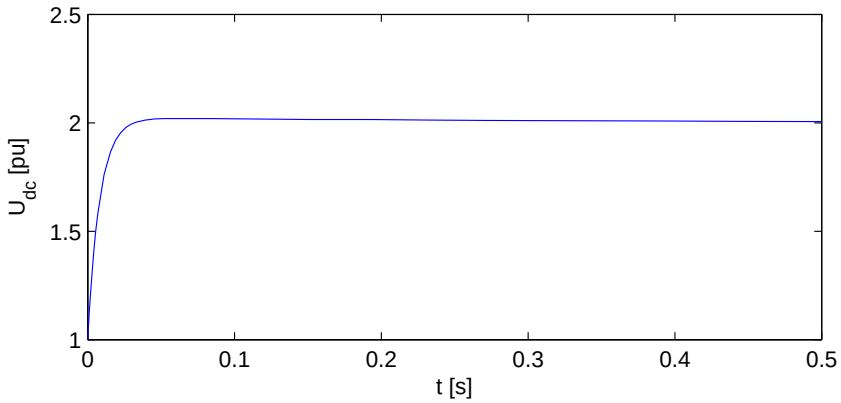

Figure 6.26: Reduced system, solved in 41 steps by implicit solver: DC voltage.

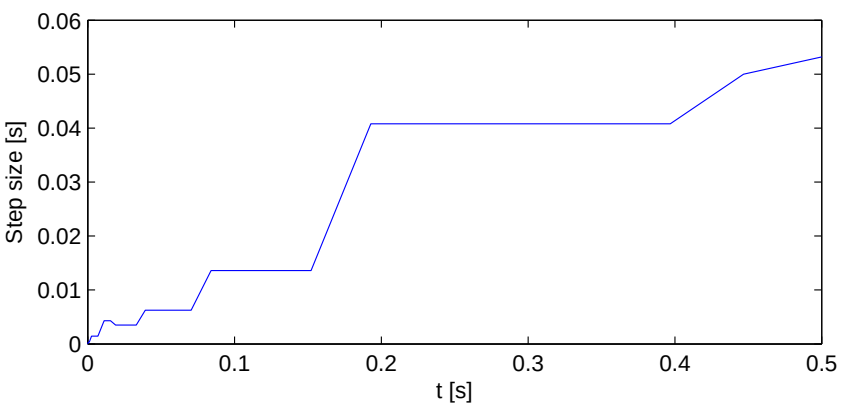

Figure 6.27: Reduced system, solved in 41 steps by implicit solver: step size.

6.10 Implementation Aspects

In order to incorporate VSC HVDC systems, drastic changes to the AC power system analysis software such as presented in Chapter 5, are required. In the following, the parts of the program that need to be altered are listed, and the changes explained.

6.10.1 Power Flow

The power flow calculation at the start of the dynamic simulation run needs to be changed. As there are now converters present, an AC/DC power flow needs to be solved. Any power flow model presented in Chapter 4 can be directly used to solve the AC/DC power flow equations. However, the power flow model should be consistent with the dynamic model: e.g. if the filter is included in the dynamic model, it should be included in the power flow model as well. If losses are taken into account in the power flow model, they have to be added to the dynamic model as well.

6.10.2 Dynamics

The dynamics of the VSC HVDC system can be entered in the same way as other dynamic equipment such as excitation systems. Two functions must be provided. The first one calculates the initial values of the state variables. This function is called after the power flow to obtain a steady-state starting point for the dynamic simulation. The second function contains the actual differential equations, that are fed into the integration subroutine, along with all other differential equations.

6.10.3 Converter Representation

A major difference with AC control equipment such as exciters is that HVDC converters inject current in the nodes. Hence, they directly alter the network equations, something they have in common with generators and FACTS devices. Due to the identity of generators' and converters' equivalent circuits, they can be represented similarly in power system analysis software. In $MatDyn$ it was chosen to represent generators as Norton equivalents. HVDC converters are therefore also represented as Norton equivalent circuits. There are two places in the program where the Norton equivalent comes into play: when building the augmented admittance matrix, the converters' Norton admittances have to be appended to the matrix, and when solving the network equations, the contribution of the converters to the injected current in the nodes has to be taken into account. In passing, it

is mentioned that the interface between the F and G set is developed in the same way as with generators: the variables of every converter are calculated in their own rotating reference frame, determined by the converter's PLL.

6.10.4 Generalised MTDC Equations

The generalised equations of the DC circuit are obviously very ill-suited to software implementation, if expressed in the form of (6.7). However, (6.7) can be represented by a matrix equation (6.51), that can be conveniently entered in a Matlab based toolbox such as *MatDyn*:

$$\left[C_{dc_i}\frac{dU_i}{dt}\right] = \boldsymbol{I_{dc}} + \mathsf{C}\boldsymbol{I_{cc}}. \tag{6.51}$$

The matrix C is the n x m incidence matrix of the directed graph describing the DC network.[3] It can be obtained as a byproduct of the construction of the DC bus admittance matrix $\mathsf{Y_{dc}}$, built only once if no topology changes occur during simulation. If topology changes, such as the loss of DC lines, do occur, the proposed formulation (6.51) remains valid but C changes. The loss of a DC line for instance, can be simulated by simply removing the line from the power flow data and rebuilding the DC bus admittance matrix $\mathsf{Y_{dc}}$, which also gives the network incidence matrix C, and matrices $\mathsf{Y_{dcf}}$ and $\mathsf{Y_{dct}}$, introduced in section 4.4.3. The dynamic equations (6.51) are automatically updated. Note that (6.8) can be directly written as a matrix equation.

If (6.51) were to be implemented in all its generality in a commercial grade power system software, it should be implemented at the source code level by the developer, as it would be very difficult or even impossible to use block-diagram based editors of commercial power system software.

6.11 Validation

The detailed model is validated by comparison with a manufacturer delivered phasor model, the HVDC Light model, that is in turn validated by a very detailed EMTP model. A normal way to proceed is to first validate the inner current loops, and subsequently the outer controllers. However, for intellectual property reasons, the manufacturer's model is delivered in compiled format. As a result, very few information is available for verification: nothing is known on the inner current loops, and the exact implementation of the control loops, nor their parameters,

[3]The incidence matrix of a directed graph is defined as a matrix with element $c_{ij} = -1$ if line i leaves node j, $c_{ij} = 1$ if line i enters node j and $c_{ij} = 0$ otherwise.

are known. In short, there is no way to get exactly the same results. Therefore, the aim is a general, but close correspondence between the models' output.

The test circuit is a two-terminal VSC HVDC system between two generators with a low short circuit ratio of 3. Three cases are simulated: a step change in active power order, a step change in AC voltage order, and a step change in DC voltage order. The results for a step change in active power order are shown in Fig. 6.28. The behaviour of the converter where the step change is applied is almost identical for both models, but the behaviour of the second converter, the lower curve, does not match perfectly. Because of the limited information at our disposal, it cannot be determined what causes the discrepancy. The results for a step change in AC voltage order are shown in Fig. 6.29. The HVDC Light model reacts slower but exhibits less overshoot. The model's parameters could be changed to obtain a closer match, but it has to be borne in mind that the model's behaviour then also changes in other simulations. The reaction of the DC voltage to a step change is shown in Fig. 6.30. There is a very good correspondence between the models. In our model more dynamics are present because the cable inductance is modelled, while this is not the case in the HVDC Light model.

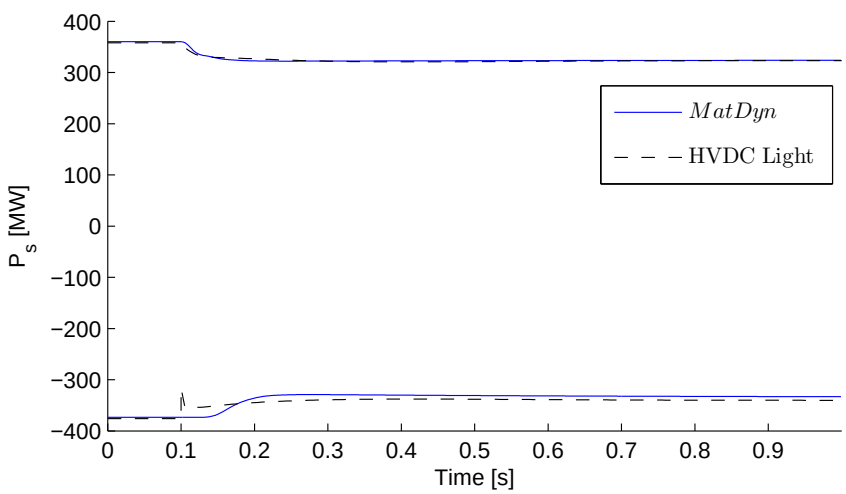

Figure 6.28: Step change active power order.

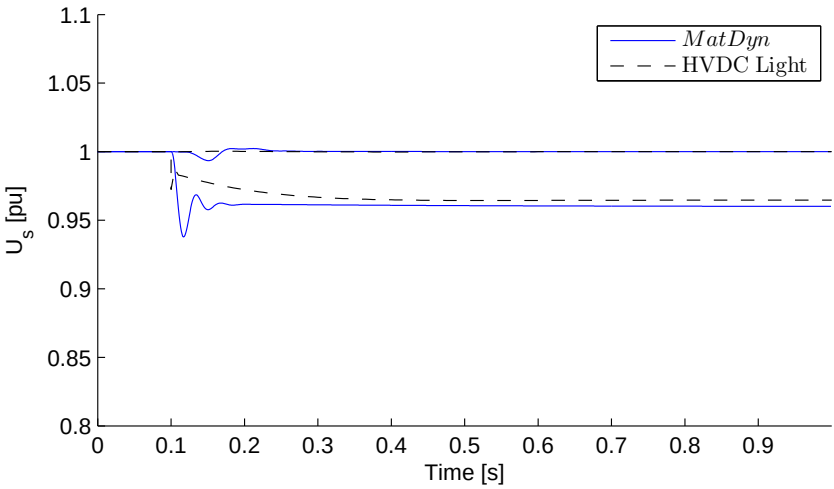

Figure 6.29: Step change AC voltage order.

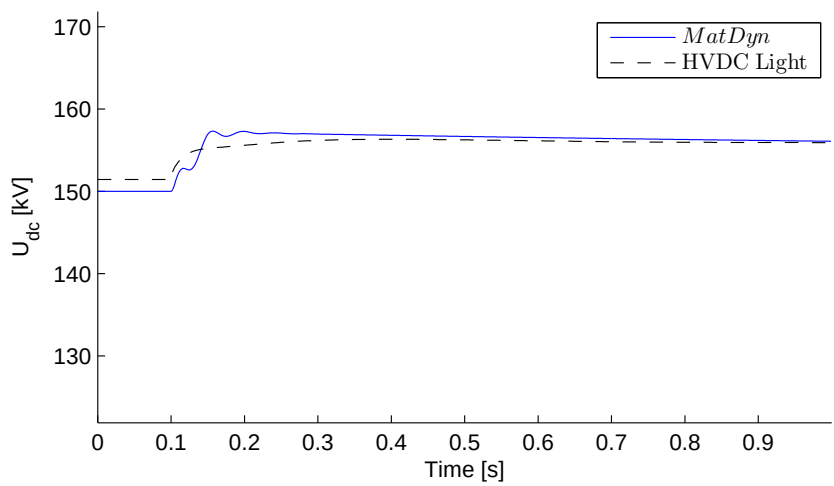

Figure 6.30: Step change DC voltage order.

6.12 Simulations

The models' performance is now verified by numerical simulation. In these simulations, the methods and tools presented in Chapters 4 to 6 are combined: the power flow model presented in Chapter 4 is integrated in *MatDyn*, where it is used to obtain a steady-state point. The dynamic models derived in this chapter are integrated in *MatDyn*, following the methods outlined in section 6.10. The whole system is solved as explained in Chapter 5. All simulations are performed using modified versions of MATPOWER[89] and *MatDyn*[90]. The ODEs are solved with a Modified Euler method with step size 1 ms.

6.12.1 Two-terminal System

First, a two-terminal VSC HVDC system installed in a 9-bus, 3-generator network is considered. The data is included in MATPOWER's `case9` and *MatDyn's* `case9dyn` data files. A single-line diagram is shown in Fig. 5.12[4]. A VSC HVDC link, described by the proposed model, is installed between buses 2 and 3. At $t = 0.2$, the DC voltage setpoint is changed. In Fig. 6.31 it can be seen that the new reference value is reached after a small transient. In all figures, dotted lines represent reference values and full lines response values. The transient propagates to the AC side. In Fig. 6.32, the influence on the system voltages is shown. At the inverter side, the transient is higher because this converter controls the DC voltage. The DC voltage step causes an instantaneous power unbalance, counteracted by the inverter active power reference. The active power reference of the rectifier remains unchanged (Fig. 6.33).

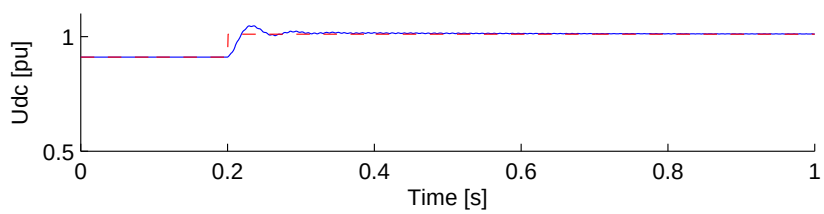

Figure 6.31: DC voltage of the two-terminal system.

[4]The power flow data of Anderson and Fouad's case and MATPOWER's casefile is identical. However, the bus numbering does not correspond. Bus numbers 1-9 in MATPOWER's casefile correspond to 1,2,3,4,6,9,8,7,5 in Anderson and Fouad's case

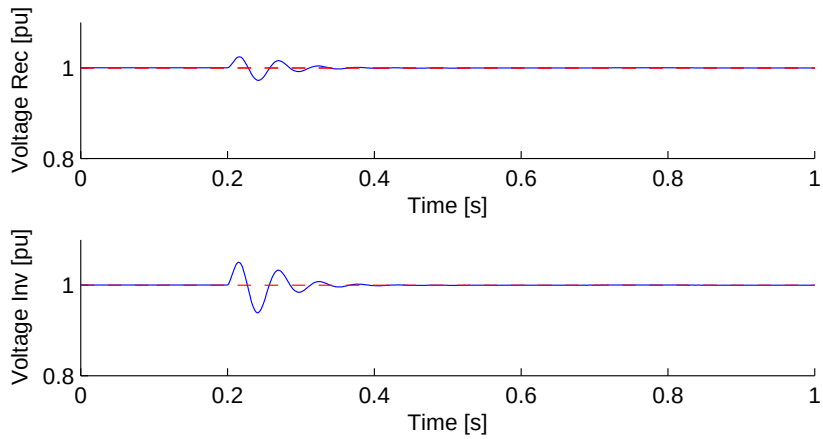

Figure 6.32: System voltages at rectifier and inverter of the two-terminal system.

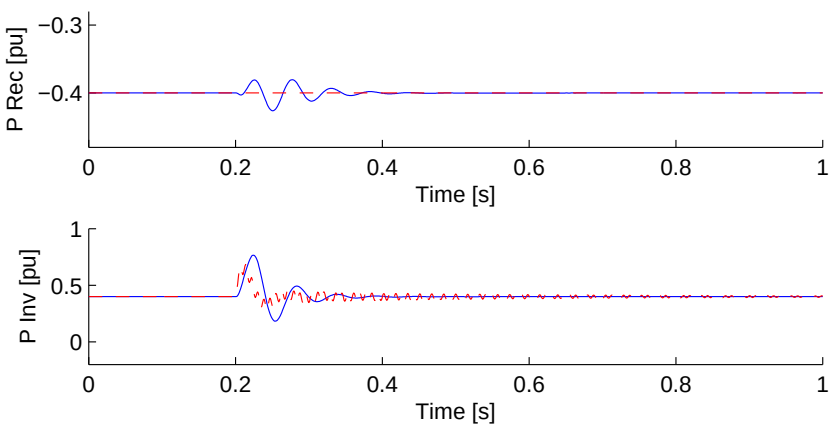

Figure 6.33: Active power at rectifier and inverter of the two-terminal system.

6.12.2 Multi-terminal System

A six-terminal VSC HVDC system is simulated to test the proposed model. The sixth converter controls the DC voltage. The DC circuit consists of seven lines, line 1-2, 1-6, 2-3, 3-4, 4-5, 4-6, and 5-6 (Fig. 6.34). For simplicity, the parameters of all DC lines are equal, and it is assumed that all converters are connected to strong AC systems. However, the validity of the model is not dependent on these conditions. At $t = 0.2$, the loss of line 5-6 is simulated. The current through the line drops to zero, and is distributed amongst the other lines (Fig. 6.35). As expected, the current through lines 1-6 and 4-6 rises to compensate for the loss of line 5-6. In Fig. 6.36 the response of the DC voltage is shown. As a result of the changed flows, the DC voltages settle to new values after the transient. Only the voltage of the slack converter, U_6, returns to its pre-fault value.

6.12.3 Anderson and Fouad's Benchmark Case Revisited

Anderson and Fouad's benchmark case presented in section 5.9.6 is revisited to study interactions between VSC HVDC systems and the AC power system. To this end, the case is changed by modelling the equipment in more detail. First of all, the fourth-order generator model is used to represent all generators instead of the more simple classical model. All data for the fourth order model is given in Table 2.1 of [99, p.39]. The single-line diagram is given in Fig. 5.12. To comply with the requirements of $MatDyn$, the q-axis transient reactance is set to the same value as the d-axis transient reactance, and the leakage reactance is neglected. In order to avoid numerical problems, the q-axis transient time constant of generator 1 is changed from 0 s to 1 ms. The resulting data is shown in Table 6.1. Secondly, an IEEE DC1A exciter model is added to each generator. Due to the small simulation interval (2 s), neither turbines nor their governors are modelled.

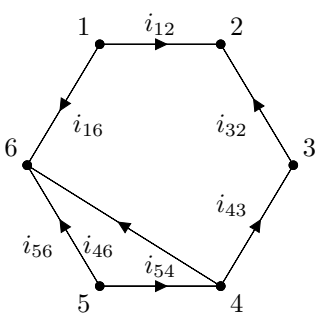

Figure 6.34: Topology of six-terminal system.

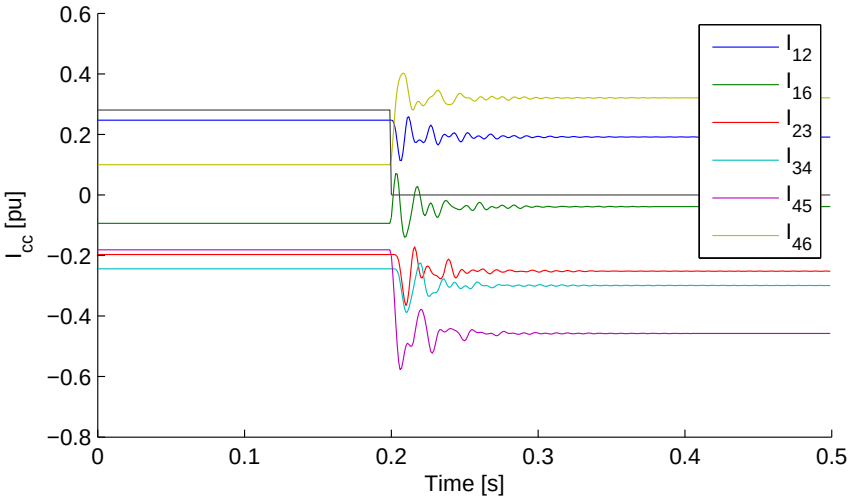

Figure 6.35: DC currents of the six-terminal system.

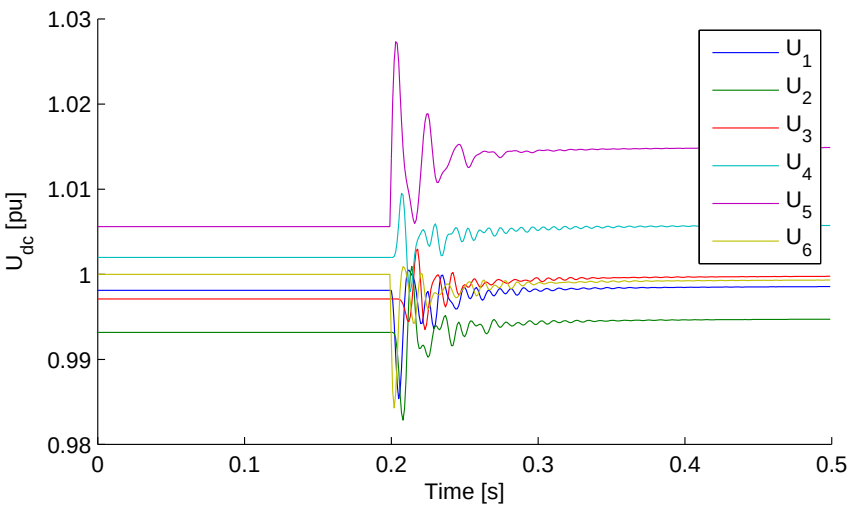

Figure 6.36: DC voltages of the six-terminal system.

The event sequence of the simulation run is:

- a three-phase fault on bus 2 at 0.1 s;
- clearing of the fault in five cycles (0.183 s);
- opening of line 5-7 at 0.184 s.

The results of the simulation with the new data are shown in Figs. 6.37 to 6.40. To assess the system's stability, angles and speeds are plotted with respect to the Centre of Inertia (COI) angle and speed respectively [121]. The system is unstable.

Table 6.1: Generator data Anderson and Fouad's benchmark case.

Generator	1	2	3
S_{nom} [MVA]	247.5	192.0	128.0
U_{nom} [kV]	16.5	18.0	13.8
x_d [p.u.]	0.1460	0.8958	1.3125
x_q [p.u.]	0.0969	0.8645	1.2578
$x'_d = x'_q$ [p.u.]	0.0608	0.1198	0.1813
T'_d [s]	8.96	6.00	5.89
T'_q [s]	0.001	0.535	0.600
H [MW $\cdot$ s]	2364	640	301

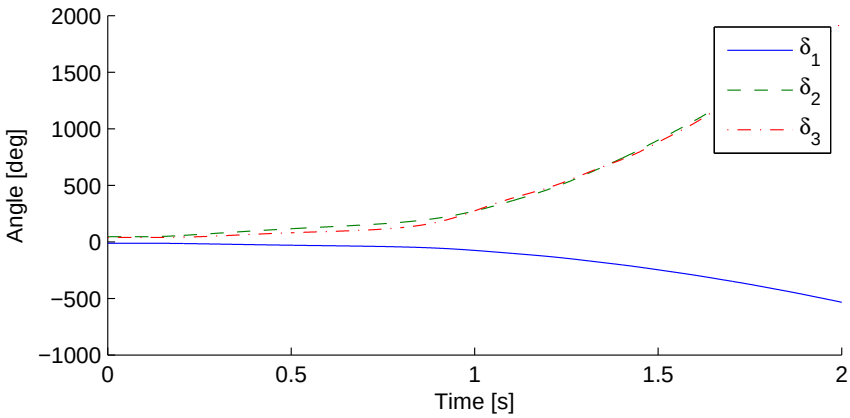

Figure 6.37: Generator angles with respect to COI without HVDC.

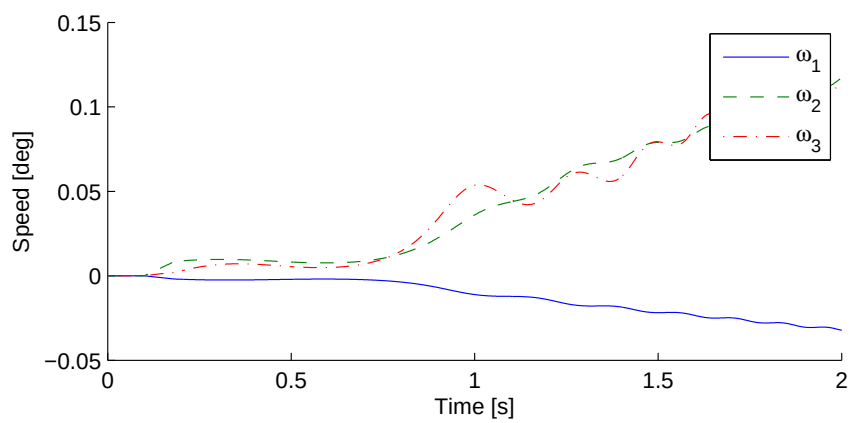

Figure 6.38: Generator speeds with respect to COI without HVDC.

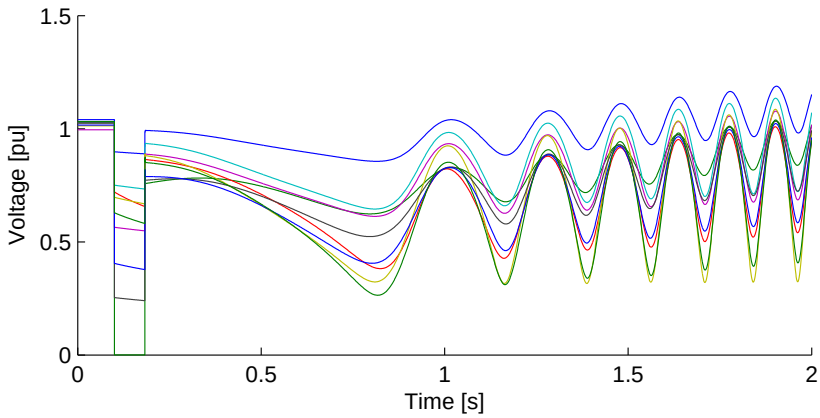

Figure 6.39: Voltages without HVDC.

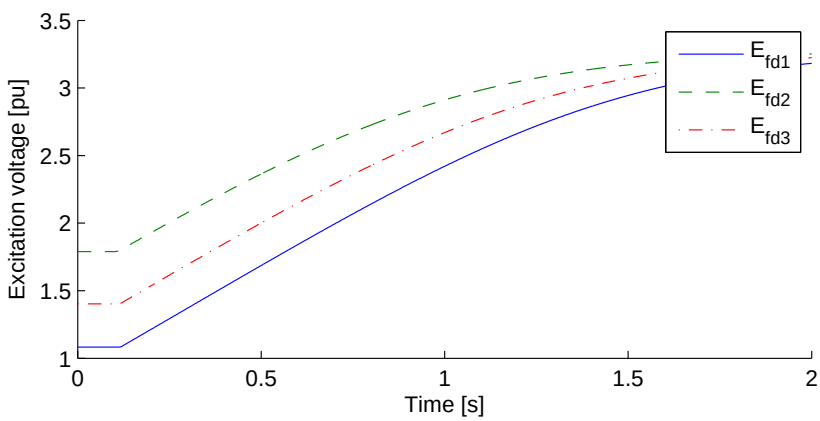

Figure 6.40: Excitation voltages without HVDC.

The simulation is now repeated for the network with a three-terminal VSC HVDC system connected between nodes 5, 6, and 8. The converters' active power setpoints are 50 MW injection in bus 5 and -25 MW injection in buses 6 and 8. The results are shown in Figs. 6.41 to 6.48. The system is stable (Figs. 6.41 and 6.42). The HVDC system's state variables (Figs. 6.45 to 6.48) reach steady-state quicker than those of the generators and their controllers (Figs. 6.41 and 6.44). The interaction between the generators' and converters' voltage controllers can be observed from these figures. It is reminded that the converter blocking during a fault is not included in the model. This is why the voltages rise during the fault, and why there is a marked overvoltage at fault clearing (Fig. 6.43).

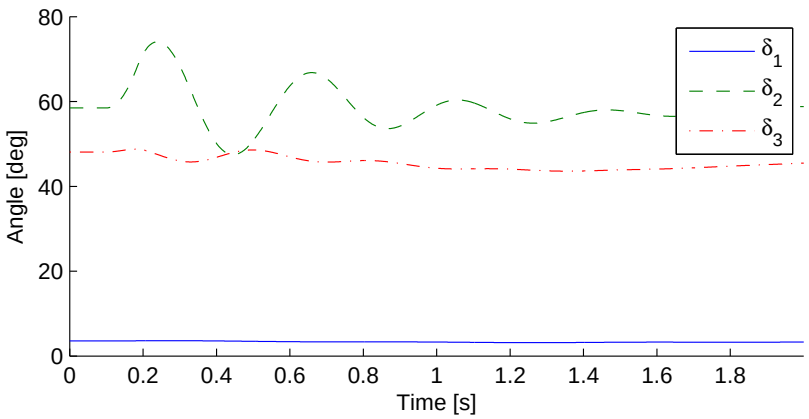

Figure 6.41: Generator angles with HVDC.

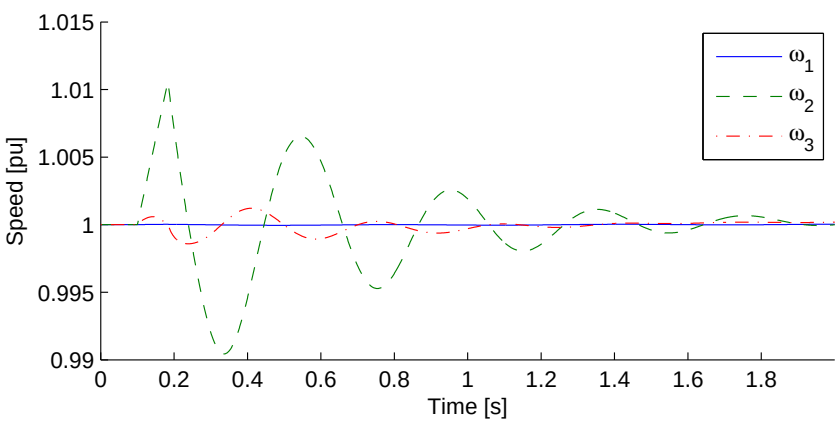

Figure 6.42: Generator speeds with HVDC.

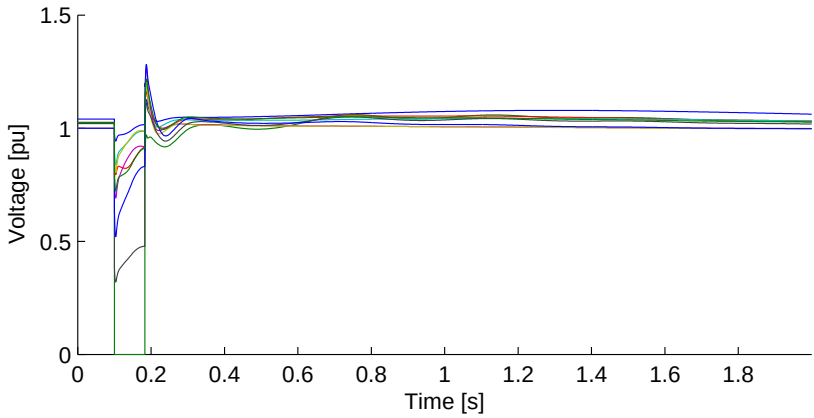

Figure 6.43: Voltages with HVDC.

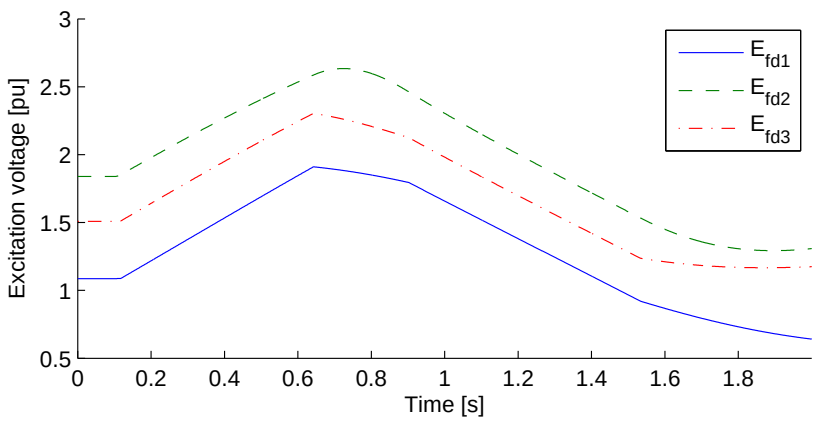

Figure 6.44: Excitation voltages with HVDC.

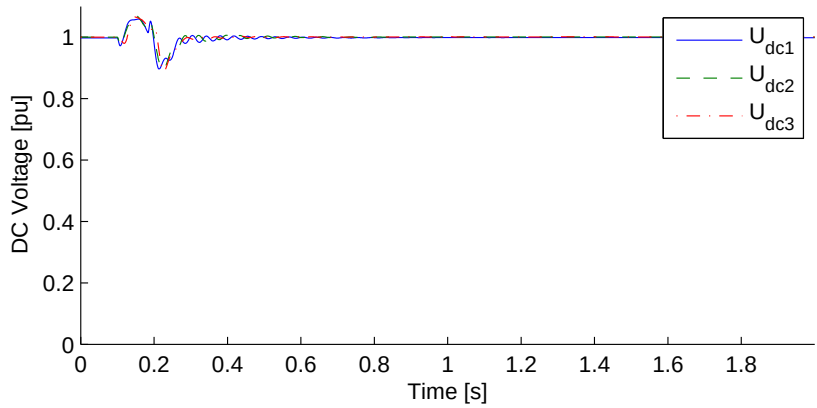

Figure 6.45: DC voltage.

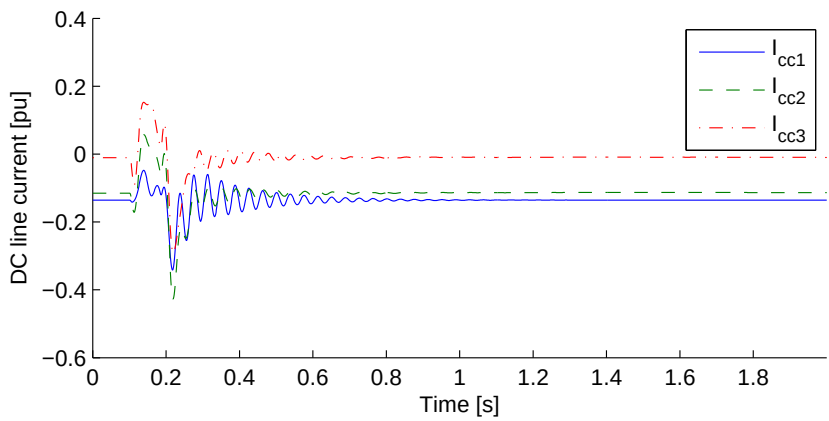

Figure 6.46: DC line currents.

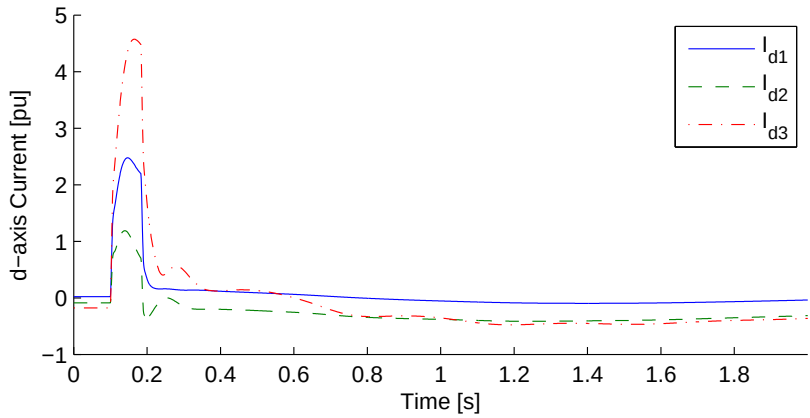

Figure 6.47: d-axis currents.

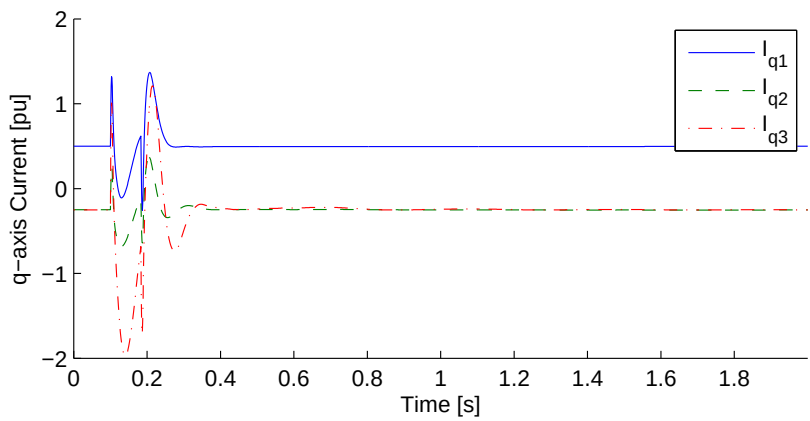

Figure 6.48: q-axis currents.

6.12.4 Simplified Model

The step response of two models is compared. The first is a full model, without filter or PLL, the second a reduced order model, neglecting T_σ, and the time constants associated with L_{dc}, and T_{dc}, as explained in section 6.9. The VSC HVDC system is connected between two infinite buses. The response to a step in DC voltage reference is shown in Figs. 6.49 to 6.54. All simulations are performed in a modified version of $MatDyn$ [90]. Operating limits are not taken into account. It can be observed that the full model responds satisfactorily to the step input in DC voltage. The reduced order model is not as accurate as the full model, but reproduces the overall dynamic phenomena.

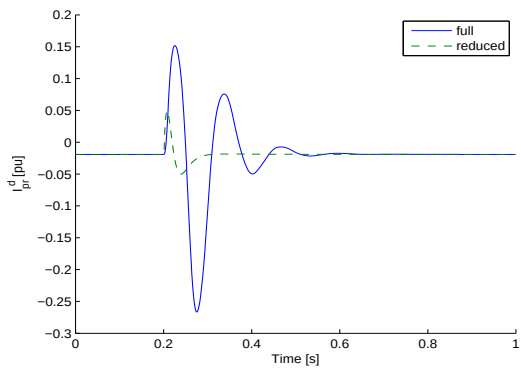

Figure 6.49: Converter d-axis current.

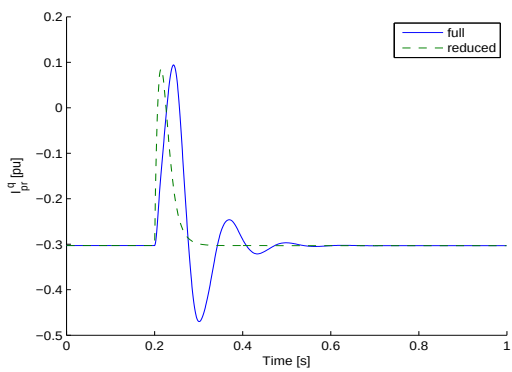

Figure 6.50: Converter q-axis current.

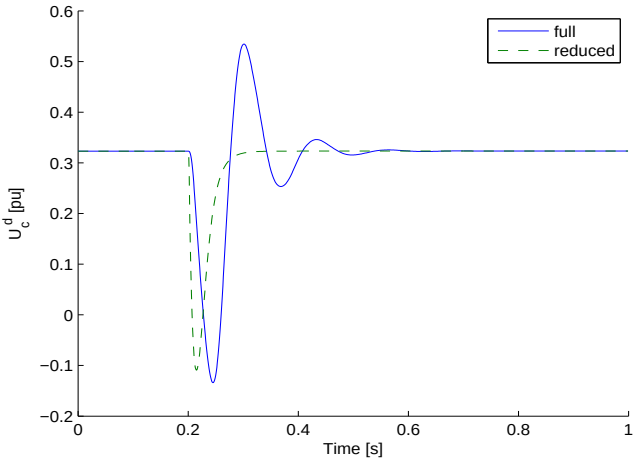

Figure 6.51: Converter d-axis voltage.

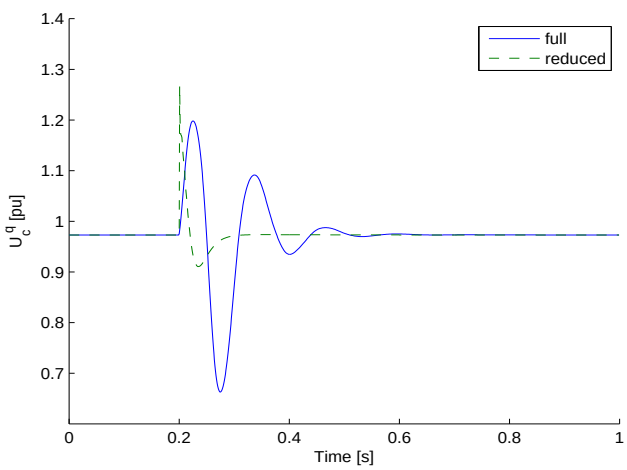

Figure 6.52: Converter d-axis voltage.

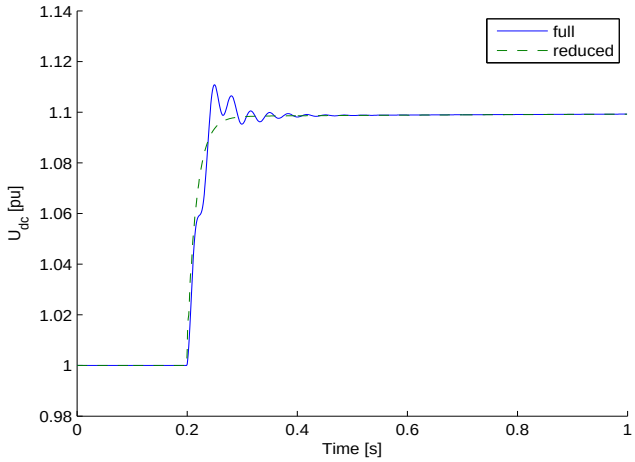

Figure 6.53: DC voltage.

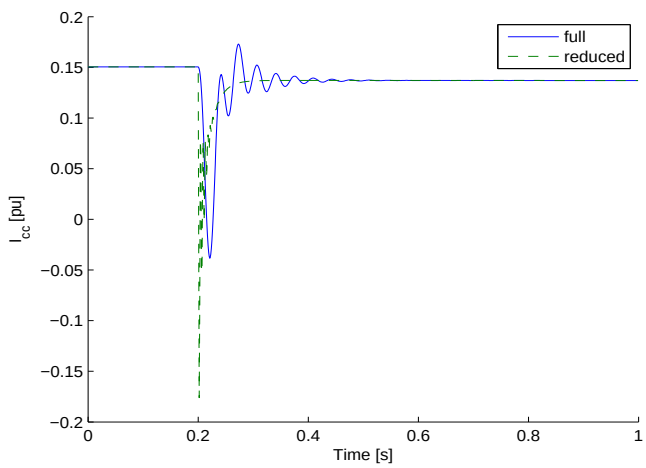

Figure 6.54: DC current.

6.13 Conclusions

A detailed VSC HVDC model has been derived starting from the basic mathematical equations. The model has been built up from the AC side equations, DC side equations, AC-DC coupling equations, and control systems. It has been explained how the filters and PLL can be included in the model. The model with and without filter and PLL are compared, and it was concluded that filter and PLL have a limited influence on system behaviour. Nowhere in the derivation, implementation specific information such as modulation index, has been used. The model does not rely on information on the converter topology and is thus truly generic. The most striking advantage of the models is that it is valid for MTDC networks of any size and topology: any MTDC system can be simulated using the same set of equations.

Implementing such a general model in power system analysis software poses a real challenge. It has been shown that this challenge can be overcome by transforming the general DC equations to a matrix equation and by intelligently building the admittance matrix. Furthermore, by rebuilding the admittance matrix, topology changes, such as adding or removing converters and lines, can be simulated straightforwardly, without having to change the model itself. Simulations on a two and six-converter system showed that the model is indeed valid for DC grids with arbitrary topologies.

Reduced order models are derived formally by neglecting small time constants. It is advised to neglect T_σ, L_{dc}, and T_{dc}. The reduced order model exhibits the same overall behaviour as the full order model. Several benefits should ensue from the simplifications, such as less data requirements, less equations and most importantly, larger step sizes. Implicit methods seem to confirm this theory. By contrast, it has been shown that for explicit methods, reduced models could actually require smaller step sizes.

Formally validating the model proves an intractable challenge due to the closed nature of the manufacturer's model. Although the results are not entirely the same, a good general correspondence has been attained, leading to conjecture that a close to perfect correspondence can be attained if all details of the manufacturer's model were to be known. Where possible, the reason for the discrepancy between our model and the manufacturer's model has been explained.

Chapter 7

Conclusions

The rising importance of VSC HVDC systems in the current grid, along with its prominent place in the vision of the future grid, calls for a serious research effort in order to fully understand all aspects related to the operation of AC/DC grids. A key point in all this is the availability of suitable models, preferably standard models, allowing simulation of integrated AC/DC systems. Such models are not available yet in most software, and those proposed in the literature, be it steady-state or dynamic, fail in one or more areas. This work addresses this vital need by proposing an array of steady-state and dynamic models for VSC HVDC systems that can act as standard models for power system analysis, and that can be readily incorporated in power system analysis software.

At the heart of VSC HVDC systems lie power electronic switches, governed by fast-acting control systems. Integrating systems with such small time constants in the power system, which contains some large time constants stemming from mechanical components, results in a system with an impractically wide range of time constants. Indiscriminately modelling all components and control systems, from the fastest firing control to the slowest boiler, would lead to a huge modelling effort and requires huge computational power. In practice, a selection of the appropriate range of time constants is made, based on the phenomena of interest. In this work, only electromechanical and steady-state models are developed: the frequency of the dynamics of interest are centred around fundamental frequency. Still a wide range of studies can be performed with such models, such as all steady-state studies, transient stability analysis, long-term dynamic analysis, and some, but not all, voltage instability phenomena. For the VSC HVDC models, this means that the very fast acting protection, and firing control, as well as switching components need not be modelled at all, and that they are submitted to all inherent limitations of the phasor modelling approach.

A VSC HVDC system can be introduced in a power flow model by representing converters by PV or PQ nodes and neglecting the DC circuit. Although such a model can be impractical in some studies, as setpoints have to be entered manually, and an estimation of losses needs to be available, such a model gives good results. The PSS/E model and the HVDC Light model are both of the simplified type. A detailed model has been developed, which is a far cry from the simplified model, and constitutes a clear step forward compared to other models proposed in the literature or commercially available. Most notably, the model supports MTDC systems, takes into account accurate limits, filters, converter losses and correctly defines power and voltage set points with respect to the system bus. The model has been thoroughly validated by comparing it to a manufacturer delivered model and a model that comes with PSS/E. It is particularly suited for detailed power flow studies. The calculation is fairly cumbersome, involving five iterative loops and limits that change at every iteration. If it is to be used just to obtain a starting point for dynamic simulations, some details can be dropped, such as detailed losses and dynamically changing limits that are of minor importance in dynamic simulations.

A detailed VSC HVDC model is derived starting from the basic mathematical equations. The model consists of AC side equations, DC side equations, AC-DC coupling equations, and control systems. It is concluded that filter and PLL have a limited influence on system behaviour. Starting from a two-terminal system, the DC equations have been generalised to MTDC systems. Reduced order models are derived formally by neglecting small time constants. It is advised to neglect T_σ, L_{dc}, and T_{dc}. The reduced order model exhibits the same overall behaviour as the full order model. Several benefits should ensue from the simplification, such as less data requirements, less equations, and most importantly, larger step sizes. Implicit methods seem to confirm this theory. By contrast, it has been shown by simulations that explicit methods could actually require smaller step sizes when solving reduced order models.

In line with the models' requirements set forth in the introduction, none of the models, be it steady-state or dynamic ones, rely explicitly or implicitly on information specifically pertaining to a given power electronic topology. The models are thus truly generic. Furthermore, both steady-state and dynamic models can be used for MTDC systems. All models are validated by comparison with commercial grade models. For steady-state models, a perfect correspondence is attained, while for the dynamic ones, a convincing but not perfect match was found. The models are thus generic, generally valid for any MTDC system, and validated, which makes them eligible for use as standard models.

The generality of the DC equations poses some serious challenges to the implementation of VSC MTDC models. A transient stability program, *MatDyn*, was developed and used as test platform for including VSC HVDC models in existing software. The program is validated by comparing with PSS/E. *MatDyn*

is flexible, provides total control over the source code, and is easy to modify. It is thus ideally suited to study the changes necessary to transform a pure AC dynamic simulation program to an AC/DC program. The parts that need to be changed are: the power flow, which needs to be extended to AC/DC power flow, the construction of the augmented Y_{bus} matrix, and the solution of network equations. The generalised equations can be implemented efficiently by writing all DC equations, steady-state and dynamic, in function of matrices that can be obtained as byproducts of the admittance matrix of the DC network. In this way, topology changes of the DC grid, even during a simulation run, can be accounted for by simply rebuilding the DC admittance matrix, without having to change the equations. It has thus been shown that it is possible to integrate both general steady-state and dynamic models in an integrated AC/DC simulation tool.

A logical continuation of the presented work would be the development of a commercial-grade model, using the principles and methods outlined here. The major advantage over all other existing models would be that multi-terminal systems with any topology can be simulated easily. Developing such a model would not require a major additional research effort, but rather an implementation effort. A commercial model should, more so as a research model, be robust and valid in all cases. The model should be extended to represent blocked converters, protection schemes, and must be able to deal with all kinds of contingencies and abnormal behaviour such as sudden islanding, loss of a converter station, and transients. Additionally, it would be useful for a commercial-grade model to relax the requirement of balanced system operation, such that asymmetrical faults can be studied. This would require modelling by Fortescue components: the negative and zero sequence model should be added.

A requirement of real MTDC systems, not accounted for in the presented models, is a suitable DC voltage control method. In the presented models, the principles from two-terminal systems are directly applied to multi-terminal systems. The DC voltage needs to remain in a very close band around its rated value. It was shown that even in two-terminal systems, each converter needs a DC voltage controller to comply with this stringent requirement. In MTDC systems this is even more so. Therefore, designating only one slack converter in a MTDC system is clearly unacceptable. It is less clear, however, which voltage control mechanism should be implemented, as it is not yet known which method is best. Two possibilities are using multiple DC slack converters, or using a distributed slack converter. All presented models support multiple DC slack converters, but if a distributed slack converter, in one form or another, is to be used as DC voltage control strategy, the model should be changed accordingly.

With ever increasing computer power, traditional lines of demarcation between phasor programs and EMTP type ones begin to fade. It becomes now viable to model small networks in full detail, and perform all types of analysis on the full system, even those traditionally reserved to phasor programs. More detailed VSC

HVDC models should then be developed, e.g. dynamic phasor models. Dynamic phasors are particularly interesting for VSC HVDC because of the pervasive presence of power electronic components. However, the phasor modelling paradigm still stands, and is expected to remain the industry standard for transient stability type of analysis in the foreseeable future.

Finally, the main contributions of the work are summarised as follows:

- A detailed multi-terminal VSC MTDC model for power flow has been developed. It is the most detailed model currently available.
- A detailed dynamic multi-terminal VSC HVDC model has been developed, together with a simplified model.
- A simulation tool, *MatDyn* has been developed.
- It is explained in detail how general VSC HVDC models can be implemented in AC power system analysis software. The presented models were successfully integrated in *MatDyn*.
- State-of-the-art numerical techniques that allow bifurcation analysis of ODE systems are extended to DAE systems and applied to a grid connected HVDC converter.

In closing, this work thus contains all necessary information, including a proof of concept, to develop multi-terminal VSC HVDC models, and integrate them in power system analysis software.

Appendix A

MatDyn User's Manual

A.1 Installation

The prerequisites for *MatDyn* are the following:

- Matlab must be installed.
- MATPOWER must be installed and added to the Matlab path. It is available from [89].
- *MatDyn* must be installed and ideally added to the Matlab path. It is available from `www.esat.kuleuven.be/electa/teaching/matdyn/` [90].

You are now ready to run a first simulation.

A.2 Running a Simulation

Dynamic simulations are run by calling the `rundyn` function:

```
>> [Angles,Speeds,Eq_tr,Ed_tr,Efd,PM,Voltages,Stepsize,...
Errest,Failed,Time]=rundyn(PFFUN,DYNFUN,EVFUN,OPTIONS);
```

PFFUN is a MATPOWER power flow data m-file or struct, DYNFUN an m-file or struct with dynamic data, and EVFUN an m-file or struct with the events such as faults. The OPTIONS vector is optional.

Examples: a simulation can be run by entering the following command at the Matlab prompt:

```
>> rundyn( 'case9','case9dyn','fault');
```

or

```
>> rundyn( 'casestagg','casestaggdyn','staggevent');
```

The EVFUN argument also accepts an empty matrix. The steady-state solution is then obtained:

```
>> rundyn( 'case9','case9dyn', [] );
```

A.3 Input Data

To perform a dynamic simulation, three m-files or structs have to be defined: one for power flow data, another for dynamic data and a last one for event data.

A.3.1 Power Flow Data

MatDyn uses the MATPOWER format for the power flow data. The matrices areas and gencost are not used by *MatDyn*. Consult the MATPOWER manual for more information on the power flow data format [73]. Alternatively, the command `help caseformat` gives a description of the MATPOWER power flow data format.

A.3.2 Dynamic Data

The dynamic data consist of general data, generator data, exciter data, and governor data. The m-file returns the matrices gen, exc, gov and the scalars freq, stepsize and stoptime. Alternatively, a struct can be defined as follows:

```
DYNFUN = struct( 'gen',gen,'exc',exc,'gov',gov,'freq',freq,...
'stepsize',stepsize,'stoptime',stoptime);
```

General Data

System frequency has to be defined, as well as the step size of the integration algoritm and the stoptime. The starttime is hard-coded and equal to $-0.02s$. The step size is only used by fixed step size algorithms (Table A.1).

Table A.1: General data

freq	network frequency [Hz]
stepsize	step size of the integration algorithm [s]
stoptime	stop time of the simulation [s]

Generator Data

The generator data is defined in the matrix gen. For the 4th order model, model 2, the columns are defined in Table A.2. For the classical generator model, model 1, the columns are defined in Table A.3. The generators are assumed to be entered from lowest to highest bus number: the generator parameters of the first row are thus from the generator connected at the bus with the lowest bus number.

Table A.2: Generator data format

	4th order model
1	*genmodel*, generator model
2	*excmodel*, exciter model
3	*govmodel*, governor model
4	H, inertia constant (p.u.)
5	D, damping constant (p.u.)
6	x_d, d-axis reactance (p.u.)
7	x_q, q-axis reactance (p.u.)
8	$x_d^{'}$, d-axis transient reactance (p.u.)
9	$x_q^{'}$, q-axis transient reactance (p.u.)
10	$T_d^{'}$, d-axis time constant (s)
11	$T_q^{'}$, q-axis time constant (s)

Table A.3: Generator data format

	Classical model
1	*genmodel*, generator model
2	*excmodel*, exciter model
3	*govmodel*, governor model
4	H, inertia constant (p.u.)
5	D, damping constant (p.u.)
6	x, reactance (p.u.)
7	$x^{'}$, transient reactance (p.u.)

Exciter Data

The exciter data is defined in the matrix exc. The matrix has as many rows as there are generators. The definition of the columns depends on the exciter model. The data in Table A.4 specifies the parameters of exciter model 2, the IEEE DC1A excitation system (Fig. A.1). Exciter model 1 means constant excitation. Only the first column, the generator number, has to be specified.

Governor Data

The governor data is defined in the matrix gov. The matrix has as many rows as there are generators. The definition of the columns depends on the governor model. The data in Table A.5 specifies the parameters of the general IEEE speed governor system of Fig. A.2). Governor model 1 means that the generator is driven

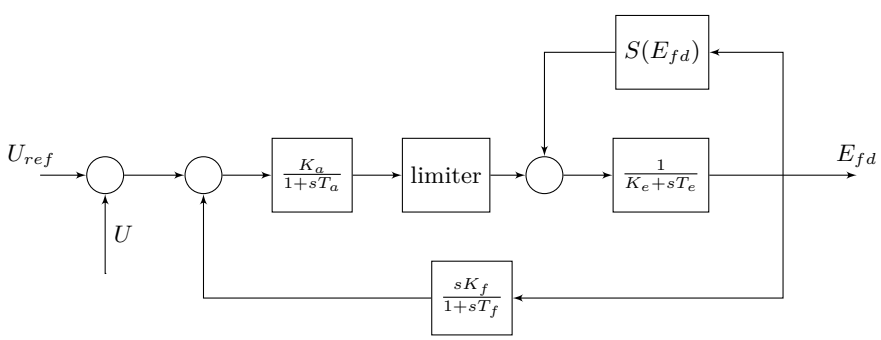

Figure A.1: IEEE DC1A excitation system.

Table A.4: Exciter data format

	IEEE DC1A model
1	gen, number of the generator
2	K_a, amplifier gain
3	T_a, amplifier time constant
4	K_e, exciter gain
5	T_e, exciter time constant
6	K_f, stabilizer gain
7	T_f, stabilizer time constant
8	A_{ex}, parameter saturation function
9	B_{ex}, parameter saturation function
10	U_{rmin}, lower voltage limit
11	U_{rmax}, upper voltage limit

by a turbine with constant mechanical output power. Only the first column, the generator number, has to be specified.

A.3.3 Event Data

The event data file defines three matrices: event, buschange, and linechange. Alternatively, a struct can be used as input argument. It has to be defined as follows:

```
EVFUN = struct( 'event',event,'fault',fault,'linechange',...
linechange,'loadchange',loadchange);
```

The event matrix contains all events that take place during the simulation (Table A.6). The first column defines the instant of the event, the second the

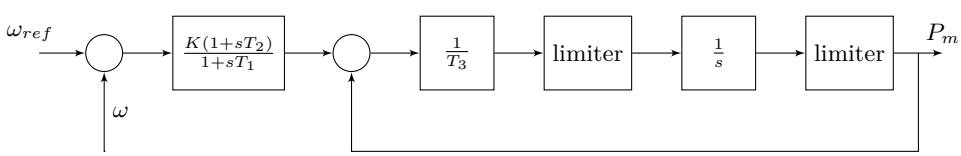

Figure A.2: IEEE general speed governing system.

Table A.5: Governor data format

	General IEEE governor model
1	*gen*, number of the generator
2	K, droop
3	T_1, time constant
4	T_2, time constant
5	T_3, servo motor time constant
6	P_{up}, upper ramp limit
7	P_{down}, lower ramp limit
8	P_{max}, maximal turbine output
9	P_{min}, minimal turbine output

type of the event.

Table A.6: Event data format

	Event data format
1	*time*, instant of change (s)
2	*eventtype*

Table A.7 shows the available event types. The program can be called with an empty event matrix to obtain a steady-state solution.

Table A.7: Event types

	Event types
1	change bus parameters
2	change line parameters

Bus Change

The bus parameters can be changed during simulation by defining the buschange matrix (Table A.8). Consult the MATPOWER manual for a list of bus parameters.

Table A.8: Bus change

Bus change data format	
1	*time*, instant of change (s)
2	*bus*, bus number
3	*parameter*, bus parameter to change
4	*newvalue*, new parameter value

Line change

The line parameters can be changed during simulation by defining the linechange matrix (Table A.9). Consult the MATPOWER manual for a list of line parameters.

Table A.9: Line change

Line change data format	
1	*time*, instant of change (s)
2	*line*, line number
3	*parameter*, line parameter to change
4	*newvalue*, new parameter value

Example: Bus Faults

Three-phase bus faults can be simulated by changing the shunt susceptance of the bus in a bus change event. Table A.10 gives the data for a zero impedance bus fault at bus 2 at t = 0. The fault can be cleared by resetting the susceptance to its original value.

A.3.4 Options

MatDyn accepts an option vector as an optional fourth input argument (Table A.11). If the option vector is not specified, the default options are used.

- method
  Selects the integration method. 1: Modified Euler, 2: Runge-Kutta, 3:

Table A.10: Bus fault

Bus change data	
1	*time*, 0
2	*bus*, 2
3	*parameter*, 6
4	*newvalue*, -1e10

Table A.11: Options

Default Options		
1	method	1
2	tol	1e-4
3	minstepsize	1e-3
4	maxstepsize	1e2
5	output	1
6	plots	1

Runge-Kutta Fehlberg, 4: Higham and Hall, 5: Modified Euler with interface error control.

- tol
  Specify the tolerance of the error. This argument is only used for the Runge-Kutta Fehlberg and Higham and Hall methods.

- minstepsize
  Sets the minimal step size. Only used by the adaptive step size algorithms: Runge-Kutta Fehlberg and Higham and Hall methods.

- maxstepsize
  Sets the maximal step size. Only used by the adaptive step size algorithms: Runge-Kutta Fehlberg and Higham and Hall methods.

- output
  Prints progress info if set to one, prints no progress info if set to zero. Errors are printed anyhow.

- plots
  Draws plots if set to one, draws nothing if set to zero.

The function mdoption returns the default option vector:

```
>> mdopt = mdoption

mdopt =

    1.0000
    0.0001
    0.0000
  100.0000
    1.0000
    1.0000
```

Remarks: The adaptive step size methods start with minimal step size. It is of interest to increase minimum step size as it speeds up the calculations. Generally, tolerance must be increased as well, or the integration will fail.

A.4 Output Data

`rundyn` returns the matrices given in Table A.12.

Table A.12: *MatDyn* output

Angles	Generator angles in degrees
Speeds	Generator speeds/synchronous speed
Eq_tr	q-axis component of the voltage behind transient reactance in p.u.
Ed_tr	d-axis component of the voltage behind transient reactance in p.u.
Efd	Excitation voltage in p.u.
PM	Mechanical output power of the turbine in p.u.
Voltages	Network voltages $U\angle\delta$ in p.u. and radians
Stepsize	Step size of the integration
Errest	Estimation of the error*
Failed	Number of failed integration steps*
Time	Vector of time steps in seconds

*Remark: Only defined for the adaptive step size methods, Runge-Kutta Fehlberg and Higham and Hall. Set to zero for Modified Euler and standard Runge-Kutta methods.

A.5 Errors and Warnings

Errors are fatal and cause the program to exit. If a warning occurs, the program will continue but it is strongly advised to recheck data.

- Warning: transient saliency not supported
  The d-axis transient reactance $x_d^{'}$ must be equal to the q-axis transient reactance $x_q^{'}$. This condition is checked for all generators, except those represented by the classical model, and enforced by setting $x_q^{'} = x_d^{'}$.
- Error: Power flow did not converge
  The dynamic simulation is only started from a steady-state condition. The power flow data should be checked.
- Error: Generator\Exciter\Governor not in steady-state
  The dynamic simulation is only started from a steady-state condition. First of all, it should be checked that the initial conditions are calculated correctly. If this is the case, the error is caused by the violation of a limit in the definition of the equipment. The data in DYNFUN should be checked: a generator's reactance that is completely off could for instance lead to an unrealistical value of excitation voltage. The power flow solution should be checked as well, as an abnormally high voltage at a generator bus could for instance impose a very high excitation voltage.
- Error: No solution found with minimum step size
  The integration alghorithm failed. Try reducing minimum step size or using a fixed step size method.

Bibliography

[1] S. Cole and R. Belmans, "Transmission of bulk power: The history and applications of voltage-source converter high-voltage direct current systems," *IEEE Ind. Electron. Mag.*, p. 6, September 2009.

[2] J. Lee. (2007, November) Off goes the power current started by Thomas Edison. New York Times. [Online]. Available: http://cityroom.blogs.nytimes.com/2007/11/14/off-goes-the-power-current-started-by-thomas-edison/

[3] R. M. Black, *The history of electric wires and cables*, ser. IEE History of Technology Series 4. Peter Peregrinus Ltd. London, 1983.

[4] W. Long and S. Nilsson, "HVDC transmission: Yesterday and today," *IEEE Power Energy Mag.*, vol. 5, no. 2, pp. 22–31, March/April 2007.

[5] B. Jacobson, Y. Jiang-Häfner, P. Rey, G. Asplund, M. Jeroense, A. Gustafsson, and M. Bergkvist, "HVDC with voltage source converters and extruded cables for up to ±300 kV and 1000 MW," in *2006 CIGRE Session*, 2006.

[6] L. Meeus, K. Purchala, and R. Belmans, "Development of the Internal Electricity Market in Europe," *The Electricity Journal*, vol. 18, no. 6, pp. 25–35, July 2005.

[7] "Council Regulation (EC) No. 2236/95 of 18 September 1995 laying down rules for granting of community financial aid in the field of trans-European networks," *Official Journal of the European Union*, September 1995.

[8] (2007, January) Inquiry pursuant to Article 17 of Regulation (EC) no. 1/2003 into the European gas and electricity sectors (final report) - Priority interconnection plan. European Commission.

[9] P. Buijs, S. Cole, and R. Belmans, "TEN-E revisited: Opportunities for HVDC technology," in *Proc. 6^{th} International Conference on the European Energy Market EEM 2009*, May 27–29, 2009, pp. 1–6.

[10] European Network of Transmission Operators for Electricity (ENTSO-E). (2010) Ten-year network development plan 2010-2020. [Online]. Available: http://www.entsoe.eu/index.php?id=232

[11] D. Van Hertem, "The use of power flow controlling devices in the llberalized market," Ph.D. dissertation, Katholieke Universiteit Leuven, ESAT-ELECTA, January 2009.

[12] (2008, January) Communication from the Commission to the European Parliament, the Council, the European Economic and Social Committee and the Committee of the regions. Commission of the European Communities. [Online]. Available: http://ec.europa.eu/commission_barroso/president/pdf/COM2008_030_en.pdf

[13] (2003, October) Wind power targets for Europe: 75,000 MW by 2010. European Wind Energy Association. [Online]. Available: http://www.ewea.org/fileadmin/ewea_documents/documents/publications/briefings/75gw.pdf

[14] (2010, April) A breath of fresh air, EWEA 2009 annual report. European Wind Energy Association. [Online]. Available: http://www.ewea.org/fileadmin/ewea_documents/documents/publications/reports/Ewea_Annual_Report_2009.pdf

[15] (2008, March) Pure power - wind energy scenarios up to 2030. European Wind Energy Association. [Online]. Available: http://www.ewea.org/fileadmin/ewea_documents/documents/publications/reports/purepower.pdf

[16] "European Wind Integration Study (EWIS) towards a successful integration of wind power into European electricity grids - final report," European Transmission System Operators, Tech. Rep., January 2007.

[17] L. Stendius and P. Jones, "The challenges of offshore power system construction: Bringing power successfully to Troll A, one of the worlds largest oil and gas platform," in *The* 8^{th} *IEE International conference on AC and DC power transmission*, 2006.

[18] S. Gilje and L. Carlsson. (2006, September) Field of the future. Power engineering international. [Online]. Available: http://pepei.pennnet.com/Articles/Article_Display.cfm?Section=ARTCL&ARTICLE_ID=273916&VERSION_NUM=2&p=17

[19] E. Spahic and G. Balzer, "Impact of the VSC HVDC connection of large offshore wind farms on power system stability and control," in *Proc. IEEE Lausanne Power Tech*, July 1–5, 2007, pp. 207–212.

[20] R. L. Hendriks, R. Völzke, and W. L. Kling, "Fault ride-through strategies for VSC-connected wind parks," in *EWEC*, Marseille, March 2009.

[21] O. A. Giddani, G. P. Adam, O. Anaya-Lara, and K. L. Lo, "Grid integration of a large offshore wind farm using VSC-HVDC transmission system in parallel with AC submarine cable," in *Proceedings of the* 44^{th} *International Universities Power Engineering Conference*, University of Strathclyde, September 2009.

[22] W. Lu, "Control and application of multi-terminal HVDC based on voltage-source converter," Ph.D. dissertation, McGill university, Department of electrical and computer engineering, Montréal, Québec, Canada, February 2003.

[23] B. Jacobson, P. F. de Toledo, and G. Asplund, "City infeed with HVDC Light and extruded cables," in 16^{th} *conference on the electric power supply industry, Mumbai, India*, November 2006.

[24] P. F. de Toledo, "Feasability of HVDC for city infeed," Master's thesis, Royal Institute of Technology (KTH) : School of Electrical Engineering, 2003.

[25] C. Du, "VSC-HVDC for industrial power systems," Ph.D. dissertation, Chalmers University of technology, 2007.

[26] S. Gordon, "Supergrid to the rescue," *Power Engineer*, vol. 20, no. 5, pp. 30–33, October-November 2006.

[27] IEEE Committee Report, "Excitation system models for power system stability studies," *IEEE Trans. Power App. Syst.*, no. 2, pp. 494–509, February 1981.

[28] ——, "Dynamic models for steam and hydro turbines in power system studies," *IEEE Trans. Power App. Syst.*, no. 6, pp. 1904–1915, November 1973.

[29] X.-P. Zhang, "Multiterminal voltage-sourced converter-based HVDC models for power flow analysis," *IEEE Trans. Power Syst.*, vol. 19, no. 4, pp. 1877–1884, Novermber 2004.

[30] G. Li, M. Zhou, J. He, G. Li, and H. Liang, "Power flow calculation of power systems incorporating VSC-HVDC," in *Proc. International Conference on Power System Technology PowerCon 2004*, vol. 2, November 21–24, 2004, pp. 1562–1566.

[31] M. Zhao, Z. Chen, and F. Blaabjerg, "Modeling of DC/DC converter for DC load flow calculation," in *Proc. 12th International Power Electronics and Motion Control Conference EPE-PEMC 2006*, August 2006, pp. 561–566.

[32] ——, "Load flow analysis for variable speed offshore wind farms," *IET renewable power generation*, vol. 3, no. 2, p. 13, 2009.

[33] Q. Chen, G.-Q. Tang, and W. Xun, "AC-DC power flow algorithm for multi-terminal VSC-HVDC systems," *Electric power automation equipment*, vol. 25, no. 6, p. 6, 2005.

[34] C. Angeles-Camacho, O. L. Tortelli, E. Acha, and C. R. Fuerte-Esquivel, "Inclusion of a high voltage DC-voltage source converter model in a Newton-Raphson power flow algorithm," *IEE Proceedings-Generation, Transmission and Distribution*, vol. 150, no. 6, pp. 691–696, November 12, 2003.

[35] L. Tang and B.-T. Ooi, "Locating and isolating DC faults in multi-terminal DC systems," *IEEE Trans. Power Del.*, vol. 22, no. 3, pp. 1877–1884, July 2007.

[36] ——, "Protection of VSC-multi-terminal HVDC against DC faults," in *Proc. IEEE* 33^{rd} *Annual Power Electronics Specialists Conference PESC 02*, vol. 2, June 23–27, 2002, pp. 719–724.

[37] H. Chen, C. Wang, F. Zhang, and W. Pan, "Control strategy research of VSC based multiterminal HVDC system," in *Proc. IEEE PES Power Systems Conference and Exposition PSCE '06*, October 2006, pp. 1986–1990.

[38] L. Tang and B.-T. Ooi, "Elimination of "harmonic transfer through converters" in VSC-based multiterminal DC systems by AC/DC decoupling," *IEEE Trans. Power Del.*, vol. 23, no. 1, pp. 402–409, January 2008.

[39] F. Lin, Z. Ma, X. You, and T. Zheng, "The grid connected converter control of multi-terminal DC system for wind farms," in *Proc. Eighth International Conference on Electrical Machines and Systems ICEMS 2005*, vol. 2, September 29–29, 2005, pp. 1021–1023.

[40] S. Zhou, "Control of multi-terminal VSC-HVDC transmission system," in *Proceedings of the* 44^{th} *International Universities Power Engineering Conference*, University of Strathclyde, September 2009.

[41] S. Lefebvre, W. K. Wong, J. Reeve, J.-M. Gagnon, and B. K. Johnson, "Experience with modeling MTDC systems in transient stability programs," *IEEE Trans. Power Del.*, vol. 6, no. 1, pp. 405–413, January 1991.

[42] S. Lefebvre, W. K. Wong, J. Reeve, M. Baker, and D. Chapman, "Considerations for modeling MTDC systems in transient stability programs," *IEEE Trans. Power Del.*, vol. 6, no. 1, pp. 397–404, January 1991.

[43] Working Group B4.37, "VSC transmission," CIGRE, Tech. Rep., 2005.

[44] Joint Task Force B4.04/A2-1, "Analysis of HVDC thyristor converter transformer performance," CIGRE, Tech. Rep., 2004.

[45] A. Suzuki, S. Nakamura, M. Matsuda, H. Tanaka, M. Shiomitsu, K. Hiraga, K. Adachi, K. Hiratsuka, K. Matsuda, M. yagi, A. Sudo, and K. Sugawara, "Installation of the world's first 500-kV XLPE cable with intermediate joints," *Furukawa Review*, vol. 19, pp. 115–122, 2000.

[46] T. Worzyk, *Submarine power cables: design, installation, repair, environmental aspects*, 1^{st} ed. Springer, 2009.

[47] S. Maruyama, N. Ishii, M. Shimada, S. Kojima, H. Tanaka, M. Asano, T. Yamanaka, and S. Kawakami, "Development of a 500-kV DC XLPE cable system," *Furukawa Review*, vol. 25, pp. 47–52, 2004.

[48] H. S. Patel and R. G. Hoft, "Generalized techniques of harmonic elimination and voltage control in thyristor inverters: Part I–harmonic elimination," *IEEE Trans. Ind. Appl.*, no. 3, pp. 310–317, May 1973.

[49] S. R. Bowes and A. Midoun, "Microprocessor implementation of new optimal pwm switching strategies," *Electric Power Applications, IEE Proceedings B*, vol. 135, no. 5, pp. 269 –280, sep 1988.

[50] A. Lesnicar and R. Marquardt, "A new modular voltage source inverter topology," in *EPE'03*, Toulouse, France, 2003.

[51] H. Huang, "Multilevel voltage-sourced converters for HVDC and FACTS applications," in *CIGRE SC B4 2009 Bergen colloquium*, Bergen, Norway, 2009.

[52] J. Arrillaga, Y. H. Liu, and N. R. Watson, *Flexible power transmission: the HVDC options*. John Wiley & Sons, Ltd., 2007.

[53] P. Kundur, *Power system stability and control*, ser. The EPRI power system engineering series. Mc Graw-Hill, 1994.

[54] M. Ilić and J. Zaborsky, *Dynamics and control of large electric power systems*. John Wiley & Sons, 2000.

[55] V. Venkatasubramanian, H. Schattler, and J. Zaborsky, "Dynamics of large constrained nonlinear systems - a taxonomy theory," *Proc. IEEE*, vol. 83, no. 11, pp. 1530–1561, November 1995.

[56] V. Venkatasubramanian, H. Schattler, and J. Zaborszky, "Global voltage dynamics: study of a generator with voltage control, transmission, and matched MW load," in *Proc.* 29^{th} *IEEE Conference on Decision and Control*, December 5–7, 1990, pp. 3045–3056.

[57] H. W. Dommel and W. Scott Meyer, "Computation of electromagnetic transients," *Proc. IEEE*, vol. 62, no. 7, pp. 983–993, July 1974.

[58] T. H. Demiray, "Simulation of power system dynamics using dynamic phasor models," Ph.D. dissertation, Swiss federal institute of technology, Zurich, 2008.

[59] A. M. Stankovic and T. Aydin, "Analysis of asymmetrical faults in power systems using dynamic phasors," *IEEE Trans. Power Syst.*, vol. 15, no. 3, pp. 1062–1068, August 2000.

[60] A. M. Stankovic, S. R. Sanders, and T. Aydin, "Dynamic phasors in modeling and analysis of unbalanced polyphase ac machines," *IEEE Trans. Energy Convers.*, vol. 17, no. 1, pp. 107–113, March 2002.

[61] J. E. Brittain, "A steinmetz contribution to the ac power revolution," *Proc. IEEE*, vol. 72, no. 2, pp. 196 – 197, feb. 1984.

[62] P. C. Krause, O. Wasynczuk, and S. D. Sudhoff, *Analysis of electric machinery and drive systems*, ser. IEEE press series on power engineering, E. M. El-Hawary, Ed. Wiley-Interscience, 2002.

[63] K. R. Padiyar, *Analysis of subsynchronous resonance in power systems*, ser. The Kluwer international series in engineering and computer science, T. A. Lipo and M. A. Pai, Eds. Kluwer Academic Publishers, 1999.

[64] R. Riaza, "Singular bifurcations in higher index differential-algebraic equations," *Dynamical systems*, vol. 17, no. 3, pp. 243–261, 2002.

[65] U. M. Ascher and L. R. Petzold, *Computer Methods for Ordinary Differential Equations and Differential-Algebraic Equations*. SIAM: Society for industrial and applied mathematics, 1998.

[66] V. Venkatasubramanian, H. Schattler, and J. Zaborszky, "Local bifurcations and feasibility regions in differential-algebraic systems," *IEEE Trans. Autom. Control*, vol. 40, no. 12, pp. 1992–2013, Dec. 1995.

[67] A. Gómez-Expósito, J. A. Conejo, and C. Cañizares, Eds., *Electric energy systems: Analysis and operation*, ser. The electric power engineering series. Taylor & Francis, Inc., 2009.

[68] *PSS/E 32.0 Documentation*, Siemens Power technologies international, Schenectady, NY, USA, June 2009.

[69] M. E. El-Hawary and S. T. Ibrahim, "A new approach to AC-DC load flow analysis," *Electric power systems research*, vol. 33, p. 8, 1995.

[70] M. M. El-Marsafawy and R. M. Mathur, "A new, fast technique for load-flow solution of integrated multi-terminal AC/DC systems," *IEEE Trans. Power App. Syst.*, vol. 99, no. 1, p. 10, January/February 1980.

[71] H. Fudeh and C. M. Ong, "A simple and efficient AC-DC load-flow method for multi-terminal DC system„" *IEEE Trans. Power App. Syst.*, vol. 100, no. 11, p. 8, November 1981.

[72] C. M. Ong and A. Hamzei-nejad, "A general-purpose multiterminal DC load-flow," *IEEE Trans. Power App. Syst.*, no. 7, pp. 3166–3174, July 1981.

[73] R. D. Zimmerman and C. E. Murrilo-Sánchez. (2007) MATPOWER, version 3.2, user's manual. Power system engineering research center, Cornell Univ. Ithaca, NY. [Online]. Available: http://www.pserc.cornell.edu/matpower/manual.pdf

[74] G. Daelemans, K. Srivastava, M. Reza, S. Cole, and R. Belmans, "Minimization of steady-state losses in meshed networks using VSC HVDC," in *IEEE PES General Meeting*, Calgary, Canada, July 2009.

[75] G. Daelemans, "VSC HVDC in meshed networks," Master's thesis, Katholieke Universiteit Leuven, Leuven, 2008.

[76] It's time to connect: Technical description of HVDC Light technology. online. ABB. [Online]. Available: www.abb.com/hvdc

[77] A. Capasso and E. Mariani, "Influence of generator capability curves representation on system voltage and reactive power control studies," *IEEE Trans. Power App. Syst.*, vol. 97, no. 4, pp. 1036–1041, July 1978.

[78] *PSS/E 32.0 Program Application Guide, Vol. II*, Siemens Power technologies international, Schenectady, NY, USA, June 2009.

[79] A. Dhooge, W. Govaerts, Y. A. Kuznetsov, W. Mestrom, A. M. Riet, and B. Sautois. (2006, Dec) MATCONT and CL_MATCONT: Continuation toolboxes in MATLAB. [Online]. Available: www.matcont.ugent.be/

[80] Y. A. Kuznetsov, *Elements of Applied Bifurcation Theory*, ser. Applied Mathematical sciences. Springer, 1995, vol. 112.

[81] X. Yue and V. Venkatasubramanian, "Complementary limit induced bifurcation theorem and analysis of Q limits in power-flow studies," in *Proc. IREP Symposium Bulk Power System Dynamics and Control - VII. Revitalizing Operational Reliability*, August 19–24, 2007, pp. 1–8.

[82] W. J. F. Govaerts, *Numerical Methods for bifurcations of dynamical equilibria*. Siam, 2000.

[83] S. Johansson, "Long-term voltage stability in power systems: alleviating the impact of generator current limiters," Ph.D. dissertation, Chalmers University of Technology, Göteborg, May 1998.

[84] J. H. Chow and K. W. Cheung, "A toolbox for power system dynamics and control engineering education and research," *IEEE Trans. Power Syst.*, vol. 7, no. 4, pp. 1559–1564, November 1992.

[85] K. Schoder, A. Hasanovic, and A. Feliachi, "PAT: a power analysis toolbox for MATLAB/Simulink," *IEEE Trans. Power Syst.*, vol. 18, no. 1, pp. 42–47, February 2003.

[86] F. Milano, "An open source power system analysis toolbox," *IEEE Trans. Power Syst.*, vol. 20, no. 3, pp. 1199–1206, August 2005.

[87] S. Ayasun, C. O. Nwankpa, and H. G. Kwatny, "Voltage stability toolbox for power system education and research," *IEEE Trans. Educ.*, vol. 49, no. 4, pp. 432–442, November 2006.

[88] M. Larsson, "Objectstab-an educational tool for power system stability studies," *IEEE Trans. Power Syst.*, vol. 19, no. 1, pp. 56–63, February 2004.

[89] MATPOWER website. [Online]. Available: http://www.pserc.cornell.edu/matpower/

[90] MatDyn website. [Online]. Available: http://www.esat.kuleuven.be/electa/teaching/matdyn/

[91] S. Cole. (2009, September) MatDyn, version 1.2. KULeuven, ESAT-ELECTA. Heverlee, Belgium. [Online]. Available: http://www.esat.kuleuven.be/electa/teaching/matdyn/

[92] F. Milano and L. Vanfretti, "State of the art and future of OSS for power systems," in *Proc. IEEE Power and Energy Society General Meeting*, July 2009.

[93] H. R. Fankhauser, K. Aneros, A.-A. Edris, and S. Torseng, "Advanced simulation techniques for the analysis of power system dynamics," *IEEE Comput. Appl. Power*, vol. 3, no. 4, pp. 31–36, October 1990.

[94] M. Stubbe, A. Bihain, J. Deuse, and J. C. Baader, "STAG-a new unified software program for the study of the dynamic behaviour of electrical power systems," *IEEE Trans. Power Syst.*, vol. 4, no. 1, pp. 129–138, February 1989.

[95] L. F. Shampine and M. W. Reichelt, "The Matlab ODE suite," *SIAM J. Sci. Comput.*, vol. 18, pp. 1–22, 1997.

[96] G. W. Stagg and A. H. El-Abiad, *Computer Methods in Power System Analysis*, ser. McGraw-Hill Series in Electronic Systems. Tokyo, Japan: McGraw-Hill Kogakusha, 1968.

[97] E. Hairer, S. P. Nørsett, and G. Wanner, *Solving Ordinary Differential Equations I: Nonstiff Problems*, 2^{nd} ed., ser. Springer Series in Computational Mathematics. Berlin, Germany: Springer, 2000, vol. 8.

[98] E. Hairer and G. Wanner, *Solving Ordinary Differential Equations II: Stiff and Differential-Algebraic Problems*, 2^{nd} ed., ser. Springer Series in Computational Mathematics. Berlin, Germany: Springer, 2002, vol. 14.

[99] P. M. Anderson and A. A. Fouad, *Power System Control and stability*, 2^{nd} ed., ser. IEEE series on power engineering, E. M. El-Hawary, Ed. Wiley-Interscience, 2003.

[100] J. Y. Astic, A. Bihain, and M. Jerosolimski, "The mixed Adams-BDF variable step size algorithm to simulate transient and long term phenomena in power systems," *IEEE Trans. Power Syst.*, vol. 9, no. 2, pp. 929–935, May 1994.

[101] P. W. Sauer and M. A. Pai, *Power system dynamics and stability*. Prentice Hall, 1998.

[102] Z. Hu, C. Mao, J. Lu, and M. Chen, "Genetic algorithm based control for VSC HVDC," in *Proc. IEEE/PES Transmission and Distribution Conference and Exhibition: Asia and Pacific*, 2005, pp. 1–5.

[103] C. Zheng, X. Zhou, and R. Li, "Dynamic modeling and transient simulation for VSC based HVDC in multi-machine system," in *Proc. International Conference on Power System Technology PowerCon 2006*, Oct. 22–26, 2006, pp. 1–7.

[104] H. Liang, G. Li, P. Li, and M. Yin, "Analysis and design of H_∞ controller in VSC HVDC systems," in *IEEE/PES Transmission and Distribution Conference and Exhibition: Asia and Pacific*, 2005, p. 6.

[105] L. Zhang and H.-P. Nee, "Multivariable feedback design of VSC-HVDC connected weak AC systems," in *PowerTech 2009*, 2009, pp. 1–8.

[106] M. Durrant, H. Werner, and K. Abbott, "A comparison of LMI and GA based robust controller designs for VSC HVDC," in *Proc.* 45^{th} *IEEE Conference on Decision and Control*, December 13–15, 2006, pp. 3990–3995.

[107] ——, "Design of LQG controllers for VSC HVDC transmission links using genetic algorithms," in *Proc. IEEE Computer Aided Control System Design IEEE International Conference on Control Applications IEEE International Symposium on Intelligent Control*, October 4–6, 2006, pp. 772–777.

[108] G. Li, G. Ma, C. Zhao, and G. Li, "Research of nonlinear control strategy for VSC-HVDC system based on Lyapunov stability theory," in *Proc.* 3^{rd} *International Conference on Electric Utility Deregulation and Restructuring and Power Technologies DRPT 2008*, April 6–9, 2008, pp. 2187–2191.

[109] C. Mao, Z. Hu, J. Lu, D. Chang, and S. Fan, "Application of an optimal coordinated control strategy to VSC HVDC," in *Proc. IEEE PES Power Systems Conference and Exposition PSCE '06*, October 2006, pp. 2141–2145.

[110] G. Terörde, *Electrical Drives and Control Techniques.* Acco, 2004.

[111] S. De Ranter, "Modeling of VSC HVDC systems for power system stability tools: Applications in Eurostag and Matlab," Master's thesis, K.U.Leuven, 2008-2009.

[112] S. Östlund, *Electrical Machines and Drives.* Stockholm, Sweden: Royal Institute of Technology (KTH) : School of Electrical Engineering, Universitetsservice, 2008.

[113] G. F. Franklin, J. D. Powell, and A. Emami-Naeini, *Feedback control of dynamic systems*, 4^{th} ed. Prentice Hall, 2002.

[114] R. E. Best, *Phase Locked Loops.* McGraw-Hill Professional, 2007.

[115] F. M. Gardner, *Phaselock Techniques.* Wiley-Interscience, 2005.

[116] A. H. Norouzi and A. M. Sharaf, "Two control schemes to enhance the dynamic performance of the STATCOM and SSSC," *IEEE Trans. Power Del.*, vol. 20, no. 1, pp. 435–442, January 2005.

[117] S. Cole and R. Belmans, "Modelling of VSC HVDC using coupled current injectors," in *Proc. IEEE Power and Energy Society General Meeting - Conversion and Delivery of Electrical Energy in the* 21^{st} *Century*, July 20–24, 2008, pp. 1–8.

[118] K. R. Padiyar and N. Prabhu, "Modelling, control design and analysis of VSC based HVDC transmission systems," in *Proc. International Conference on Power System Technology PowerCon 2004*, vol. 1, November 21–24, 2004, pp. 774–779.

[119] J. M. Mauricio and A. G. Exposito, "Modeling and control of an HVDC-VSC transmission system," in *Proc. IEEE/PES Transmission. Distribution Conference and Exposition: Latin America TDC '06*, August 15–18, 2006, pp. 1–6.

[120] C. Du, E. Agneholm, and G. Olsson, "Comparison of different frequency controllers for a VSC-HVDC supplied system," *IEEE Trans. Power Del.*, vol. 23, no. 4, pp. 2224–2232, October 2008.

[121] Y. Ni, Z. Lan, L. Zhu, K. Poon, D. Gan, H. Zhu, and Z. Cai, "Area center of inertia - a potential unified signal for synchronous and frequency stability control of interconnected power systems under short and long time spans," in *Proc. International Conference on Electrical Engineering*, 2007.

Publications

Reviewed Journals

1. P. Buijs, D. Bekaert, S. Cole, D. Van Hertem, and R. Belmans, "Transmission investment problems in Europe: going beyond standard solutions," submitted to *Energy Policy*, 2010.
2. S. Cole, K. Srivastava, M. Reza, and R. Belmans, "New numerical techniques for bifurcation analysis of power systems," submitted to *European Trans. Elec. Power*, 2010.
3. S. Cole, and R. Belmans, "*MatDyn*, a new Matlab based toolbox for power system dynamic simulation," submitted to *IEEE Trans. Power Syst.*, 2010.
4. S. Cole, and R. Belmans, "A proposal for standard VSC HVDC dynamic models in power system stability studies," submitted to *Electric Power Systems Research*, 2010.
5. S. Cole, J. Beerten, and R. Belmans, "Generalized dynamic VSC MTDC model for power system stability studies," *IEEE Trans. Power Syst.*, vol. 25, no. 3, pp. 1655-1662, August, 2010.
6. L. Meeus, L. Vandezande, S. Cole, and R. Belmans: "Market coupling and the importance of price coordination between power exchanges," *Energy*, vol. 34, no. 3, pp. 228-234, 2009.
7. S. Cole, D. Van Hertem, L. Meeus, and R. Belmans: "Energy storage on production and transmission level: a SWOT analysis," *WSEAS Trans. Power Syst.*, vol. 1, no. 1, pp. 31-38, January, 2006.

Reviewed Magazines

1. S. Cole, and R. Belmans: "Transmission of bulk power. The history and applications of voltage-source converter high-voltage direct current systems," *IEEE Ind. Electron. Mag.*, pp. 19-24, September, 2009.

International Conferences

1. J. Beerten, S. Cole, and R. Belmans, "A sequential AC/DC power flow algorithm for networks containing multi-terminal VSC HVDC systems", *Proc. IEEE Power & Energy Society General Meeting PES GM '10*, July 2010.

2. G. Daelemans, K. Srivastava, M. Reza, S. Cole, and R. Belmans, "Minimization of steady-state losses in meshed networks using VSC HVDC," *Proc. IEEE Power & Energy Society General Meeting PES GM '09*, July 2009, pp. 1 - 5.

3. P. Buijs, S. Cole, and R. Belmans, "TEN-E revisited: opportunities for HVDC technology," *Proc. 6^{th} International conference on The European Electricity Market EEM'09*, May 2009.

4. S. Cole, D. Van Hertem, and R. Belmans, "VSC HVDC as an alternative grid investment in meshed grids," *Proc. Int. Conf. on Infrastructure Systems*, November 2008.

5. S. Cole, and R. Belmans, "Modelling of VSC HVDC using coupled current injectors," *Proc. IEEE Power & Energy Society, 2008 General Meeting Conversion and Delivery of Electrical Energy in the 21^{st} Century*, July 2008.

6. S. Cole, D. Van Hertem, I. Pardon, and R. Belmans, "Randstad HVDC: A case study of VSC HVDC bulk power transmission in a meshed grid," *Proc. Security and Reliability of Electric Power Systems, Cigré regional meeting*, June 2007, pp. 83-89.

7. S. Cole, D. Van Hertem, and R. Belmans, "Connecting Belgium and Germany using HVDC: A preliminary study," *Proc. IEEE Power Tech 2007*, July 2007.

8. D. Van Hertem, J. Verboomen, S. Cole, W. Kling, R. Belmans, "Influence of phase shifting transformers and HVDC on power system losses," *Proc. IEEE PES 2007 General Meeting*, June 2007.

9. L. Meeus, L. Vandezande, S. Cole, and R. Belmans, "Pricing approach for coupled exchanges and the use of LMP," *Proc. World Energy Systems Conference*, June 2006.

10. S. Cole, L. Meeus, and R. Belmans, "Assessment of a market coupling implementation based on price differences," *Proc. 3^{rd} IEEE Benelux Young Researchers Symposium in Electrical Power Engineering*, April 2006.

11. S. Cole, D. Van Hertem, L. Meeus, and R. Belmans, "The influence of renewables and international trade on investment decisions in the grid of the

future," *Proc. ICREPQ'06 International Conference on Renewable Energies and Power Quality*, April 2006.

12. S. Cole, D. Van Hertem, L. Meeus, and R. Belmans, "SWOT analysis of utility side energy storage technologies," *Proc. 5^{th} WSEAS/IASME Int. Conference on Electric Power Systems, High Voltages, Electric Machines*, December 2005.

13. S. Cole, D. Van Hertem, L. Meeus, and R. Belmans, "Technical Developments for the Future Transmission Grid," *Proc. International conference on future power systems*, November 2005.

Curriculum Vitae

Stijn Cole
Born July 17, 1982 in Wilrijk, Belgium

1994 - 2000	Latin-Mathematics Sint-Gummaruscollege, Lier
2000 - 2005	Master of Science: Electrotechnical Engineering K.U.Leuven
2005 - 2009	Master in Sinology K.U.Leuven
2005 - 2010	PhD in Engineering Electrical Engineering Department, ESAT Division Electrical Energy and Computer Architectures, ELECTA K.U.Leuven

Arenberg Doctoraatsschool Wetenschap & Technologie
Faculteit Ingenieurswetenschappen
Departement Elektrotechniek
Afdeling Elektrische Energie en Computerarchitecturen
Kasteelpark Arenberg 10 bus 2445
B-3001 Leuven